CHALMERS

A joint model of heavy truck, tyres, and operating environment for tyres selection

Master's thesis in Automotive Engineering

PETR KOLÁŘ

Department of Applied Mechanics
CHALMERS UNIVERSITY OF TECHNOLOGY
Göteborg, Sweden 2015

MASTER'S THESIS IN AUTOMOTIVE ENGINEERING

A joint model of heavy truck, tyres, and operating environment for tyres selection

PETR KOLÁŘ

Hogeschool van Arnhem en Nijmegen

HAN Automotive Institute
HAN UNIVERSITY OF APPLIED SCIENCES
Arnhem, The Netherlands 2015

Faculty of Mechanical Engineering
CZECH TECHNICAL UNIVERSITY IN PRAGUE
Prague, Czech Republic 2015

CHALMERS

Department of Applied Mechanics
Division of Vehicle Engineering and Autonomous Systems, Vehicle Dynamics group
CHALMERS UNIVERSITY OF TECHNOLOGY
Göteborg, Sweden 2015

A joint model of heavy truck, tyres, and operating environment for tyres selection
PETR KOLÁŘ

Master's thesis 2015:12
ISSN 1652-8557
Department of Applied Mechanics
Division of Vehicle Engineering and Autonomous Systems, Vehicle Dynamics group
Chalmers University of Technology
SE-412 96 Göteborg
Sweden
Telephone: +46 (0)31-772 1000

Cover:
courtesy of Volvo GTT

Chalmers Reproservice
Göteborg, Sweden 2015

A joint model of heavy truck, tyres, and operating environment for tyres selection
Master's thesis in Automotive Engineering
PETR KOLÁŘ
Department of Applied Mechanics
Division of Vehicle Engineering and Autonomous Systems, Vehicle Dynamics group
Chalmers University of Technology

Abstract

Improving fuel efficiency is one of the core targets when minimizing the transport cost of a vehicle combination. Hence, it is crucial to optimize the design and selection of all vehicle components, including tyres. Volvo Group Trucks Technology (GTT) and Chalmers University of Technology run a common research project TyreOpt—Fuel consumption reduction by tyre drag optimization. This master thesis is supporting the TyreOpt research project by verification of a computationally efficient model for an evaluation of the operating costs by a newly developed joint model of the vehicle, environment, and tyres, which is based on one of the existing tools within Volvo GTT.

Selection of the proper Volvo GTT analysis tool, which serves as a base for the newly developed joint model, was supported by Volvo experts' experience. Theory of tyre was reviewed in order to support modelling of the transient-linear tyre model and implementation of the rolling resistance model, which was developed within the TyreOpt research project. Representation of the computationally efficient model of the operational cycle and all relevant parameters was transformed to the newly developed model. Simple driver and power-train models were developed in order to evaluate vehicle performance for selected operational environments. Feasability of constraining events implementation to the high-fidelity model is discussed and candidates for new constraints are proposed.

Verification of the computationally efficient model concludes performance and limitations of this computationally efficient model, developed within the TyreOpt research project. The tyre model is parameterised in tyre design parameters, such as tyre width, radius and pressure. The computationally efficient and the newly developed model are investigated in qualitative manner in order to list differences in behaviour under various specification parameters of the vehicle, the tyres and the operating environment. Improvements of the computationally efficient model are proposed. Sensitivity analysis aims to investigate energetic behaviour of both models with respect to changing tyre design variables. Results proved considerable influence of different fidelity of the model on transport costs, mainly due to inverse kinematic principle of computationally efficient model, which can not cope with velocity transients and different control strategies. Trends of the energy consumption for different tyre design variables are compared with the rolling resistance theory, which was summarized in the literature review.

Keywords: Vehicle dynamics, tyres, rolling resistance, fuel consumption, optimization.

To my mother Jana..

Preface

This thesis work is an integral part of the programme Master of Automotive Engineering (MAE) governed by Czech Technical University (CTU) in Prague, Czech Republic and Hogeschool van Arnhem en Nijmegen (HAN), the Netherlands. Thanks to already 10 years of cooperation of both universities, I have been able to get insight into Vehicle dynamics and apply for the thesis project "A joint model of heavy truck, tyres, and operating environment for tyres selection", governed by the Chalmers University of Technology and Volvo Group Trucks Technology (GTT).

Academic supervision of the thesis was carried out by Zuzana Šabartová and Pär Pettersson from Chalmers University of Technology and Karel Kůral from HAN. Industrial supervisor was Peter Lindroth from Volvo GTT.

Almost six months ago, I moved to Göteborg in Sweden and I started to work on my thesis, which brought me valuable experience due to many interesting issues and cooperation with experts from industrial and academic environment. It is a pleasure to thank Volvo GTT and FISITA Student Travel Bursary for covering part of my living expenses of my stay in Göteborg, Sweden. Their support is greatly appreciated.

At Chalmers University of Technology, I would like to acknowledge amazing cooperation with professor Bengt Jacobson, Zuzana Šabartová, and Pär Pettersson. Their help and comments to my work are highly appreciated.

At Volvo GTT, I would like to acknowledge great support from the department Chassis&Vehicle Dynamics, where I received perfect support and conditions for my work. My industrial supervisor Peter Lindroth gave me motivation and many comments which dragged my work further on.

At HAN and CTU, I would like to acknowledge way of lectures and personal approach of Saskia Monsma, Karel Kural, and Gabriela Achtenová. Their work accelerated my passion for automotive industry.

I owe my deepest gratitude to my family. I thank to them for who I am.

Contents

Nomenclature

α	slip angle of the wheel
α_{slmax}	start-ability constraint threshold, i.e. maximum road slope
α_{sl}	slope angle
δ	radial tyre compression
δ_0	nominal radial tyre compression
Δx	logitudinal offset of the wheel normal reaction resultant
$\dot{\Omega}$	angular wheel acceleration
η	understeer gradient
η_{min}	understeer gradient threshold
γ	wheel camber angle
κ	longitudinal wheel slip
κ_{max}	limit of the longitudinal slip
μ	road-tyre friction coefficient
μ_x	normalized longitudinal force F_x
μ_y	normalized lateral force F_y
ν	steering angle
Ω_{y0}	rotational velocity of the free rolling wheel
Ω_y	rotational velocity of the wheel under tractive forces
ρ	air density
σ_α	relaxation length for slip angle α
σ_κ	relaxation length for longitudinal slip κ
τ	human sensoric delay
$\mathbf{p}$	vector of vehicle and environment parameters
$\mathbf{x}$	vector of tyre design variables
ξ	approximation constant
a	contact patch length
a_{dr}	driver's acceleration request
b	experts evaluating Volvo analysis tools
c	criteria
c_{dz}	damping coeficient of the tyre in the vertical direction
c_{F_α}	lateral slip stiffness
c_{F_γ}	camber stiffness
c_{F_κ}	longitudinal slip stiffness
c_{M_α}	aligning torque stiffness
c_{M_γ}	aligning torque stiffness
c_w	air drag coefficient
c_x	longitudinal stiffness
c_y	lateral stiffness
d_0	unloaded diameter of the tyre
d_{dr}	driver's preview distance
dep	tread depth

e	expert's rating of a tool with respect to the given criteria
e_∞	steady state error
e_κ	longitudinal slip error
E_{tr}	tractive energy
e_{vx}	velocity error
f	rolling resistance coeficient
F_c	total fuel consumption
f_c	fuel consumption
f_{R_l}	regression function of the loaded radius
F_{RR}	rolling resistance force in the wheel plane
F_{tr}	vehicle tractive force
F_{x0}	longitudinal force in absence of side force F_y
F_{xcomp}	road slope compensated longitudinal force F_x
F_{xFz}	slope compensation of the longitudinal force
F_x	longitudinal force component in the wheel plane
F_{y0}	lateral force in absence of brake or drive force F_x
F_{ycomp}	road camber compensated lateral force F_y
F_{yFz}	slope compensation of the lateral force
F_y	lateral force in the wheel plane
F_{z0}	nominal tyre load
F_z	normal reaction of the wheel
G	resultant of the gravitational force
g	gravity acceleration
G_d	driver's proportional gain
G_{TC}	proportional gain of the traction controll
H	wheel profile height
HU	calorific value of the fuel
$I_{red,i}$	moment of intertia of the powertrain components
I_{yy}	moment of inertia of the wheel
k	project stakeholder
l_1	distance from the front axle to the vehicle center of gravity
l_2	distance from the rear axle to the vehicle center of gravity
m	vehicle mass
M_f	wheel resistive moment from air and wheel hub drag
m_F	vehicle translational weight
m_t	tyre weight
M_{yRR}	rolling resistance moment
M_y	tractive torque on the wheel
M_{z0}	aligning moment of the wheel from pure lateral slip
M_z	aligning moment of the wheel
n_w	total number of wheels
n_{as}	number of tyres per axle side
p	inflation pressure of a tyre

P_{dr}	driver's power demand
P_{max}	maximal engine power
P_{RR}	rolling resistance power
P_{tr}	tractive power
q_{Sy1}	rolling resistance moment coeficient
q_{Sy2}	rolling resistance moment depending on F_x
q_{Sy3}	rolling resistance moment depending on velocity v_x
q_{Sy4}	rolling resistance moment coeficient depending on velocity
q_{V1}	tyre radius growth coeficient
R	sum of vehicle resitances
r	human request to the pedal
R_0	unloaded tyre radius
r_κ	correction of the pedal request
R_a	resistane of rotating masses
r_{dyn}	dynamic wheel radius
R_e	effective rolling radius of tyre
R_l	loaded wheel radius
R_{sl}	slope resistance
R_w	air drag resistance
s	overall rating of a Volvo analysis tool
S_w	frontal vehicle area
T	air temperature
T_{dr}	driver's preview time
T_{ITC}	integration constant of the traction controll
tr	velocity error threshold
u_s	displacement of the spring in longitudinal direction
v_{crit}	critical velocity of the wheel
v_{ref}	refference velocity for rolling resistance measurement
v_{sx}	longitudinal wheel slip velocity
v_{sy}	lateral wheel slip velocity
v_s	displacement of the spring in laterall direction
v_w	longitudinal component of the relative wind velocity
v_x	longitudinal component of the tyre velocity
v_y	lateral component of the wheel velocity
w	criteria weight
w_t	tyre width
x	distance along the track
x_{stop}	vehicle stopping distance
z_r	road vertical coordinate in global coordinate system
z_w	wheel hub vertical coordinate in global coordinate system
B	stiffness factor in Pacejka's Magic Formula
C	shape factor in Pacejka's Magic Formula
D	peak factor in Pacejka's Magic Formula
E	shape factor in Pacejka's Magic Formula

SI units and radians used

1 Introduction

The current commercial vehicle market competition creates a demand for innovations. Not only the purchase cost of the vehicle contributes to the overall cost, since the operating costs, such as service, fuel, tyres, and labour costs are also significant. Saving the fraction of the operating costs of the truck leads to a remarkable competition benefit for the producer, the customer and also for the society (CO_2 savings). However, such task is very complex, since trucks are not subject to the classical market segmentation as in the case of passenger vehicles. Number of possible truck combinations at Volvo GTT is about 10^{150}, see [20]. That is making heavy duty vehicle industry very special.

1.1 Background

Improving the fuel efficiency is one of the core targets when minimizing the transport cost of a vehicle combination. Hence, it is crucial to optimize the design and selection of all vehicle components. Volvo GTT and Chalmers University of Technology run a common research project TyreOpt—Fuel consumption reduction by tyre drag optimization, which is described in [34], [35], [36], [21], and Section 2.1. The main aim of the research project is to identify the optimal tyre configuration for each vehicle and operating environment specification. The scope of this thesis project is to contribute to the research project connecting the optimization and the modelling framework, illustrated in Figure 1.1, by establishing a high fidelity joint model of the heavy truck, tyres, and operating environment. The required structure of this model is schematically described in Figure 1.2, where it can be seen that a joint model is used in order to evaluate the objective function and constraints for the simulation based optimization, see [18], [15], [5], [7].

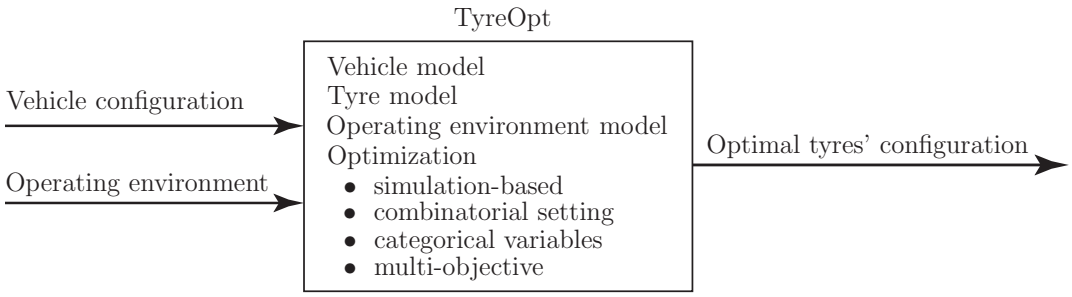

Figure 1.1: *Illustration of the optimization routine and vehicle dynamics modelling [34]*

The desired high fidelity model should be able to evaluate the objective functions and constraints based on fixed input operating vehicle parameters and tyre design variables. The model will be later utilized to evaluate tyre related functions selected in the research project and verify the results of the project.

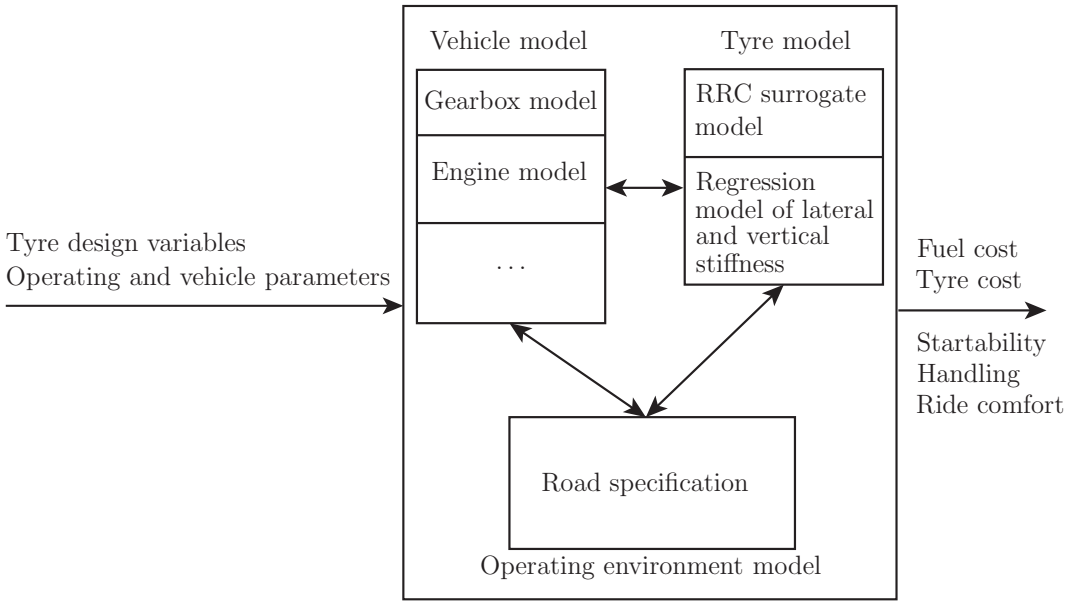

Figure 1.2: *Joint model structure [34]*

1.2 Problem statement

Tyres significantly contribute to the overall vehicle operating costs, due to different losses of energy during driving denoted as rolling resistance and costs of the tyres itself. The frequency of tyres changing depends on their wear and brings a significant cost especially for trucks, where tyres are quite expensive. A small decrease in rolling resistance leads in a long term comparison to large savings. Nevertheless, the tyre selection problem is not the same for every customer, because of other performance based constraints and operating costs, which varies for different vehicle and environment combinations.

The simulation-based optimization framework, described briefly in Section 2.2, aims to solve the tyres selection problem. These algorithms require preferably a computationally efficient model both the objective function and the constraints which were introduced in [10]. Such model should provide a simple, but trustworthy representation of the reality in order to reflect the real interaction of vehicle, tyres, and environment. The quality of the optimal solution obtained by the optimization algorithms is only as good as the used joint model.

1.3 Envisioned solution

The purpose of this thesis is to generate the joint model (further referred to as model B), containing detailed model of the truck, tyres, and environment based on the current analysis tools, resources, and the expert knowledge available in Volvo GTT. The existing computational efficient model described in [10] (further referred to as model A) will be verified by the model B. Special attention will be paid to the evaluation of the objective function. Possible deviations between the models and their relation to the real truck behavior will be discussed.

1.4 Objective

The core objective of the work is to make a high fidelity joint model of the truck (model B), which should help to answer if the computationally efficient model (model A) reflects the influence of tyre design changes on objective function (cost) and constraints well enough.

1.5 Deliverable

The thesis deliverable are the following:

- high-fidelity joint model (model B) of the truck, tyre and environment, including
  - integration of tyre design variable dependent tyre model,
  - development of the simplified power-train and longitudinal driver model, and
  - integration of power-train and driver model.
- verification of the model A, including
  - selection of vehicle and operating cycle,
  - selection of comparison quantities, and
  - propose most important changes to model A and/or B.

1.6 Limitations

Project requirements come from the TyreOpt research project demands. This thesis project is therefore aimed to support it by providing sufficient models for the tyre optimization, not to develop mathematical optimization routines itself. The following list defines the project boundaries which are based on the thesis project plan. In case agreed activities are finished before the scheduled plan, model B could be further improved within a new set of activities agreed by all involved parties.

Thesis will include

- truck model based on the existing software of Volvo GTT,
- environment specification in a sufficient format for the model B, including velocity and topography,
- verification of the objective function (energy consumption) evaluation of model A with alternative representation in model B,
- implementation of tyre design variable dependent tyre model from TyreOpt,
- a modified tyre definition based on the previous research performed within TyreOpt research project, and
- list of constraints which can be evaluated by model B.

Thesis will not include

- verification of the model A tyre wear costs,
- road definition (curvatures, micro-structure, etc.),
- tyre model considering brake/load torque and tread material influence on rolling resistance,
- verification of many vehicle and environment combinations,
- interaction of tyre with deformable surfaces (only rigid road surface representation),
- slippery road conditions,
- complex power-train model, and
- complex driver model.

2 Tyre selection research project

2.1 TyreOpt

TyreOpt—Fuel consumption reduction by tyre drag optimization is a research project aiming to propose a new tyre selection process based on utilizing scientific methodology combined with the existing expert knowledge. The current practice for selection of the tyres' configuration at Volvo GTT is usually based on experience and customers' input. Nowadays, the competition between heavy duty vehicle manufacturers requires an improved method for selecting the optimal set of tyres for particular vehicle-operating environment combination.

The selection of the optimal set of tyres in order to minimize the operating costs is a very complex task, because of the great variety of environments and vehicle combinations. This makes every customer a unique formulation of the optimization task, closer described in [34], and in Section 2.2. This master thesis aims together with [10] to explore and create the joint models of varying fidelity. University of Ontario in Canada, Institute of Technology (UOIT) contributes to the project by its research aimed on structural modelling of the truck tyre based on finite element method (FEM).

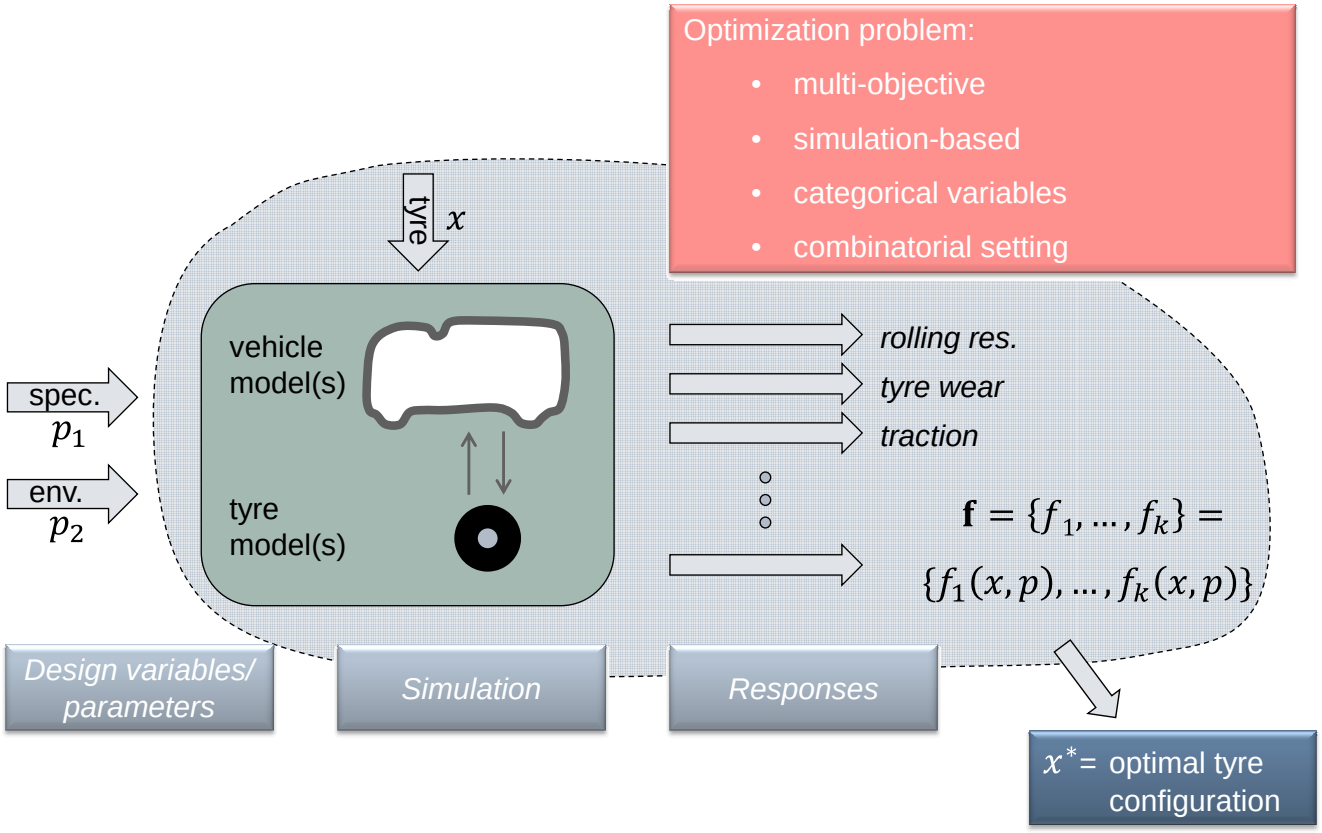

Figure 2.1: *Optimization of tyre selection*

2.2 Optimization

The TyreOpt project aims to treat the tyre selection problem in a structured mathematical way. Core of this project is to reduce the rolling resistance while balancing other tyre depending criteria. The optimization model of the tyres selection problem approved by Volvo GTT, is to minimize the sum of the fuel and tyre costs subject to the start-ability, the ride comfort, and the handling comfort ([34]). Tyre selection process is visualized in Figure 2.1. The list of constraints selected may be updated in the future.

Following tyre design variables $\mathbf{x}$ are selected within the optimization model of the tyres selection problem as those that considerably influence rolling resistance:

- inflation pressure p,
- tyre width w_t,
- tyre diameter d_0, and
- groove depth dep.

Vector $\mathbf{p}$ represents operating parameters, describing selected vehicle and operating environment. One possible formulation of the truck tyres selection optimization problem is to

$$\text{minimize } f_{fuelcost}(\mathbf{x}, \mathbf{p}) + f_{tyrewear}(\mathbf{x}, \mathbf{p}), \tag{2.1}$$

subject to the following set of constraints

$$g_{startability}(\mathbf{x}, \mathbf{p}) \leq 0, \tag{2.2}$$

$$g_{ridecomfort}(\mathbf{x}, \mathbf{p}) \leq 0, \tag{2.3}$$

$$g_{handling}(\mathbf{x}, \mathbf{p}) \leq 0, \tag{2.4}$$

and boundary restriction of variables ([34]). This thesis considers only fuel cost, not tyre wear cost.

Surrogate modeling

A detailed FEM model of the tyre, developed in UOIT, described in [2],[9],[3], is computationally expensive. FEM simulation of the tyre model for specific conditions takes several hours on an average workstation. This tyre model is parametric, therefore the influence of the tyre design variables can be investigated. The simulation results could be interpreted as a sample point for the rolling resistance coefficient (RRC) function f, defined in Section 4.3, for given values of the tyre design variables $\mathbf{x}$ (p, w_t, dep, d_0), normal tyre load F_z, longitudinal velocity of the tyre v_x, defined in Section 4.3 and [34]. That computationally expensive process of FEM simulation is replaced in [34] by a surrogate model, which is realized by relatively fast analytical function for obtaining actual value of rolling resistance by providing vehicle states F_z, v_x and tyre design variables $\mathbf{x}$. Such approach is standard in simulation based optimization [7]. Even high fidelity vehicle models with high frequency of state changing could be supported with such a technique. Another advantage of sample points interpolations with analytical function is possibility to evaluate function even for non-existing tyre combinations within operational range of surrogate model, introduced in Table 2.1, which was derived from the set of sample points supplied by UOIT. The interpolation of sample points is based on the radial basis function integrated with the existing expert knowledge about the rolling resistance coefficient to create the final surrogate, see [35].

variable	**units**	**operational interval**
tyre inflation pressure p	[psi]	$\langle 55; 165 \rangle$
unloaded section width w_t	[mm]	$\langle 227.66; 455.31 \rangle$
tread depth dep	[mm]	$\langle 0; 23.93 \rangle$
unloaded tyre diameter d_0	[mm]	$\langle 916.57; 1120 \rangle$
normal tyre load F_z	[lbs]	$\langle 1e03; 1e04 \rangle$
longitudinal tyre velocity v_x	[kph]	$\langle 0; 120 \rangle$

Table 2.1: Operational range of the surrogate model

3 Identification of the project requirements

One of the main goals of the thesis work is to introduce the high fidelity joint model of the truck. Truck is a very complex system, which has to be always simplified to a certain extent. Allowable level of simplification is the compromise with other project criteria. Certain requirements has to be specified in order to select which Volvo GTT analysis tool, described in Section 5.4, would serve as a base for the model B, because each of these tools is specified and developed for different purposes. Hence different levels of simplification are valid for each tool. However, the right decision which analysis tool to choose requires good knowledge of all GTT analysis tools. It is not even possible to get insight to all of them within the time denoted for this thesis. Therefore an alternative approach which involves multi-criterial analysis based on the expert knowledge is utilized. Even though the choice of tool is rather subjective task, the process described bellow aims to provide a systematic way for choosing a proper software solution.

3.1 Criteria

The model has to be able to verify model A, introduced in [10], which is based on the longitudinal dynamics of the vehicle. It is preferable to use one of the Volvo GTT dynamic analysis tools, because of modularity (different truck combinations, environments, tyres definition) and good correlation of these models with reality for specified region of tasks. The fact that the existing tool will be used means significant time savings in contrast to the case when high-fidelity model should be developed from the beginning.

The main requirements for the Volvo vehicle dynamics tool selection are following:

- possibility to verify the objective functions and constraints as modelled in the model A,
- possible substitution of the model A by the model B in the optimization routine,
  - satisfaction of demands of the optimization routine (computational efficiency, possibility to continuously change tyre design variables),
- modularity (different truck combinations and environment), and
- to meet available resources (time, knowledge, software).

3.2 Criteria specification

One of the possible set of criteria for selection of Volvo vehicle dynamics tool is the following:

1. possibility to verify the objective functions and constraints as modelled in model A
   (a) simple vehicle longitudinal drive cycle simulation (normal forces on each of the wheels, lateral&longitudinal slip, rotational velocity of the wheel),
   (b) definition of the resistances,
   (c) power-train definition,
   (d) vehicle comfort related simulations,
   (e) vehicle start-ability related simulations,
   (f) definition of the tyre working with rolling resistance, and
   (g) vehicle stability (handling) related simulations.
2. optimization routine requirements
   (a) computational efficiency, and
   (b) continuous change of the tyre design parameters (inflation pressure, diameter, width, groove depth).

3. modularity&robustness

   (a) possibility to define variety of truck types and combinations easily, and

   (b) possibility to change the environment.

4. available resources

   (a) learning time,

   (b) approximate time spent to set the simulation, and

   (c) edit-ability.

3.3 Suitable tools and environment

With respect to the lack of documentation and this thesis's time limitation the multi-criterial analysis for the analysis tool selection was utilized. Experts aware of all the software tools at Volvo GTT were asked to fill in a questionnaire containing evaluation of each software tool wrt. the selected criteria. The results of the questionnaire were then processed and the most suitable truck model was selected based on these results.

First, we have to specify relevant criteria c which was done in previous section 3.2 and assign them weights w_i, where $i = \{1, 2, 3, ..., 14\}$, index i denotes specified criteria. Personalized weights w_{ki} are assigned by the project stakeholder k to each criteria i, where $k = 1, 2, 3, 4, 5$. Project stakeholders will evaluate each of the relevant criteria to analysis tools. Higher values of personalized weights w_{ki} express higher priority. Such evaluation will ensure that all stakeholders will express their needs. Finally the overall weight for each criteria will be specified as

$$w_i = \frac{\sum_{k=1}^{5} w_{ki}}{5}. \tag{3.1}$$

Experts $b = 1, 2, 3, 4, 5$ aware of all tools were asked to evaluate weights e_{ij}, which reflects to what extent each of the Volvo analysis tools $j = 1, 2, 3, 4, 5$ matches the selected criteria i, where $e_{ij} \in \{1, 2, 3, 4, 5\}$. Higher values of e_{ij} express higher rate of meeting the criteria i for given tool j.

Final rating of each tool is described by following relation

$$s_j = \sum_{b=1}^{5} \frac{\sum_{i=1}^{14} w_i e_{ij}}{n_{bj}}, \tag{3.2}$$

where n_{bj} is the number of criteria evaluated wrt. each tool j by expert b. Volvo analysis tool j with highest value of rating $max\,(s)$ would be considered as a model B base platform.

3.4 Conclusions

Questions were posed via questionnaires to all five stakeholders for evaluation of the criteria weights. Resulting weights can be seen in Table A.3. Five experts at Volvo GTT were approached with evaluation of the analysis platforms by matching rate of satisfaction of each criteria for every platform, see Table A.4.

From the overall results of the requirement analysis can be seen, that CVM achieved best platform rating s. However, It would be very hard to implement the surrogate model of the rolling resistance coefficient due to the fact that vehicle is described in NASTRAN FEM software which requires special training for operation and providing changes in the tyre definition. Also the computational time needed by CVM is much higher than the time needed by other available tools. Final choice is VTM, which we select for further development of model B, as it achieves second highest platform rating s. It meets resources available in this thesis (training, knowledge) and it is relatively fast when compared to CVM. VTM vehicle templates can capture dynamic behavior of the chassis, therefore its influence on the objective function can be investigated.

4 Theory of tyres

First of all, when considering the tyre behavior it is necessary to be aware of the fact that the tyre is a very complex structure, and it is not possible to simplify the structure for universal use. The tyre's behavior is related to the deformation and to the ground contact.

The basic task of a tyre is to provide support of the vehicle in the normal direction to the road, smooth the road irregularities, and transmit forces in ground plane that allow motion along the desired trajectory ([37]). In addition to the basic tasks we can find whole subsets of other criteria which are expected from the modern tyre, related to e.g. comfort, handling performance, rolling resistance, etc.

4.1 Tyre operation

One of the basic tasks of tyre is to transmit forces between the vehicle and the road. These forces are in most cases generated by two main phenomena, adhesion and deformation of the tyre and the road, see [14]. As tyres are very complex structures, so is the tyre's behavior. Therefore some simplifications have to be made in models, leading to a limited range of use of such models. This thesis is focused solely on the rigid road surfaces. Hence, we can allow to neglect deformations of the road, because it plays only minor role for the vehicle behavior on rigid surfaces, such as tarmac, concrete etc., see [37]. This assumption leads to major simplification of drive cycle modeling . Another situation which is not in the scope of the thesis is operation in wet conditions. The vehicle behavior under such conditions is very different, as is the modelling of the tyre behavior. This is modelled with help of fluid dynamics that complicates the matter significantly, see [14].

Adhesion effects are moreover caused by mutual molecular attraction between the tyre and the road. Tyre polymer structure consists of adhesive sites, which interact with the road in the contact patch. Adhesive sites are interacting until a maximum relative displacement is reached. When contact is broken, the material is oscillating, because of released potential energy from the contact stress. Because the material in a tyre is not purely elastic, but also has some viscous properties, certain amount of energy is dissipated between road and ground under the wheel. This mechanism ensures that displacement of the tyre generates a corresponding reaction force. Adhesion depends on temperature, damping properties and deformation of contacting surfaces ([14]).

Deformation of the tyre is caused by the forces loading the tyre structure. Deformation of the tyre contact patch generates reaction force with the road. Therefore vehicle can be controlled in longitudinal and lateral direction. A rolling tyre is being consistently deformed due to the road contact and centrifugal forces acting on the tyre mass. The contact patch is compressed at the front and stretched out at the end. This phenomena is producing contact patch pressure difference which compacts the ground under the wheel, which creates better friction due to stronger interaction with the road micro-profile ([14]).

4.2 Basic tyre relations

One of the main thesis activities is modeling of the vehicle behavior, therefore it is crucial to define basic tyre mechanic relations influencing dynamic properties of the vehicle. Notation used within this thesis follows ISO standards. In order to distinguish between different tyres on the vehicle, supporting indexes i, j were utilized. Index i denotes axle order, where $i = 1$ is assigned to the front axle and index increases towards rear of the vehicle. Side index $j = 1$ denotes left hand tyres and $j = 2$ right hand tyres. In case of more than 2 tyres on the axle, combinations of i, j represent more tyres. For instance, in case of twin-tyre on the rear axle, F_{z22} represents combined normal load for both tyres.

Effective rolling radius R_e expresses the virtual distance of the instantaneous wheel rotation center on the vertical tyre axis. Kinematics of the tyre and resulting slip could be expressed with use of effective rolling radius as introduced in [30]. It does not reflect the real radius of the tyre. Free rolling tyre is defined by the ratio, see Eq. 4.1, between longitudinal wheel hub velocity component of the speed v_x and rotational velocity of the wheel Ω_{y0}. Free rolling tyre is not driven nor braked. It means that sliding is not present in the contact patch,

$$R_e = v_x / \Omega_{y0}. \tag{4.1}$$

Previous relation is valid only for a free rolling tyre. When we bring additional torque to the wheel, the wheel is braked or driven, we can define longitudinal slip κ as

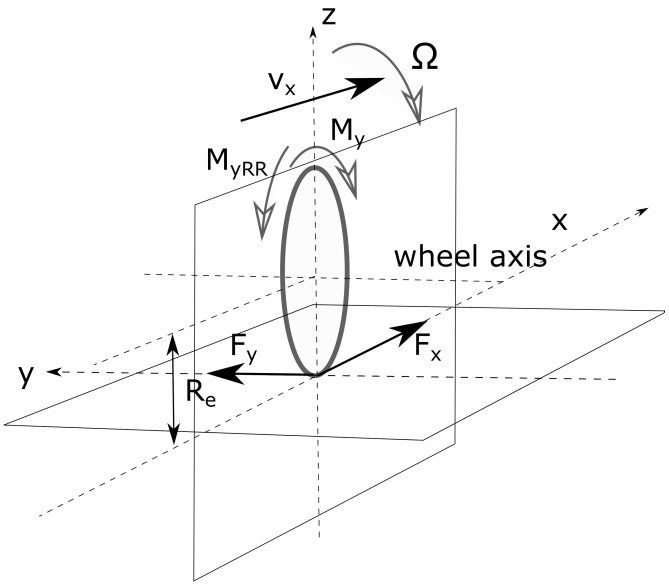

Figure 4.1: *Wheel coordinate system and notation according to the ISO 8855*

$$\kappa = -\frac{v_x - R_e\Omega_y}{v_x} = -\frac{\Omega_{y0} - \Omega_y}{\Omega_{y0}}, \tag{4.2}$$

where Ω_y is real angular velocity of the wheel. Sign of slip κ and longitudinal force F_x are positive while driving. Under slippery conditions, κ can attain large values for the same input torque, see [29].

The effective radius R_e varies with the normal load F_z until certain threshold where it is saturated. Empirical approximation of the effective radius R_e

$$R_e = R_0 - \delta_0 \left[F \arctan\left(G\frac{\delta}{\delta_0} \right) + H\frac{\delta}{\delta_0} \right], \tag{4.3}$$

as introduced in [30]. Deflections of the tyre δ, or δ_0 for nominal load are defined as

$$\delta = \frac{F_z}{c_z} = R_0 - R_l, \tag{4.4}$$

where F_z, or F_{z0} are tyre loads, which are normal to the road surface. The vertical stiffness of the tyre c_z is defined as

$$c_z = \frac{\delta}{F_z}. \tag{4.5}$$

Empirical coefficients F, G, H are described in Table 4.1 ([30]). Alternative empirical description of the effective rolling radius R_e can be found in [29].

coefficient	**note**	**interval**
F	tyre structure (bias, radial)	$[3; 12]$
G	tread height coefficient (new, worn)	$[0.2; 0.4]$
H	slope of $R_e - F_z$ for large loads (bias usually higher)	$[0.03; 0.25]$

Table 4.1: Empirical coefficients for effective rolling radius R_e [30]

Another important quantity which has to be defined is wheel slip angle α, defined as

$$\tan\alpha = \frac{v_y}{v_x}, \tag{4.6}$$

which is ratio between longitudinal v_x and lateral v_y velocity component of the wheel, see [29].

Now we can finally define the force generated by the tyre. Reaction forces of the tyre in longitudinal F_x, lateral F_y directions and self-aligning moment M_z are defined as positive with respect to coordinate system, see

Figure 4.1. These forces and moments are results of the deformation of the tyre, which we can express as slip dependent quantities by following functions

$$F_x = F_x(\kappa, \alpha, \gamma, F_z), \tag{4.7}$$

$$F_y = F_y(\kappa, \alpha, \gamma, F_z), \tag{4.8}$$

$$M_z = M_z(\kappa, \alpha, \gamma, F_z), \tag{4.9}$$

of slip quantities κ and α, camber angle γ and normal load F_z. Camber angle γ is angle between vehicle vertical axis z_v and the wheel plane $z_w x_w$. Positive camber angle is when the top of the tyre lean outwards, as defined in [29].

Simplest linear representation of tyre force generation is by a simple longitudinal slip stiffness $c_{F\kappa}$, lateral slip stiffness $c_{F\alpha}$, camber stiffness $c_{F\gamma}$, aligning toque stiffness dependent on slip angle $c_{M\alpha}$ and camber angle $c_{M\gamma}$, see [29]. Nevertheless, such simplification could be done only for very small tyre deformations, because for larger lateral and longitudinal accelerations becomes the tyre behavior highly non-linear. This limitation requires set operation range of the tyre model and control it during simulation. Linear tyre model can be, according to [29], expressed as

$$F_{x0} = c_{F\kappa}\kappa, \tag{4.10}$$

$$F_{y0} = c_{F\alpha}\alpha + c_{F\gamma}\gamma, \; and \tag{4.11}$$

$$M_{z0} = -c_{M\alpha}\alpha + c_{M\gamma}\gamma. \tag{4.12}$$

Non-linear behavior of the tyre is necessary to take into account, e.g. for larger lateral accelerations of the vehicle. Semi-empirical model of the wheel forces with respect to slip quantities can be represented by empirical expression, so called "Magic Formula" (MF) have following expression:

$$y(x) = D\sin[C\arctan\{Bx - E(Bx - \arctan(Bx))\}], \tag{4.13}$$

introduced in [29], where B is stiffness factor $B = C_{F\alpha}/CD$, D is peak factor $D = \mu F_z = F_{ypeak}$ and cornering stiffness $C_{F\alpha} = BCD$, shape factors C, E ([29]).

It is important to keep in mind that these relations are not independent on each other. Deformation in longitudinal direction is also influences the maximum possible lateral force and vice versa. It means that longitudinal and lateral force components have to be within the friction circle (ellipse), respectively their normalized forces μ_y, μ_x, defined in Eq. 4.14. Both normalized forces, have to obey the condition 4.15, which is called ellipse approximation, see [30].

$$\mu_y = \frac{F_y}{F_z};\; \mu_x = \frac{F_x}{F_z}, \; and \tag{4.14}$$

$$\mu_x^2 + \mu_y^2 \leq \mu^2. \tag{4.15}$$

4.3 Rolling resistance

Rolling resistance is caused by deformation of the road and tyre. Between the sections where a compound enters and leaves the contact patch is tyre being deformed. This leads to the heat dissipation, which is caused by viscous-elastic material properties. Rolling resistance can be modeled as rolling resistive moment M_{yRR} defined as

$$M_{yRR} = F_z \Delta x, \tag{4.16}$$

where a resultant of the normal force F_z is shifted by an horizontal offset Δx (from the wheel center axis the forward direction). Longitudinal offset Δx is a shift of the normal force resultant, given by the pressure distribution along

the contact patch. Therefore the rolling resistive moment M_{yRR} counteracts the rolling direction. Steady state solution of the rolling resistance can be expressed as

$$F_{RR} = \frac{F_z \Delta x + M_f}{R_l}, \tag{4.17}$$

where M_f represents moment counteracting wheel rotation, which is caused by air and wheel hub drag. In case of driving, M_f is substituted with the difference between driving/braking torque and resistive moments $M_y - |M_f|$. The tyre is being braked if $M_y < 0$ and driven when $M_y > 0$, see Figure 4.1.

However, pressure distribution in the contact patch is hard to model. Therefore rolling resistance could be expressed by use of the experimental relation

$$F_{RR} = f F_z, \tag{4.18}$$

where f is called the rolling resistance coefficient ([27]). There are other empirical relations that include more quantities influencing the rolling resistance in order to bring more fidelity relation of the rolling resistance, see [30], [14].

In order to be able to choose the relation that best suits our needs, dependency of the rolling resistance on different quantities has to be investigated. The most important phenomena are discussed bellow.

Wheel velocity

The rolling resistance increases with increasing longitudinal wheel velocity v_x ([37]). Increasing qualitative tendency of the rolling resistance has been also achieved with the UOIT FE tyre model, described in the Section 2.2, rolling resistance trend of the FE tyre model for different design variables is discussed in [2]. Surrogate model for rolling resistance coefficient f, described in Section 2.2, is based on the sample points from FE tyre model and its dependency on the velocity v_x is visualized in the Figure 4.2. Velocity dependance of the rolling resistance coefficient from the surrogate model for the rolling resistance coefficient seems to be significantly more sensitive to the velocity v_x than tendencies found in [37], [30], which also displays non-zero values of rolling resistance coefficient for very small velocities. Different tendency of the surrogate model can be caused by interpolation methods used in the surrogate model and/or qualitatively inaccurate results from FEM simulations of truck tyres.

Increase continues until a critical velocity v_{crit} is reached, where the natural frequency of the tyre is exceeded ([14]). It is due to vibrational phenomena. Back part of the contact patch is lifted by the standing wave. Hence the pressure resultant moves forward to the frontal zone. Tyre tread oscillations become under-damped. Such oscillations are accompanied with an enormous increase of deformations all across the wheel circumference. Therefore, due to the viscous characteristic of the tyre material, the deformations cause a large increase of the tyre temperature, overheating and possibly destroying the tyre. Such velocity limit is not within the recommended tyre operation area ([14]). Therefore each tyre has a speed index, which denotes maximal operational speed sufficiently far away from the critical tyre speed. For instance indexes H and S restrict maximum speed to 180 kph, respectively to 210 kph ([30]).

Material and structure effects

Material nature and tyre structure play significant roles when determining the rolling resistance and the critical velocity. Both can be optimized for specific application, vehicle and environment. Different applications have specific priorities. Therefore tyres for racing will have quite different structure and material than tyres for long-haul trucks.

From the material perspective it is important what are the tyre structure damping properties. Especially tread is very important. Damping is influenced by fillers, which are used in the rubber compound. Natural rubber usually display lower damping rates than a synthetic rubber, see [14].

Effect of tread wear

Tread wear decreases mass of the tyre tread, where the most of the losses due to the material hysteresis occurs. Tread material reduction results in less heat dissipation, hence rolling resistance decreases as well ([30]). Also the natural frequency of the tyre tread tends to be lower with reduction of tread mass. Lower frequency means lower critical velocity v_{crit} ([14]). Such tendency cannot be proved by the surrogate model, because the surrogate model is not directly dependent on the profile height, which is required for evaluation of tread wear influence to the rolling resistance coefficient.

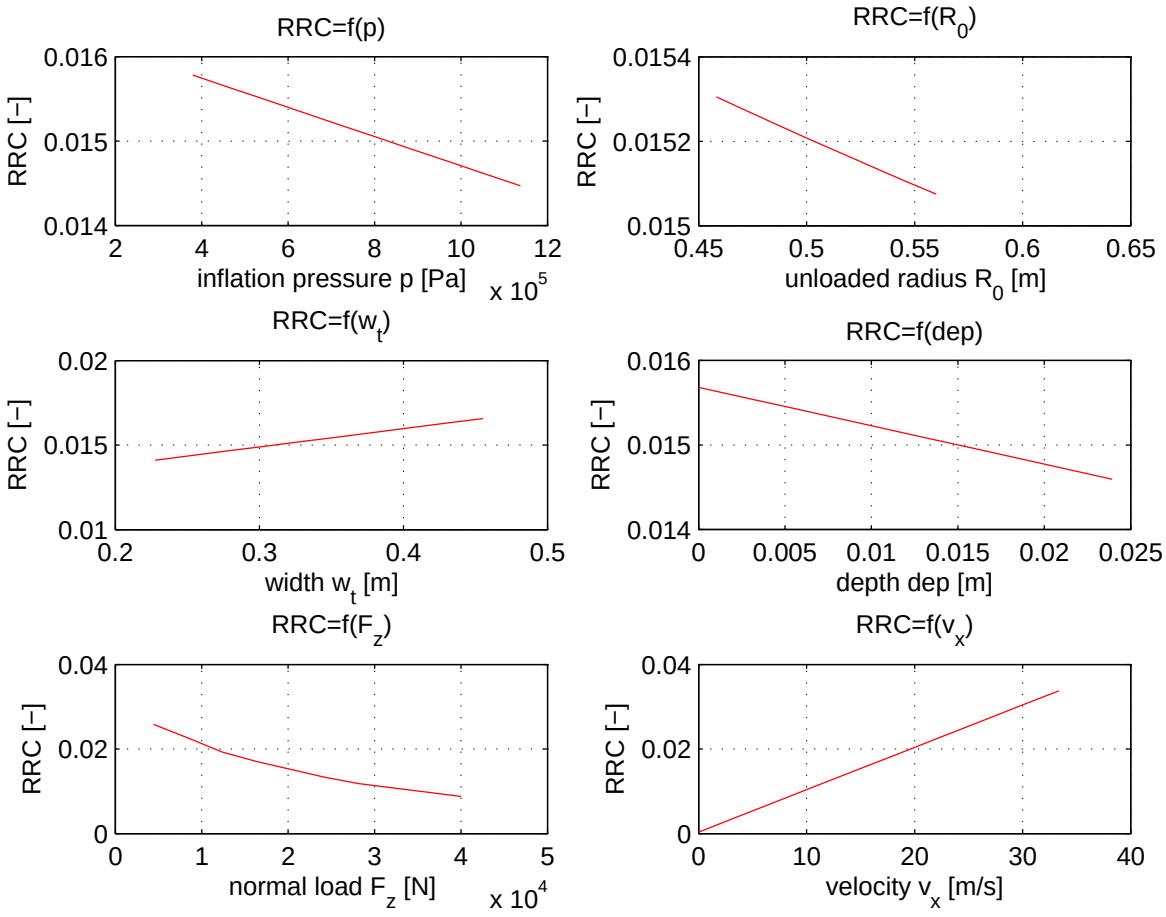

Figure 4.2: *Rolling resistance f trends from the surrogate model, when varying single design parameters around the design point: inflation pressure $p = 7.16e05$, tyre width $w_t = 0.329$, tyre diameter $d_0 = 1.006$, and groove depth $dep = 0.012$.*

Temperature

Friction between the tyre and the road decreases with increasing temperature which leads to reduction of the local sliding contribution in rolling resistance. Also internal damping of the tyre material decreases which results in lower rolling resistance due to lower heat dissipation. Higher temperature of the tyre structure increases inflation pressure, because the convective terms within tyre increases the air pressure in order to stabilize the tyre structure (less deformation around the circumference of the tyre tread) ([14]).

Inflation pressure and vertical load

With increasing inflation pressure p and vertical load F_z, the rolling resistance coefficient f decreases and the critical speed v_x increases, because of less tyre-tread deformation and heat dissipation ([14]).

Increasing tyre inflation pressure p leads to a decrease of the rolling resistance, until tyre design limitations ([14]). Similar qualitative tendency of the rolling resistance has been achieved with the UOIT FE tyre model, discussed in [2]. Surrogate model for rolling resistance coefficient f dependencies on the inflation pressure p and vertical load F_z are visualized in Figure 4.2.

Tyre dimensions

A design parameter that has a large influence on rolling resistance is aspect ratio H/w_t, where H represents tyre profile height and w_t its width. Decrease of the aspect ratio H/w_t results in decreased rolling resistance coefficient f

due to the lower material deformation around tyre circumference. Also the critical velocity v_{crit} is increased ([14]).

With increasing unloaded radius R_0, the rolling resistance coefficient f tends to decrease, see [30]. It can be also directly seen from the Eq. 4.17. Increasing qualitative tendency of the rolling resistance has been achieved with the UOIT FE tyre model, discussed in [2]. Surrogate model for rolling resistance coefficient f dependencies on the unloaded radius R_0, tyre width w_t, and tread depth *dep* are visualized in Figure 4.2. Increasing qualitative tendency of the rolling resistance coefficient with increasing tread depth were achieved with the UOIT FE tyre model, see [2], whereas results from the surrogate model displays decreasing rolling resistance coefficient with increasing tread depth, visualized in Figure 4.2. TyreOpt researchers claims that dependency of the rolling resistance coefficient on tread depth from surrogate model can vary with choice of different design points. Sample points from the FE truck tyre were conducted on the rim with constant radius ([2]). Therefore we cannot distinguish what is the influence of the aspect ratio and tyre diameter, because aspect ratio increases with increasing unloaded radius of a tyre. Constant aspect ratio simulations of the FE truck tyre are required in order to investigate rolling resistance coefficient dependency on the aspect ratio.

Longitudinal forces

The increase of rolling resistance with longitudinal forces is rather small. However, when strong tractive/braking forces are applied, change of rolling resistance should be considered. Sliding means that even more energy is lost. It is interesting that small driving force can sometimes actually lower the rolling resistance coefficient. This is favorable when considering vehicles with more driven axles ([30]).

Side-slip angle

Side-slip angle causes strong increase of the resistance force on the vehicle, because lateral forces are acting in the wheel plane. Because of the toe angle, lateral force F_y is projected in the direction of the velocity vector of the vehicle F_{RR}. Hence, we can express the rolling resistance as

$$F_{RR} = F_x cos\alpha + F_y sin\alpha, \tag{4.19}$$

when considering only the linear relation of the cornering stiffness and making the small angle approximation, according to [14] can be relation simplified to

$$|F_{RR}| = |F_x| + c_{F\alpha}\alpha^2. \tag{4.20}$$

Compliance effects

Aligning torque M_z caused by the camber angle acts in accordance with the rolling resistance force F_{RR}. Hence this moment is added to other resistances

$$F_{RR} = \frac{F_z \Delta x cos\gamma + M_z sin\gamma + M_f}{R_l}. \tag{4.21}$$

The total contribution of the aligning moment is very small since camber is usually small, and therefore also the aligning moment ([14]).

5 Modelling

This chapter aims to provide overview of the modeling techniques, principles and its implementation to the model B. Modelling of the simple linear tyre is documented and its range of applicability is discussed in Section 5.1. Surrogate model for rolling resistance coefficient is implemented to both, the simple linear tyre and MF tyre model. Resistances influencing truck and their implementation to the model B are described in Section 5.2. The simple representation of the driver and power-train of the model B and its implementation are described in Section 5.3. Different joint models of the vehicle are briefly introduced in Section 5.4, where is also described the computationally efficient model A, which is verified in Chapter 6. Constraining event modelling is briefly outlined in Section 5.6.

5.1 Implementation of the tyre model

The requirements of model A verification resulted in development of two different tyre models, see Figure 5.1. The surrogate model, described in Section 5.1, was implemented to the original representation of the VTM tyre model, see Section 5.4. Such tyre model is able to provide rolling resistance moment, which is influencing dynamic behavior of the vehicle.

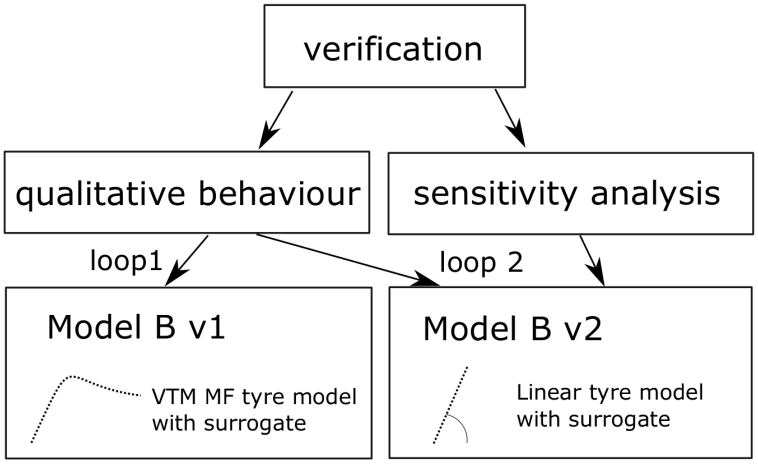

Figure 5.1: *Tyre representation in model B*

Limited set of tyres available in VTM can be used for the first loop of verification, see Section 6.2. This requires to propagate relevant tyre parameters to model A. All required parameters for representation of the tyre in model A can be supplied, except of the wear related coefficients and the tyre depth *dep*, which was not provided in the tyre definition files, used in VTM. Tyre depth is therefore set to the center point of the interval of surrogate model, $dep = 0.012$, for all simulations, see Table 2.1.

Second loop of the verification, see Section 6.2, requires continuous change of the tyre design parameters, corresponding to the operational range of surrogate model, see Table 2.1. Therefore VTM's semi-empirical tyre model cannot be used, because of lack of testing data. Analysis of the Volvo GTT tyre resources, proved availability of approximation relations for linear tyre characteristics, described in Section 5.1. Such data are sufficient for supplying of the linear tyre model, combined with the RRC surrogate model with relevant tyre characteristics. Approximations are using deflection of the tyre δ, see Eq. 4.4, which requires approximation of loaded radius R_l for tyre design variables. Regression model of loaded radius is introduced later in this section.

Approximations for linear tyre characteristics

Approximations of linear tyre characteristics, see Eq. 5.1 to 5.5, described in [6], were suggested by the experts from Volvo GTT, because they provide satisfactory results for the tyres with higher profile numbers $H/w_t > 0.5$. Coefficients ξ of the approximations were tuned for truck tyres by Volvo GTT, see Table D.5. Lateral slip stiffness $c_{F\alpha}$ is defined as

$$c_{F\alpha} = \xi_1 w_t^2 \left(p + 0.44 p_r\right) \left[1.2 \frac{\delta}{2R_0} - 8.8 \left(\frac{\delta}{2R_0}\right)^2\right], \tag{5.1}$$

where ξ_1 is the coefficient provided by Calspan and Bridgestone measurements, cf. D, p is tyre pressure, p_r is rated tyre pressure, δ is compression of the tyre, defined in Eq. 4.4 and R_0 unloaded tyre radius. Lateral stiffness of the tyre c_y is defined as

$$c_y = \xi_2 w_t \left(p + 0.24 p_r\right) \left[1 - 0.7 \frac{\delta}{w_t}\right], \tag{5.2}$$

where ξ_2 is an empirical constant, cf. D, which depends on the tyre width. Longitudinal stiffness c_x is defined as

$$c_x = c_y \xi_3, \tag{5.3}$$

where ξ_2 is an empirical constant, cf. D, which differs for the driven and steered axle types. Longitudinal slip stiffness $c_{F\kappa}$ is defined as

$$c_{F\kappa} = c_x \xi_4 a, \tag{5.4}$$

where ξ_4 is an empirical coefficient, cf. D, a is the contact patch length approximated as

$$a = \xi_5 R_0 \sqrt{\frac{\delta}{2R_0} - \left(\frac{\delta}{2R_0}\right)^2}, \tag{5.5}$$

where ξ_5 is an empirical coefficient, cf. D, and varies for the different tyre widths. Relaxation lengths for longitudinal slip σ_κ and slip angle σ_α, described in [29], are approximated as

$$\sigma_\kappa = \frac{c_{F\kappa}}{c_x}, \; and \tag{5.6}$$

$$\sigma_\alpha = \frac{c_{F\alpha}}{c_y}. \tag{5.7}$$

No particular approximation for vertical stiffness was available. However, the deflection of the tyre at nominal tyre load F_{z0} corresponds to a difference between the unloaded tyre radius R_0 and the loaded radius R_l. Therefore the resulting vertical stiffness can be written as

$$c_z = \frac{F_{z0}}{R_0 - R_l}. \tag{5.8}$$

Loaded tyre radius R_l for different tyre loads is calculated by using the vertical tyre stiffness (flexibility)

$$R_l = R_0 - \frac{F_z}{c_z}. \tag{5.9}$$

Moment of inertia I_{yy} approximation is

$$I_{yy} = m_t \left(\xi_6 R_0\right)^2, \tag{5.10}$$

where m_t is weight of the tyre and ξ_6 is an empirical constant, cf. D.

Regression of loaded radius

The regression model of the loaded tyre radius R_l has been done in order to get the tyre deflection δ and the vertical stiffness c_z for any tyre design variables within operating boundaries, defined in Table 2.1.

Since the tyre database which was chosen as a source of data for regression model does not contain tread depth *dep*, data, it was not possible to satisfy dependency of the loaded radius regression model on all tyre design variables, defined in Section 2.2. Therefore the resulting tyre model does not capture influence of tread depth on linear tyre characteristics.

First, for the sake of simplification of the multivariate regression of the loaded tyre radius, rated pressure p_r was set as constant. This helps to decrease a dimension of the regression to $\mathbb{R}^3$. However certain tradeoff in form of restriction of available sample points to tyres measured at $p_r = 900kPa$ was made, because of most points with the same constant pressure p_r. Therefore only 9 sample points satisfying such condition were used for regression.

For approximation of these points were used different regression functions accessible in MATLAB's curve fitting toolbox, see [23], [24]. This method is using least square method, described in [26], in order to select such coefficients of regression, which provide minimum of the least square sum.

First, scaling of the vertical load F_{z_i}, unloaded radius R_{0_i} and loaded radius R_{l_i} by scaling coefficients was made in order to provide consistent orders or variables for numeric solver. Scaled tyre quantities are described as

$$F_{zsc} = \frac{F_z}{maximum(F_z)},\ R_{0sc} = \frac{R_0}{maximum(R_0),}\ and\ R_{lsc} = \frac{R_l}{maximum(R_l)}. \tag{5.11}$$

Regression of loaded radius R_l for scaled normal load F_{zsc} and unloaded tyre radius R_0 was made. Different orders of approximation surfaces represented by the coefficients $q1$ and $q2$ were used

$$R_{lsc} = p(F_{zsc}, R_{0sc}) = \sum_{t=0}^{q1}\sum_{u=0}^{q2} a_{ut} F_{zsc}^{u} R_{0sc}^{t}. \tag{5.12}$$

Even though orders higher than 2 of approximations $q1$ and $q2$ results in lower residuals, such functions are not convenient for the extrapolation of the approximated region, because they are growing away from the sample points even in proximity of tested interval boundaries. Resulting functional value of loaded radius R_l is

$$R_l = R_{lsc} maximum(R_l). \tag{5.13}$$

Cross validation, described in [31], helps to evaluate regression quality. One sample point is left out from the regression base and regression is created. Functional value of R_l in subtracted point is compared with original value R_l of this point, related to the tyre database. This values provide an information how the function behaves outside of sample points. First order approximation has been chosen.

Tyres from standard tyre database were used in order to find whether the approximation of loaded tyre radius R_l by 9 sample points correlates with the rest of the tyre database. We can directly compare values of R_l from approximation f_{R_l} with measured values from Standard tyre database by evaluating of the residuals

$$\Delta R_l = R_l - f_{R_l}\left(F_z, R_0\right), \tag{5.14}$$

visualized in Figure 5.2.

Linear tyre model

Second loop of the operation cycle verification, see Section 6.2, requires change of tyre design variables. Custom tyre could be modeled with use of linear tyre model further explained in this chapter. Necessary linear tyre characteristics are supplied by approximations and regression model of the loaded radius. Operational range of the linear tyre model is discussed at the end of this section.

Tyre-road contact is simulated with help of the single-contact point transient model, described in [29]. This model concentrates force generated by the contact patch to single point. This point is connected to the rim by the longitudinal and lateral springs. Hence displacement of the spring in longitudinal u_s and lateral v_s direction, introduced in [29], could be translated to the resulting slips κ', α', by following differential equations

$$\frac{du_s}{dt} + \frac{1}{\sigma_x}\left|v_x\right| u_s = \left|v_x\right| \kappa = -v_{sx}, \tag{5.15}$$

$$\frac{dv_s}{dt} + \frac{1}{\sigma_\alpha}\left|v_x\right| v_s = \left|v_x\right| \alpha = -v_{sy}, \tag{5.16}$$

where slip velocity v_{sx} is defined as

$$v_{sx} = v_x - \Omega_y R_e, \tag{5.17}$$

for representation of the effective rolling radius were utilized empirical relation, see Eq. 4.3. Tyre forces are generated with help of linear slip stiffness. For the pure longitudinal slip force holds

$$F_{x0} = c_{F_\kappa}\kappa' = c_{F_\kappa}\frac{u}{\sigma_\kappa},\ and \tag{5.18}$$

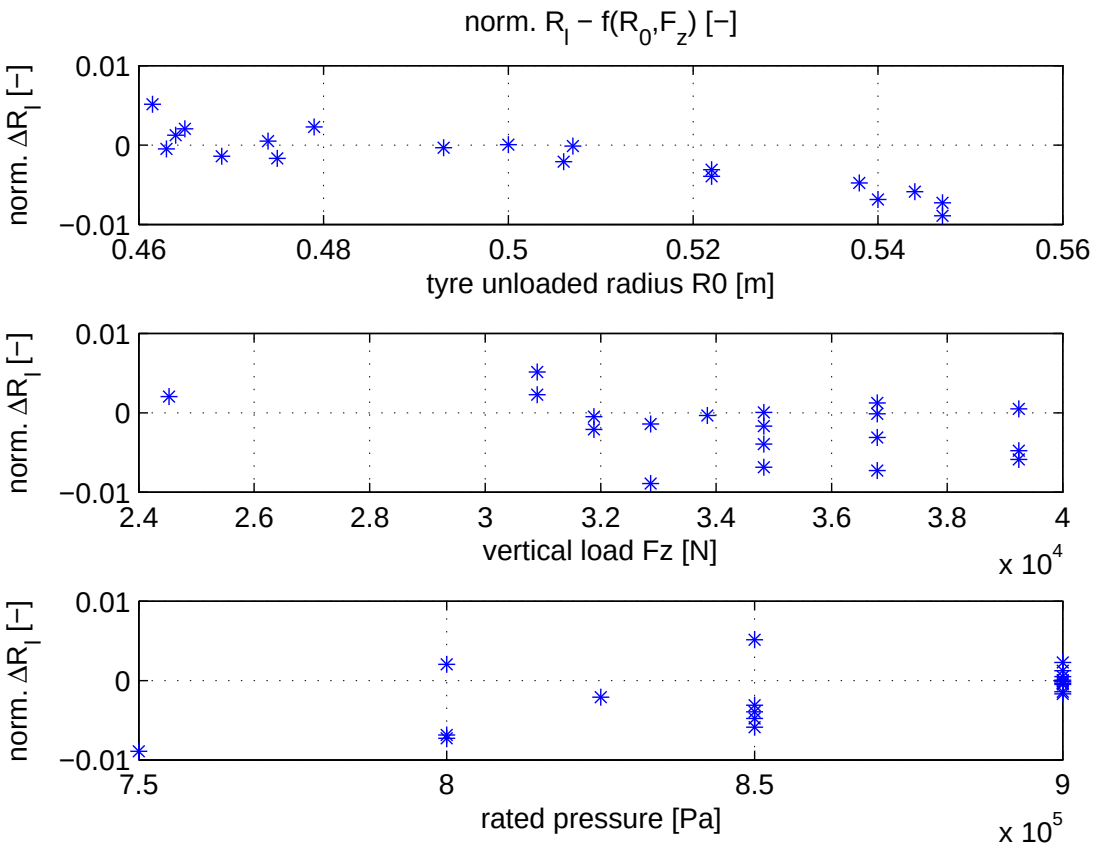

Figure 5.2: *Normalized residuals ΔR_l of the loaded radius R_l regression*

for the pure lateral force holds

$$F_{y0} = c_{F_\alpha}\alpha' = c_{F_\alpha}\frac{v_s}{\sigma_\alpha}. \tag{5.19}$$

The elliptic approximation for combined tyre characteristics, defined in Eq. 4.15, ensures that combined forces are approximating a real tyre behavior, when the tyre is loaded in the lateral and longitudinal direction. The Euler equation of motion of the wheel rotation provides angular acceleration $\dot{\Omega}_y$ of the wheel around wheel rotation axis

$$I_{yy}\dot{\Omega}_y = -M_{yRR} - F_x R_l + M_y, \tag{5.20}$$

which is integrated in order to obtain angular wheel velocity Ω_y. Slip velocity v_{sx} is calculated by Eq. 5.17, where velocity v_x comes from the vehicle model. Slip velocity v_{sx} is used in order to calculate deflection of the spring u_s in Eq. 5.15, which serves for calculating transient slip κ', and tractive force F_{x0}, see Eq. 5.18. This approach enables future implementation of a more detailed definition of the vehicle power-train. Longitudinal version of the linear tyre created in the Simulink is visualized in the Figure 5.3. Combined tyre model can be implemented by using relations, which were introduced in this section.

Alternatively, the wheel rotational inertia effect in Eq. 5.20 can be neglected, as were neglected rotating masses inertia of the power-train, see Section 5.2. This solution would simplify the tyre model significantly. Angular wheel velocity Ω_y can be obtained directly from the inverse slip model, see Eq. 5.23, 5.28, and 5.27, because the tractive force F_x is known from Eq. 5.20 with neglected wheel inertia term.

Linear tyre model provide only rough approximation of the real tyre behavior. Therefore it is crucial to be aware of the range of applicability of the linear tyre model and its limitations. Empirical MF tyre model, described in Section 4, follows the real tyre behavior even for the higher values of slip angle α and longitudinal slip κ, see Figures D.1 and D.2, where could be seen behavior of linear and tyre model on selected tyre, described in Table D.1. From figures D.1 and D.2 can be seen large difference of stiffness between linearized MF tyre model and stiffness obtained by approximations. However validation of such results are out of scope of this thesis.

Investigation of the error between the linear and non-linear tyre model, on tyres described in Tables D.1, D.2, D.3, and D.4, helps us to decide what are the maximal allowable slips α_{max} and κ_{max}, which can not be crossed

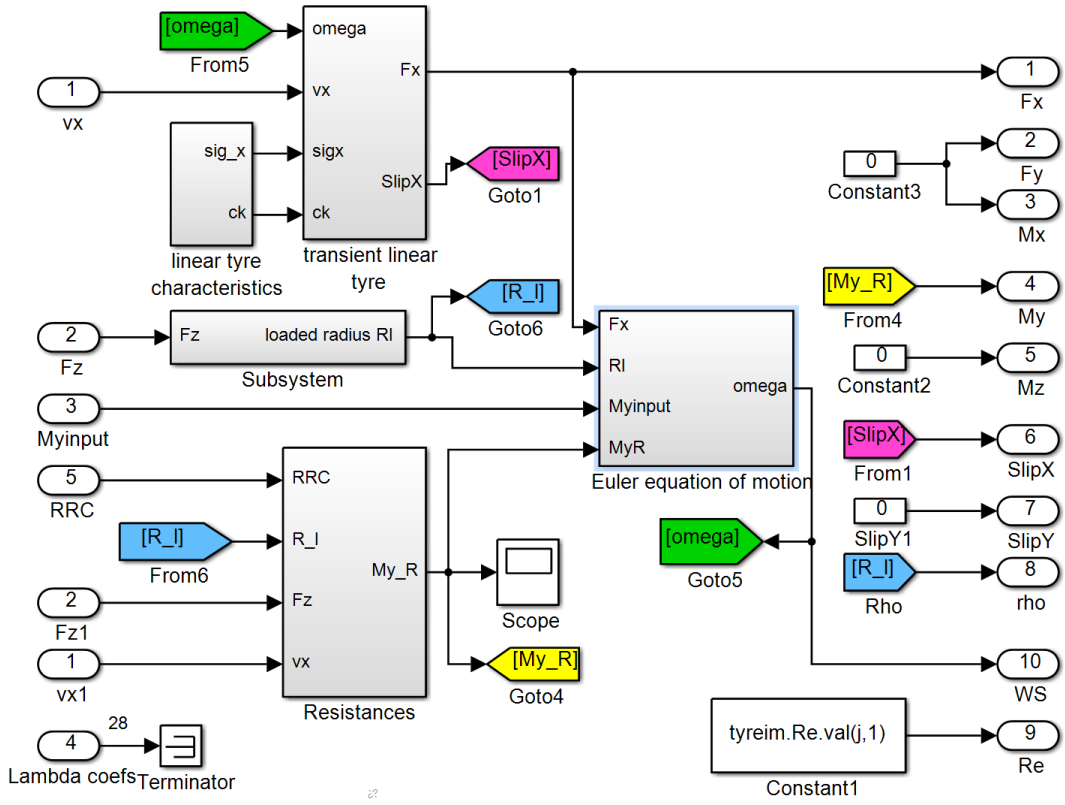

Figure 5.3: *Longitudinal version of the linear tyre subsystem, i.e. block "Linear tyre model" in Figure 5.5, block "linear tyre characteristics" is visualized in Figure B.1, block "transient linear tyre" is visualized in Figure B.2, block "subsystem" is visualized in Figure B.4, block resistances is visualized in Figure 5.6, block "Euler equation of motion" is visualized in Figure B.5.*

in the simulations using the linear tyre model. Simulations of various drive cycles proved that longitudinal slip exceeds longitudinal slip $\kappa > 0.1$ only in special cases. Linearization error in case of the longitudinal slip $\kappa = 0.1$ seems reasonable, see Figure 5.4. Therefore maximal longitudinal slip used in the simulation is $\kappa_{max} = 0.1$. For instance acceleration of the vehicle in the uphill or downhill sections has to be controlled with the traction control, described in Section 5.3, in order to keep longitudinal slip κ bellow $\kappa < \kappa_{max}$. Available torque capacity of the power-train can not be fully utilized in special cases. Linearization of the lateral tyre characteristics seems to be more sensitive on the linearization error, see Figure D.3. In order to be consistent with the previous selection, the maximal error of the linearization of lateral tyre behavior should be kept the same.

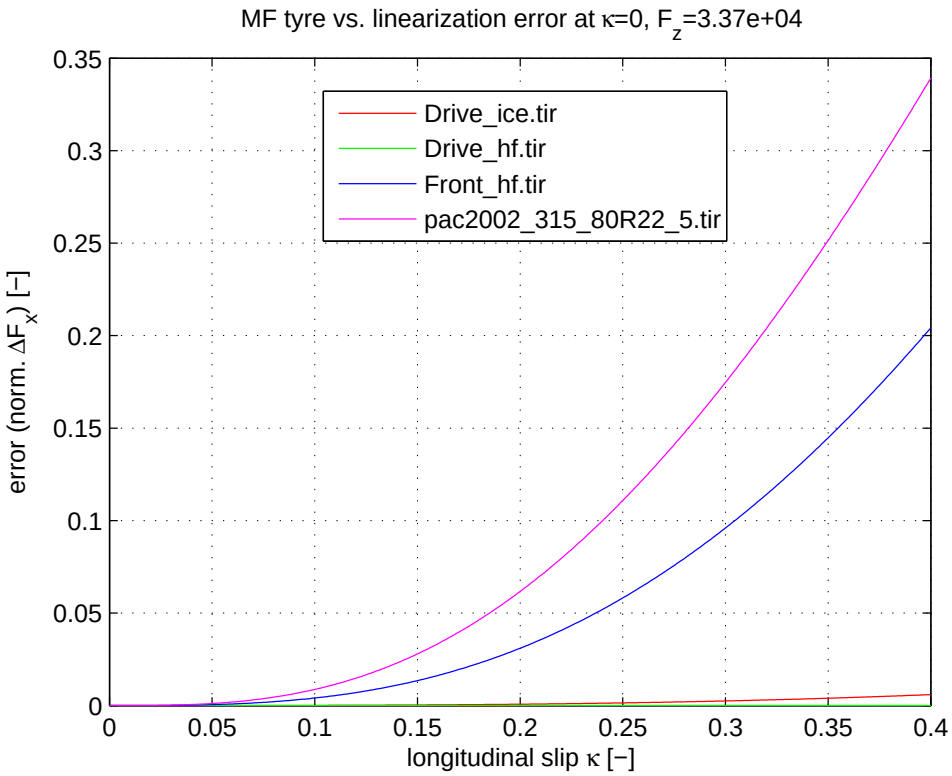

Figure 5.4: *Linearization error of normalized longitudinal force F_x on various tyres*

Surrogate model of the rolling resistance coefficient

The surrogate model is an interpolation of the FEM based sample points and it is expressed as a function for describing the rolling resistance coefficient of the truck tyre. Radial basis function interpolation of the sample points is relatively fast analytical function. For generation of the surrogate model were developed MATLAB scripts, described in [35]. Input to this function is a set of sample points computed by detailed FE tyre model at UOIT, described in [2], [9], [3]. Function is generated when all the sample points have been simulated. Interpolation parameters needed for the surrogate model are initialized at the beginning of the simulation of model B. Surrogate model was transformed and wrapped into a MATLAB function, which is integrated to the VTM tyre model, described in Section 5.4.

Tyre design variables $\mathbf{x}$ (p, w_t, dep, d_0) are loaded from the initialization file at the beginning of the simulation, together with other parameters needed for the construction of the surrogate model. Verifications run with the fixed tyre design variables $\mathbf{x}$. Normal tyre load is received from the multibody model structure. Elastic and viscous properties of the tyre in vertical direction are taken into account in equation of motion in normal direction from the road and normal load is compensated with respect to the road slope, see Section 5.4. Resulting normal load of the tyre in wheel hub F_z (in lbs) and longitudinal velocity of the tyre v_x (in kph) serve as an input to the surrogate.

For implementation of the surrogate to the VTM tyre model, described in Section 5.4, was necessary to modify Magic Formula (MF) tyre S-function, described in [25], by adding a new inputs, supplying rolling resistance coefficient f from the surrogate model and air drag resistance force R_w, described in 5.2. Equations 5.50, respectively 5.51 were replaced with

$$M_{yRR} = fF_z(R_0 - \delta), \tag{5.21}$$

where δ represents radial deflection of the tyre. Hence, $(R_0 - \delta) \approx R_l$ is loaded radius of the tyre. Representation of the radial deflection of the tyre δ in MF tyre model, as introduced in [29] and [1], is following

$$\delta = R_0 - R_l + q_{V1}R_0\left(\frac{\Omega R_0}{V_0}\right)^2, \tag{5.22}$$

where q_{V1} is empirical tyre radius growth coefficient. Resulting tyre model is a combination of semi-empirical MF tyre model and surrogate model for the rolling resistance, see Figure D.4, where can be seen the connection of the MATLAB function to the MF tyre model.

Unfortunately, the evaluation of the rolling resistance coefficient model in every time step could considerably slow down the simulation performance. Distance of current sample point from all sample points (504) has to be calculated in every time step in all tyres models. This can result in rapid slow down of the simulation, especially when the fine step times are needed. Therefore surrogate MATLAB function's step size were increased to $10ms$ in order to provide sufficient performance of the simulation which is desirable for evaluation of the long cycles.

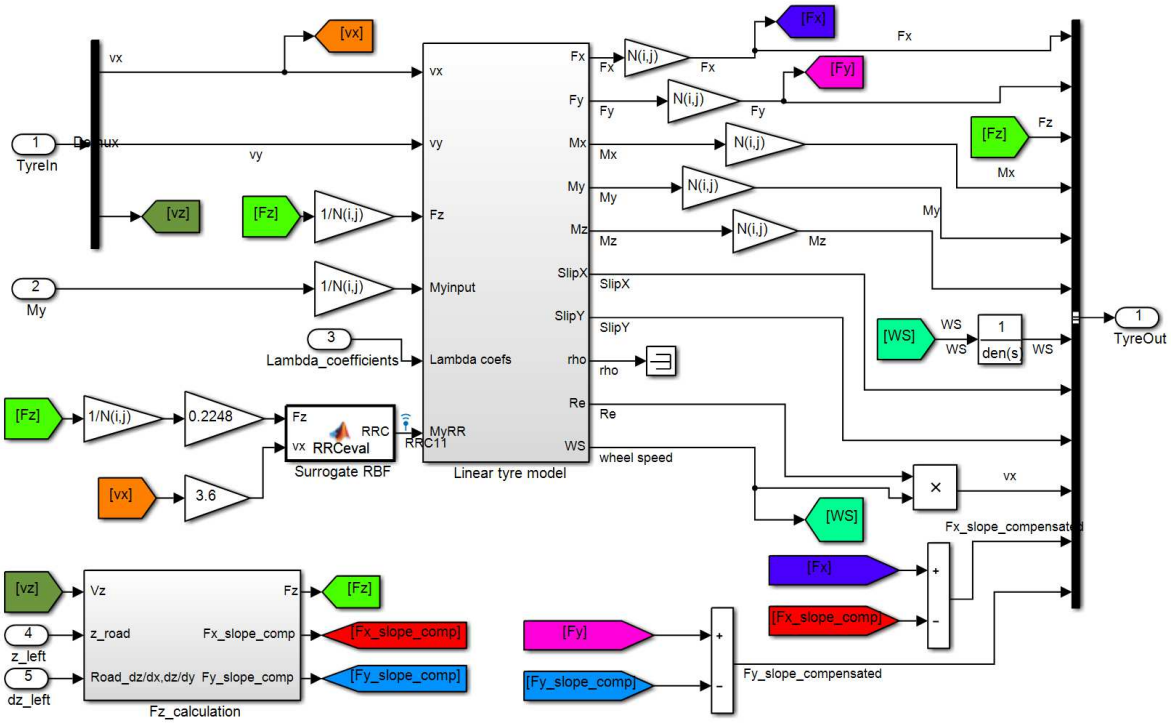

Figure 5.5: *Implementation of the Surrogate model to the tyre model, "linear tyre model" subsystem is visualized in Figure 5.3, normal load calculation block "Fz_calculation" is visualized in Figure 5.21, implementation into VTM defined by signals "TyreIn" and "TyreOut" are same as in Figure D.4.*

5.2 Resistances influencing truck

Rolling resistance has large influence on the truck transport task efficiency. However it is not the only source of resistance. Resistances could be divided into following categories:

- air drag R_w,
- slope resistance R_{sl},
- rolling resistance F_{RR}, further described in Section 4.3, and
- acceleration resistance R_a.

Alternatively could be added resistances from trailer units and auxiliary components of the vehicle. Overall resistance R acting to the vehicle is according to [27] a sum of all listed resistances

$$R = R_w + R_{sl} + F_{RR} + R_a. \tag{5.23}$$

Overall longitudinal dynamics of the truck is described in [22] as the following first order differential equation

$$m_F \frac{dv_x}{dt} = F_{tr} - R. \tag{5.24}$$

Air drag

Air flow around and through the vehicle is a consequence of relative motion between the vehicle and air flow. Air drag is a resistive force, which acts in vehicle longitudinal direction. It consists of air pressure drag caused by turbulence and surface resistance, both in and outside of the vehicle. Air drag is significantly contributing to the overall vehicle losses, especially for commercial vehicles [27]. It can be expressed by simplified expression

$$R_w = \rho c_w S_w \frac{v_w^2}{2}, \tag{5.25}$$

representing dynamic air pressure and product of frontal area S_w and shape related drag coefficient c_w for straight flow, which is experimentally evaluated on scaled models, computational fluid dynamics (CFD) models or on real vehicle in wind tunnels. Air density ρ is a function of air temperature T, humidity and pressure. Velocity v_w is a longitudinal component of the relative vehicle speed with respect to wind velocity. For the sake of a simplification is assumed no wind condition. Therefore

$$v_w = v_x. \tag{5.26}$$

Typical values for rigid truck are $c_w = [0.55; 0.85]$, $S_w = [6; 10]\, m^2$. ([27])

Slope resistance

Resultant of the gravitational force G is a product of the vehicle mass m and gravitational acceleration g. It is acting to the center of gravity of the vehicle. Slope of the road is denoted as α_{sl}. Slope resistance can be expressed as a component of the gravitational force in direction of the road slope

$$R_{sl} = G \sin \alpha_{sl}. \tag{5.27}$$

Acceleration resistance

Acceleration resistance R_a can be approximated as

$$R_a = m_{rot} a, \tag{5.28}$$

where a denotes vehicle acceleration in longitudinal direction and m_{rot} reduced vehicle mass, described as

$$m_{rot} = \frac{\sum I_{red,i}}{r_{dyn}^2}, \tag{5.29}$$

where all the rotating components of the power-train which are accelerated due to the braking by engine and propulsion are reduced to the driven axle. Power-train inertia $I_{red,i}$ of components within the torque flow changes with shifted gear, operation of the clutch, etc. Tyre dynamic radius r_{dyn} is calculated from the distance which is traveled at 60kph of the free rolling wheel, see [27]. Acceleration of the vehicle translational mass m_F is already included in the longitudinal equilibrium Eq. 5.24.

Implementation of the resistances

Slope resistance R_{sl} was already present in the VTM tyre model, see Section 5.4. Acceleration resistance of the rotating masses R_a was not included, because it would require more detailed representation of the power-train, including model of the gearbox. Air drag resistance has been implemented to both tyre models of the model B in order to avoid modification of the VTM vehicle template structure. Therefore, the modularity of the VTM is preserved and changes required when implementing new vehicle combinations are minimized. Air drag resistance R_w has been implemented, according to the Eq. 5.25 on each wheel

$$R_{wij} = \frac{R_w}{n_w}, \tag{5.30}$$

where n_w denotes total number of wheels in the vehicle combination. Resultant of the air drag force R_w is assumed to act at the road level and distribution of the air drag among the wheel is uniform. Implementation of the resistances into the linear tyre is visualized in the Figure 5.6. MF tyre model required implementation of the resistances to the S-function. It has to be noted that this approach is simplifying air drag resistance, because the moment from the air drag resultant around the vehicle center of gravity is neglected.

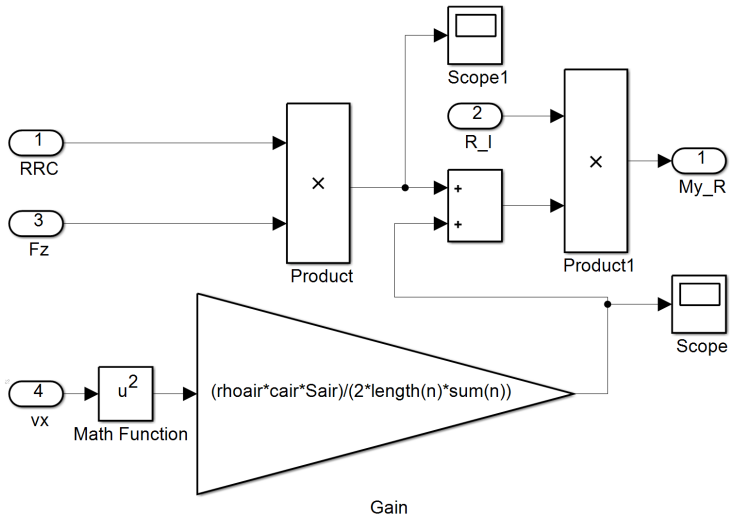

Figure 5.6: *Resistance block in the linear tyre model, i.e. block "Resistances" in 5.3.*

The most important resistance for the verification part of this thesis is the rolling resistance F_{RR}, which is calculated independently on each wheel with known normal force of the wheel F_z

$$F_{RRij} = F_{zij} f_{ij}, \tag{5.31}$$

where f is produced by the surrogate model. Implementation of the surrogate model is described in the Section 5.1.

5.3 Driver and power-train modeling

Multibody vehicle template of the rigid truck provided in VTM lacks any representation of power-train and driver model (control strategy). Therefore both of these model subsystems have to be implemented in order to be able to simulate different operation cycles as in case of Model A, further described in Section 5.4, and [10]. It is important to keep in mind that model A has no driver representation and its model of power train does not influence vehicle dynamics. Such type of model is described in [12], [13] as kinematic approach to vehicle modeling. Such model is based on inverse dynamics, visualized in Figure 5.7, where we can see feed forward transformation of the drive cycle data to resulting fuel consumption. The rotational velocity of the engine is calculated from the velocity

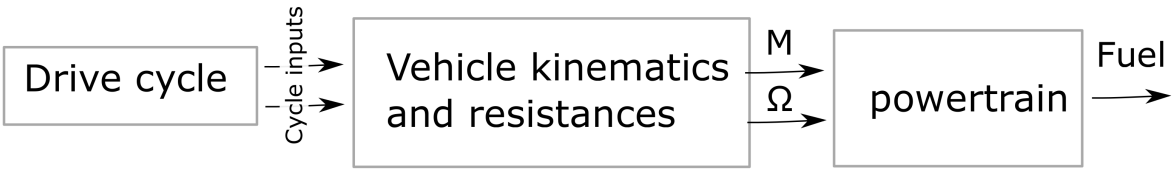

Figure 5.7: *Inverse dynamic approach of vehicle modelling*

profile of the operating cycle. Drive torque required by the engine is a function of the resistances influencing truck, described in Section 5.2. However, this modeling technique does not describe transients, because it lacks connection to vehicle dynamics feedback and any sort of driver model. Nevertheless this kind of model is very effective from the point of view of computational efficiency and can be used as a rough estimation of the vehicle fuel consumption. Quasi-static approach, described in [12], [22], combines prepared cycle inputs with driver model controlling vehicle velocity. Simulated system can be called quasi-static, because main systems are described with steady state maps. This kind of model could be used for evaluation of the vehicle performance (e.g. consumption), including transients. High fidelity representation of transients needs to be modeled in a greater detail with the dynamic approach, described [12], [22], which brings complete dynamic representation of the vehicle power train components.

Model B representation of both power-train and driver could be kept as simple as possible, because verification aims to focus on qualitative comparison of rolling resistance related behavior. Hence adding complexity of the model by detailed power-train and driver models makes even harder to identify tyre contribution to the complete vehicle behavior. Driver-powertrain model can be broken down into the driver part, human-machine interface (HMI), traction control and power-train models, visualized in Figure 5.8.

Verification of the model A with the developed model B will be performed on the road definition used in the model A. Simple driving cycle consists of sample points of the set speed v_{set} with respect to distance along the track x and vertical profile of the track z_{tr} with respect to the distance along the track x.

Velocity driven control of the vehicle was utilized, see [28]. Error of velocities e_{vx} is defined as

$$e_{vx} = v_{set} - v_x, \tag{5.32}$$

where v_{set} is set (input) velocity, defined in velocity profile $v_{set} = f(x)$ and actual velocity v_x, which is feedback from the vehicle plant, see Figure 5.9. Such error could be used as input signal for the controller, representing human behavior. Driver sensoric and controlling task can be replaced by the open loop transfer function, see [13], [8], described as

$$\frac{r(t)}{e_{vx}(t)} = G_d \frac{(T_L s + 1)}{(T_I s + 1)} e^{-\tau s}, \tag{5.33}$$

where output $r(s)$ is the driver's request to the human-machine interface (HMI). Human sensoric delay is represented by the time constant τ. Integral part of the driver transfer function, represented by the integration constant T_I, which ensure maintaining speed without large steady state error e_∞ difference between set v_{set} and actual velocity v_x, described in [28]. Driver's proportional gain G_d was selected as the ratio of actual power demand P_{dr} and maximum power of the engine P_{max}, according to the vehicle performance capabilities

$$G_d = \frac{P_{dr}}{P_{max} e_{vx}}, \tag{5.34}$$

where P_{dr} is a power demand which driver expects from the vehicle. Simplified model of a driver's power demand P_{dr} is depending on the tractive force F_{tr}, described in the Eq. 5.24, and velocity of the vehicle v_x

$$P_{dr} = F_{tr} v_x. \tag{5.35}$$

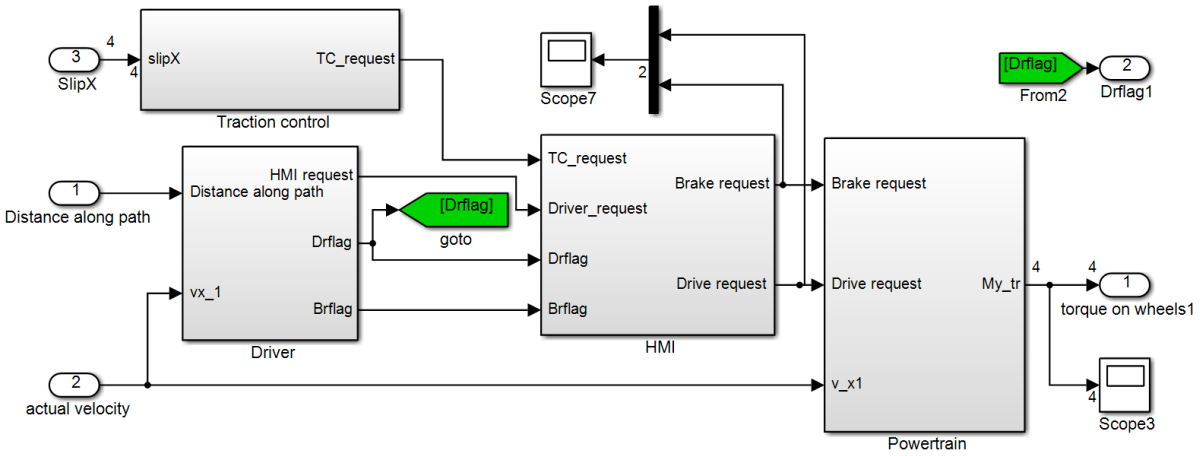

Figure 5.8: *Driver and power-train model, i.e. subsystem "Driver-powertrain model" in Figure 5.23.*

parameter	value
G_d	1
T_L	0
T_I	0.1
τ	0.1

Table 5.1: Parameters of the driver's transfer function

Tractive force F_{tr} requested from the driver is simplified to the function of the desired acceleration a_{dr}, which is required in order to maintain the set velocity v_{set}

$$P_{dr} = ma_{dr}v_x = \frac{me_{vx}v_x}{T_{dr}} = \frac{me_{vx}}{d_{dr}}, \tag{5.36}$$

where preview time T_{dr} express the period for matching the vehicle with set velocity v_{set}. This period could be given into the context with the preview distance of the driver d_{dr}, which simplifies the whole term of power demand P_{dr}. Larger preview distance d_{dr} results in a smaller magnitude of control requests from the driver, which makes the velocity profile smoother and it also reduces vehicle jerk. However, larger preview distance results in longer rise times of vehicle's velocity, when the set velocity v_{set} changes. Parameters of the driver model were tuned in order to keep the velocity of the vehicle v_x within the range of $e_{vx} \leq 1\, m.s^{-1}$ on constant velocity intervals of the road, described in the Figure 6.1. Selected parameters of the driver model are shown in Table 5.1.

Due to the fact that braking and propulsion modes are not equivalent from the point of view of sign and magnitudes the of available torque M_y, we have to distinguish between that modes. Design of brakes allows usually larger torques than engine could provide, see [14]. For positive values of error e_{vx} is assigned propulsion mode and braking is assigned for negative values of the error e.

$$e_{vx} \in (0; \infty) \Rightarrow propulsion, \tag{5.37}$$

$$e_{vx} \in (0; -\infty) \Rightarrow braking. \tag{5.38}$$

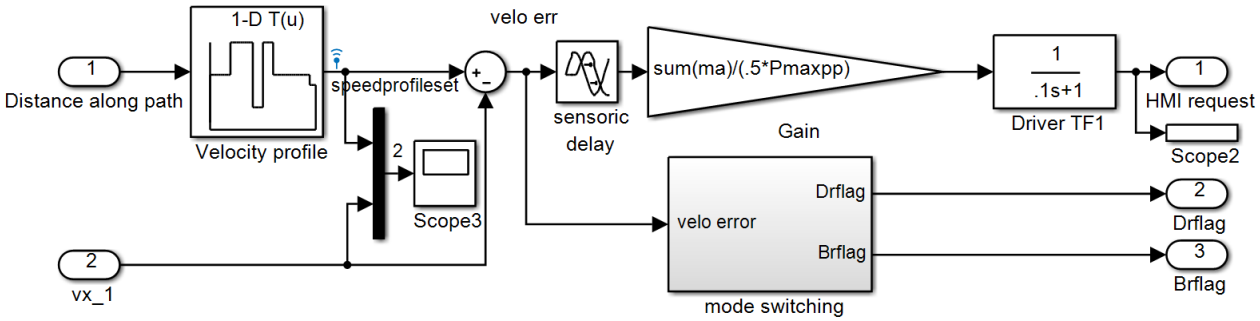

Figure 5.9: *Driver model, , i.e. block "Driver" in Figure 5.8.*

However this solution in combination with low steady state error e_∞ leads to high frequency of mode changing, because of high frequency of zero crossing, caused by the sharp transition between intervals. This could be reduced by introducing additional hysteresis which reduces rapid change of mode.

$$e_{vx} \in (tr; \infty) \Rightarrow propulsion, \tag{5.39}$$

$$e_{vx} \in [-tr; tr] \Rightarrow coasting, \tag{5.40}$$

$$e_{vx} \in (-\infty; tr) \Rightarrow braking, \tag{5.41}$$

where the threshold tr defines range of error e_{vx} between 3 control modes. However, for high values of proportional gain occurs chattering of the torque request M_y during step change of the set velocity v_{set}. This has been solved by implementing delays simulating actuating neuro-muscular lag when changing mode (pressing accelerator/brake pedal). Model of the driver's logic is visualized on the Figure 5.10. Such delay ensures that dynamic of the vehicle plant increase error from switch-point, therefore fast switching is suppressed.

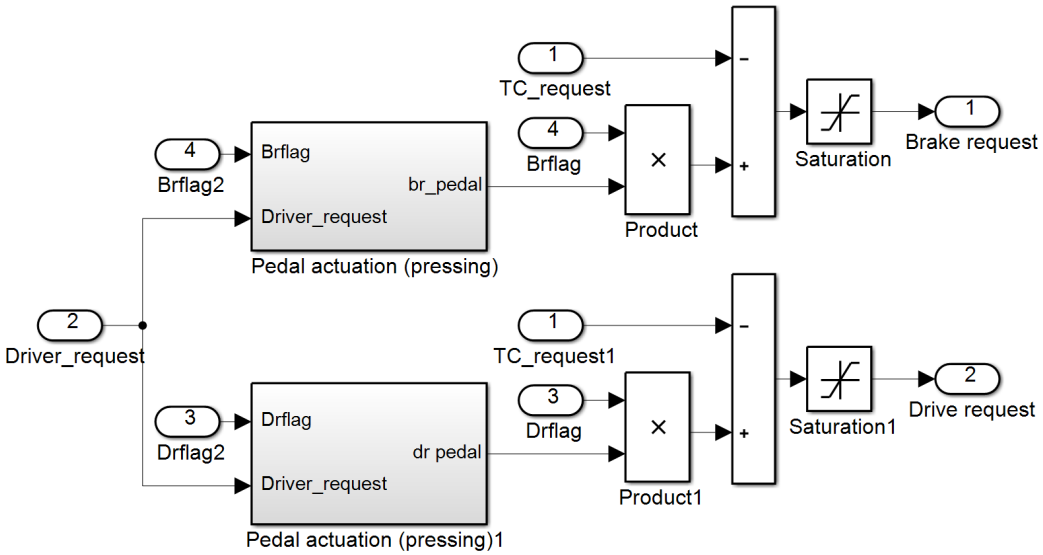

Figure 5.11: *HMI model, i.e. block "HMI" in Figure 5.8.*

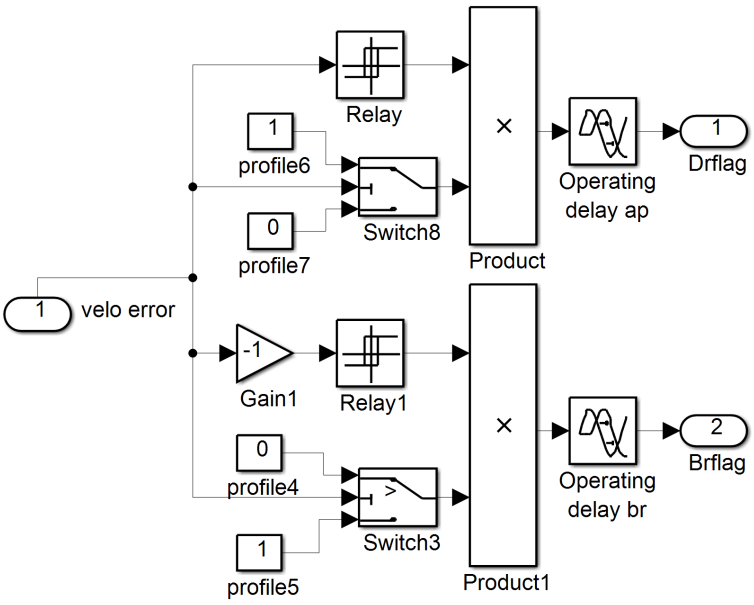

Figure 5.10: *Driver's logic, i.e. block "mode switching" in Figure 5.9.*

HMI model is visualized on the Figure 5.11. It aims to bring realistic behavior of the driver. This solution avoids unrealistic switching between power-train modes, because operating of the brake and accelerator pedal is modelled, see Figure 5.12.

HMI block is connected to the power-train subsystem, where the propulsion or braking is selected, see Figure 5.13. As a substitution of the engine dynamics may serve us a transfer function, see [11], visualized on the Figure 5.14. However this demand has to respect maximum power capacity of the engine P_{max}. This is realized by limiting engine with maximum tractive torque related to vehicle longitudinal velocity v_x. Even though this solution is not matching real control strategy of the truck, because real control strategy is influenced by many complex components of the power-train such engine, clutch, gearbox dynamics, it seems satisfactory for use in verification.

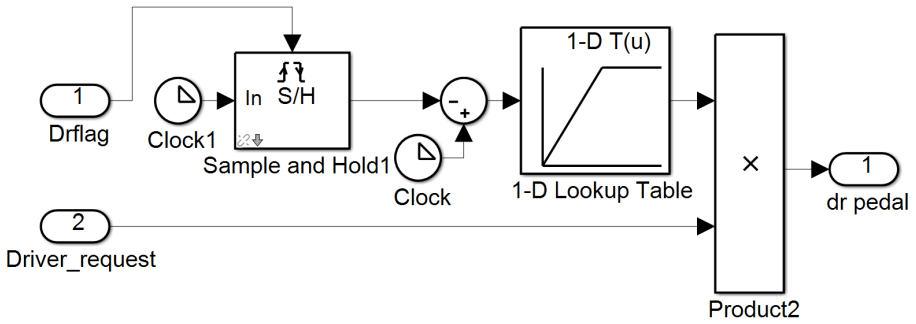

Figure 5.12: *Pedal actuation mode, i.e. blocks "Pedal actuation" in Figure 5.11.*

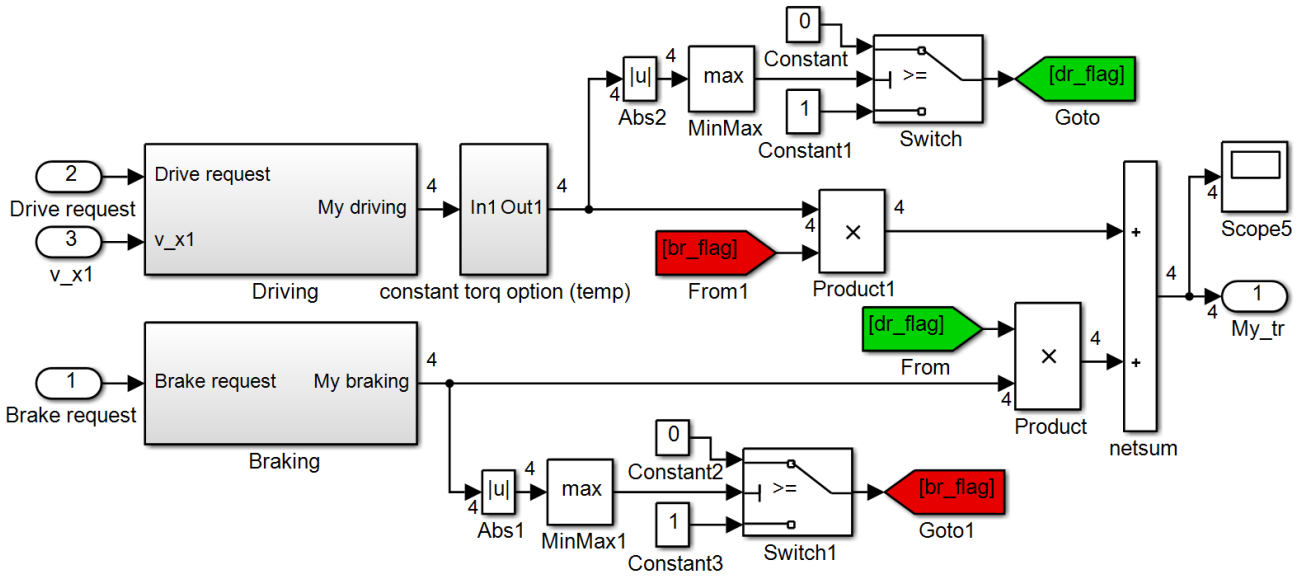

Figure 5.13: *Power-train subsystem, i.e. block "Powertrain" in Figure 5.8.*

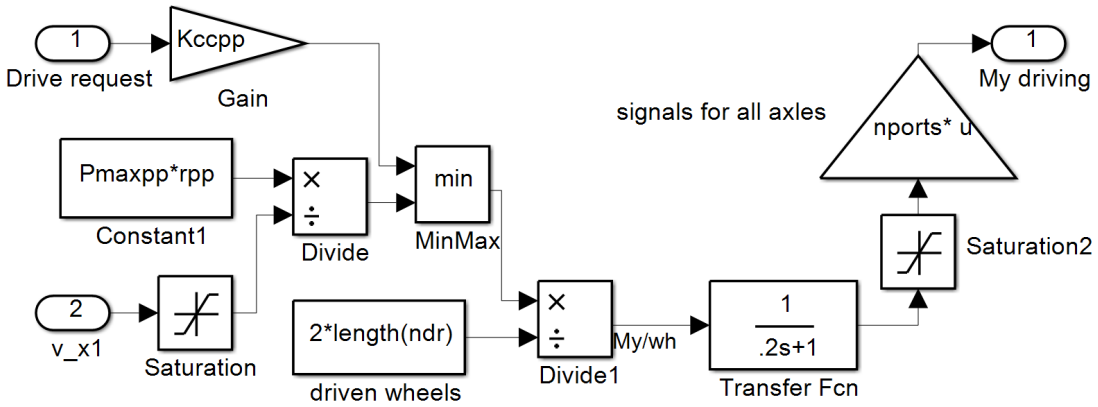

Figure 5.14: *Simple power-train model (propulsion), i.e. block "Driving" in Figure 5.13.*

parameter	value
G_{TC}	10
T_{ITC}	0.1

Table 5.2: Parameters of the traction control transfer function

Therefore power-train acts as an ideal actuator, which does not consider energy needed to accelerate rotating parts in the power-train, energy losses due to gear shifts, and varying combustion efficiency of the engine (engine fuel map and gear selection). Representation of the braking system is rather simple, see Figure 5.15, and does not capture detailed behavior such brake moment fading, and other dynamics of the braking system. Vehicle behavior should follow real use of the tractive limits. However, proposed solution of vehicle control can produce demands of the wheel torques, which results in a saturation of the wheel force. This results in excessive values of the longitudinal slips κ, which does not follow real vehicle behavior. Therefore simple traction control were introduced, see Figure 5.16, in order to reduce demand of tractive force, when the longitudinal slip κ' exceeds limit value κ_{max}, defined in Section 5.1. Traction control is supplied with the maximal wheel slip κ', from the tyre models. Input to the traction control is the longitudinal slip error e_κ

$$e_\kappa = \kappa' - \kappa_{max}. \tag{5.42}$$

Output of the control can be described with the transfer function

$$\frac{r_\kappa(t)}{e_\kappa(t)} = G_{TC}\frac{1}{(T_{ITC}s+1)}, \tag{5.43}$$

where r_κ represents correction of the driver's pedal request, G_{TC} represents proportional gain, and T_{ITC} is integration constant. Selected parameters of the transfer function are described in the Table 5.2.

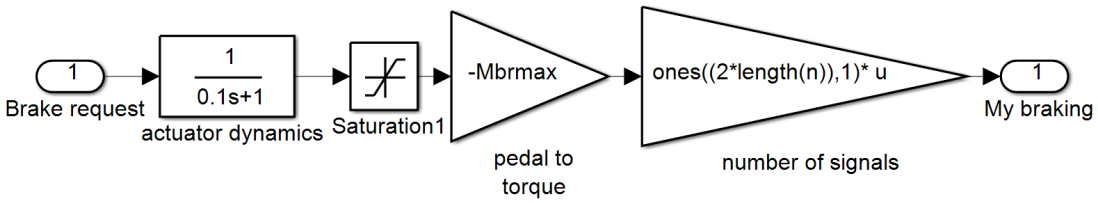

Figure 5.15: *Simple power-train model (braking), i.e. block "Braking" in Figure 5.13.*

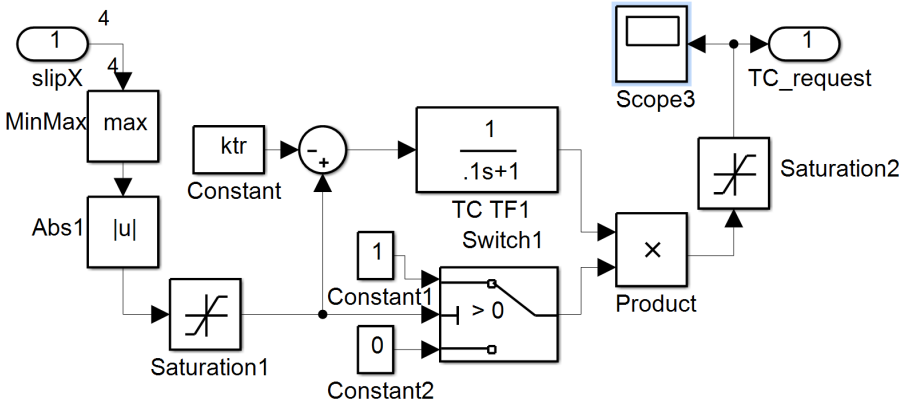

Figure 5.16: *Simple traction control, i.e. block "Traction control" in Figure 5.8.*

5.4 Joint models

Joint models considered in this thesis are set of models, which represent vehicle, environment and tyres. Therefore mutual interaction of the vehicle, tyres and environment can be investigated. This section aims to summarize joint model model A, platforms of Volvo GTT and overview of model B.

Efficient model A

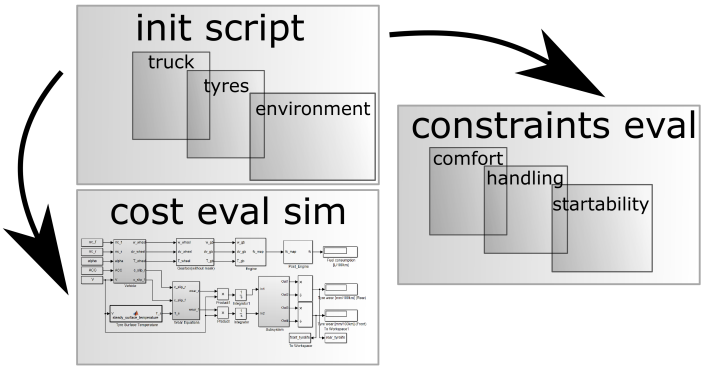

Figure 5.17: *Scheme of the model A structure*

The computationally efficient model of a heavy duty truck which was made for the TyreOpt research project purposes within master thesis project is described in [10]. The model was built in the MATLAB/Simulink environment, where constraints are represented in the form of scripts, and objective function evaluation is implemented by combination of scripts and Simulink simulation.

Definition of all necessary parameters, used in the simulation and constraining events is governed by the initializing script, which can be seen in the Section 5.17. Vehicle parameters are defined wrt. the type of cargo and load distribution. The script responsible for definition of the environment loads sample points representing vertical and velocity profile of the track transforms the inputs to the simulation. The script defining tyres calls the surrogate model described in Section 2.2. The surrogate model builds the RBF interpolation for the rolling resistance coefficient and evaluates it for all desired tyre input variables. This is also transformed to the formatted structure, which serves as an input to the simulation of the drive cycle.

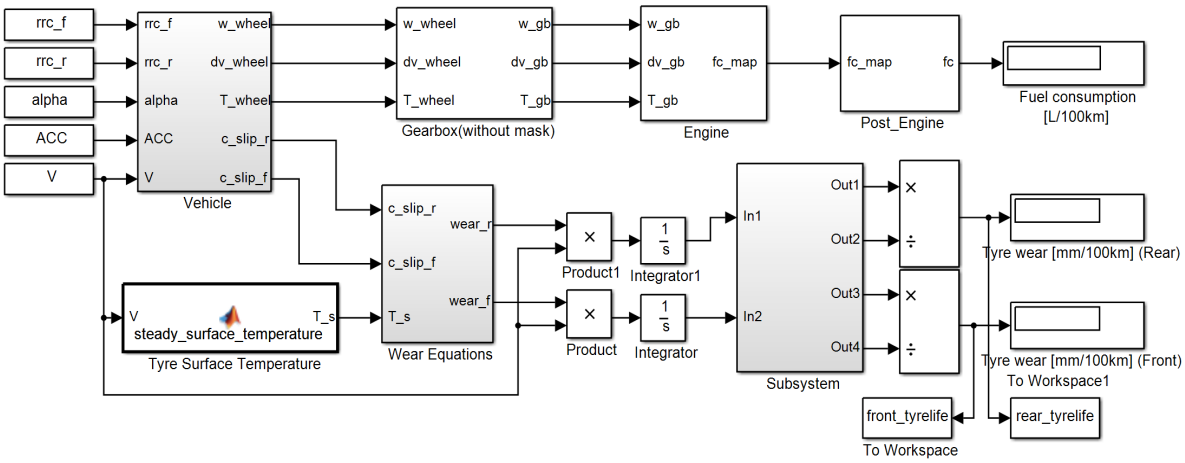

Figure 5.18: *The objective function models used in model A*

Objective function

The inverse dynamics principle is used in the simulation for computation of fuel consumption, see Section 5.3. Vehicle dynamics data such as vehicle velocity, acceleration, rolling resistance and others are calculated a-priori in MATLAB scripts and then serve as input to the simulation, as illustrated in Figure 5.18. The models of the tyre wear and the fuel consumption are simulated over the operating cycle. In order to get vehicle fuel consumption, simple model of the power-train based on the QSS toolbox was utilized [17]. QSS toolbox is a tool for simple implementation of the vehicle power-train to Simulink vehicle models. The tyre wear model is dependent on the wheel slip and environment temperature, described in [16]. One of the indisputable advantages of such a model is computational efficiency, which is highly appreciated, especially when a lot of simulations have to be run for different tyre parameters and different vehicle combinations. However, one of the tradeoffs of such simplification is lack of dependencies between vehicle and power-train. The control strategy of the vehicle depends only on resistive forces. This can lead to unrealistic values of power produced by the power-train and control strategy which does not respect power train limitations. Another simplification is that normal reactions on the wheels are fixed during the simulation, which is a simplification limiting use of the model to level roads, small accelerations and no cornering. Model A does not consider vehicle inertia when it is evaluates resistance forces. Power-train losses are not represented within the relation for resistive forces.

Constraining events

The set of constraining events is evaluated in form of MATLAB scripts and do not depend on the simulation. Start-ability, ride-comfort and handling are evaluated.

The start-ability is one of the most critical longitudinal performances which indicate vehicle ability to start from stand-still and maintain steady forward motion on specified grade α_{slmax}, when operating at maximum laden mass m ([10]). Start-ability definition in the model A is using simplified equilibrium equation in the vehicle longitudinal direction, introduced in [10]. The start-ability constraint is fulfilled when

$$F_x \geq R. \tag{5.44}$$

Model of resistances R considers only resistances from road slope R_{sl} and rolling resistance F_{RR}. Acceleration of rotating masses R_a and air drag R_w were neglected. Simplified model of resistances R is

$$R = \sum_{i=1}^{2} f_i F_{zi} \cos\left(\alpha_{slmax}\right) + mg \sin\left(\alpha_{slmax}\right), \tag{5.45}$$

where α_{slmax} denotes constraint threshold. Rolling resistance coefficients f_i for axles are constant and do not use surrogate model for rolling resistance coefficient evaluation, see [10]. Tractive force F_x is modeled as the minimum of tractive and friction forces.

$$F_x = \min\left[2T_{max} g_{r1} g_f / d_0,\ F_{z2} \mu \cos\left(\alpha_{max}\right)\right]. \tag{5.46}$$

Handling constraining event model in model A, described in [10], depends on the under-steer gradient of the vehicle η, defined as

$$\eta = \frac{c_{F\alpha 2} l_2 - c_{F\alpha 1} l_1}{c_{F\alpha 1} c_{F\alpha 2} \left(l_1 + l_2\right)}, \tag{5.47}$$

where l_1 and l_2 denotes distance from the center of gravity to the front and rear axle, respectively. The start-ability condition is fulfilled when

$$\eta > \eta_{min}, \tag{5.48}$$

where η_{min} is under-steer gradient threshold.

Ride-comfort is important factor expressing passenger feel. Vibration issues mainly arise from the vehicle body which is a subject of the environment perturbations mainly induced from the road profile ([37]). Tyre design properties such tyre mass m_t, vertical damping c_{dz}, and vertical stiffness c_z, significantly influence vertical dynamics of the vehicle combination. Ride-comfort constraint model in model A, described in [10], utilizes simple 4DoF vertical model of the front part of the vehicle, consisting of front axle, frame, cab, and seat masses, mutually connected with the spring and damper combinations. Weighted root mean square (RMS) acceleration of the seat a_{RMS}, with ISO 2631 filter, described in [37], evaluates response of the vehicle in the frequency domain for various road profiles. Several set of roads representing various road conditions are evaluated. Vehicle with selected tyres has to fulfill ride-comfort condition

$$a_{RMS} \leq a_{RMS_{max}}, \tag{5.49}$$

which aims to limit maximal discomfort for the passenger $a_{RMS_{max}}$ to the tyre selection process.

PERF

PERF is a vehicle analysis tool capable to evaluate the truck's power-train performance criteria on simple longitudinal driving cycles. It mainly aims to assess fuel economy, and suitability of particular vehicle specification for a desired environment.
The main focus of calculations in PERF is to:

- optimize vehicle specification by evaluating of the performance,
- compare different drive-lines, and
- simulate different road conditions.

PERF is written in FORTRAN and therefore it is not suitable to edit without knowing that particular programming language. This seriously limits any changes of tyre definition, because the used tyre model is very simple. A constant rolling resistance coefficient does not reflect a change in tyre parameters. Therefore using this tool would require close cooperation with programmers.

The tool is equipped with a graphic user interface, visualized in Figure 5.19, where all truck components and parameters can be easily defined. Choosing truck systems (engine, gearbox, etc.) is done in a set of menus. The desired operating environment (driving cycle) is chosen from a list. After execution of the program, a simple overview of the truck is provided (economy speed range, speed range top gear, max. nominal speed, grade speed, max. grade-ability, grade-ability, start-ability). A comparison based on vehicle performance is possible ([32], [33]).

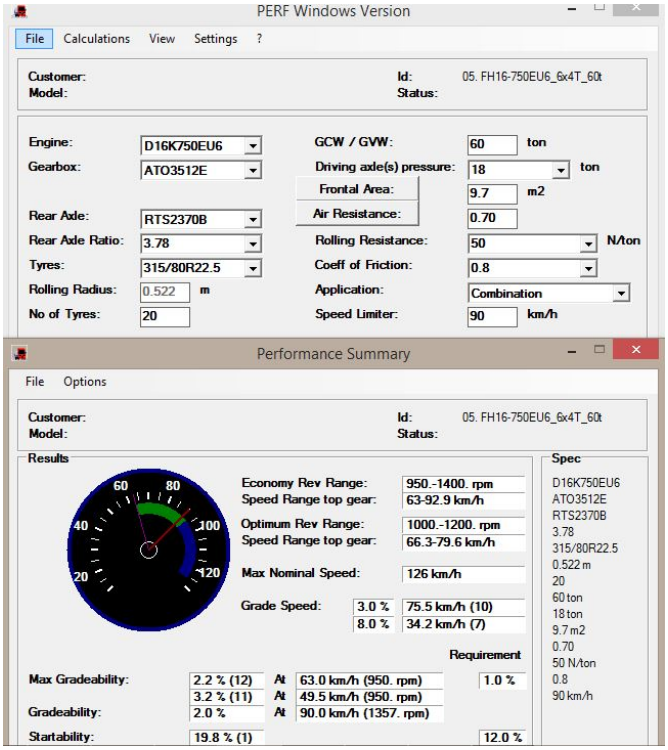

Figure 5.19: *PERF graphical interface*

Volvo Transport Models (VTM)

The basic purpose of this environment is to assess vehicle dynamic behavior. The simulation environment is based on the Simulink toolbox SimScape, SimMechanics, see [25]. Therefore this environment can be edited. The VTM library contains different vehicle templates, controllers and other blocks which can be easily added to the model. This environment is a multibody modeling system, which evaluates the structure of the model. It formulates automatically the equations of motion and all necessary transformation matrices without any special knowledge. The template library contains different vehicle plants such as tractor-trailer combinations and rigid trucks.

The road definition can be very detailed, including 3D track profile, which is interpolation of the sample points in lateral and longitudinal direction. Therefore logged track data can be utilized and simulated. The vehicle is lacking a description of the power-train which is a considerable disadvantage for the purpose of the verification.

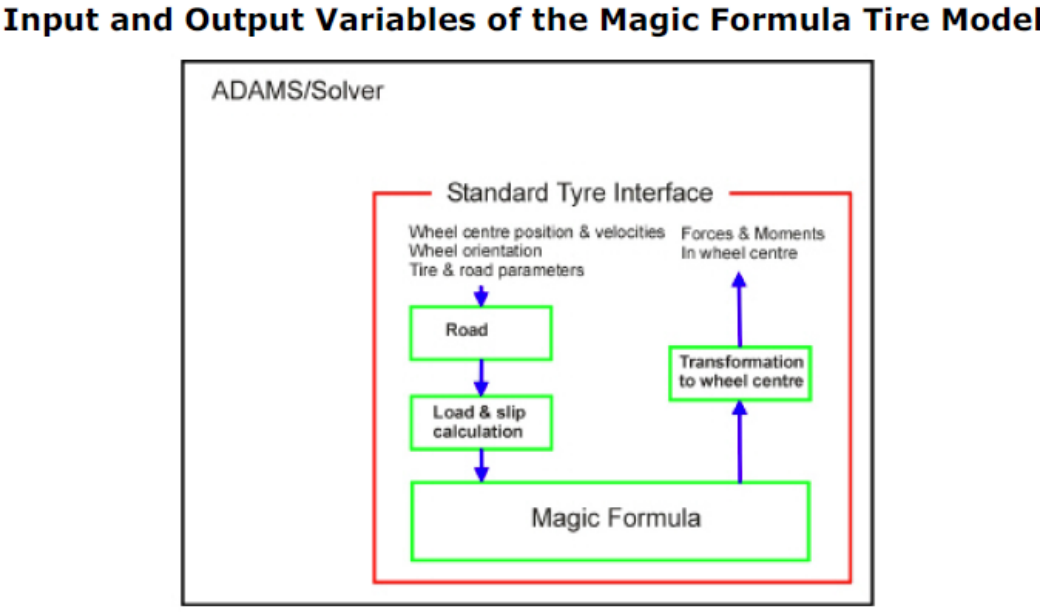

Figure 5.20: *Tyre interface causality scheme, [1]*

coefficient	explanation
q_{Sy1}	rolling resistance moment coefficient
q_{Sy2}	rolling resistance moment depending on F_x
q_{Sy3}	rolling resistance moment depending on velocity v_x
q_{Sy4}	rolling resistance moment depending on velocity^4

Table 5.3: Rolling resistance coefficients explanation

Vehicle templates consist of several building blocks/bodies which interacts with each other according to prescribed constraints. Components influencing vehicle behavior are modelled. Special attention is given to steering system, frame, axle definition, suspension, tyres and truck cab.

Tyre definition

The tyre model utilized in VTM, cf. Figure 5.20, is based on Pacejka's Magic Formula PAC2002, see [1]. The tyre model is written in the C programming language as the Simulink LEVEL 2 S-function, see [25], and compiled to MEX function in order to be implemented within Simulink environment.

Tyre-road interaction is rather simple. Tread is modelled as a rigid disc and every time step the wheel-ground contact point is computed in the tangent plane to the track profile.

Parameters of the tyre are provided by script which reads tyre data from the TYDEX file format, described in [1], and translates them into the variables used within the Simulink environment. A large number of tyre data and testing is necessary in order to get all data required by the tyre models.

VTM's MF tyre model is represented as an S-function Simulink block, see [25]. MF tyre relation used in VTM for rolling resistance moment, developed in [1], [29], is empirical approximation of rolling resistance

$$M_{yRR} = R_0 F_z \left[q_{Sy1} + q_{Sy2} \frac{F_x}{F_z} + q_{Sy3} \left| \frac{v_x}{v_{ref}} \right| + q_{Sy4} \left(\frac{v_x}{v_{ref}} \right)^4 \right], \tag{5.50}$$

where V_{ref} is velocity of the tyre when it was tested. Empirical coefficients used in approximations of rolling resistance are explained in Table 5.3. If the coefficients q_{Sy1} and q_{Sy2} are zero, alternative relation, introduced in [1], [29], is used

$$M_{yRR} = R_0 \left(S_{Vx} + K_x S_{Hx} \right). \tag{5.51}$$

Scaling coefficients are used in order to enable changing various tyre characteristics during the simulation.

Normal load F_{zij} in the wheel hub is generated from the equilibrium equation in the vertical direction

$$F_{zij} = (z_{wij} - z_{rij}) c_{zj} + (\dot{z}_{wij} - \dot{z}_{rij}) c_{dzj} + m_{ij} g, \tag{5.52}$$

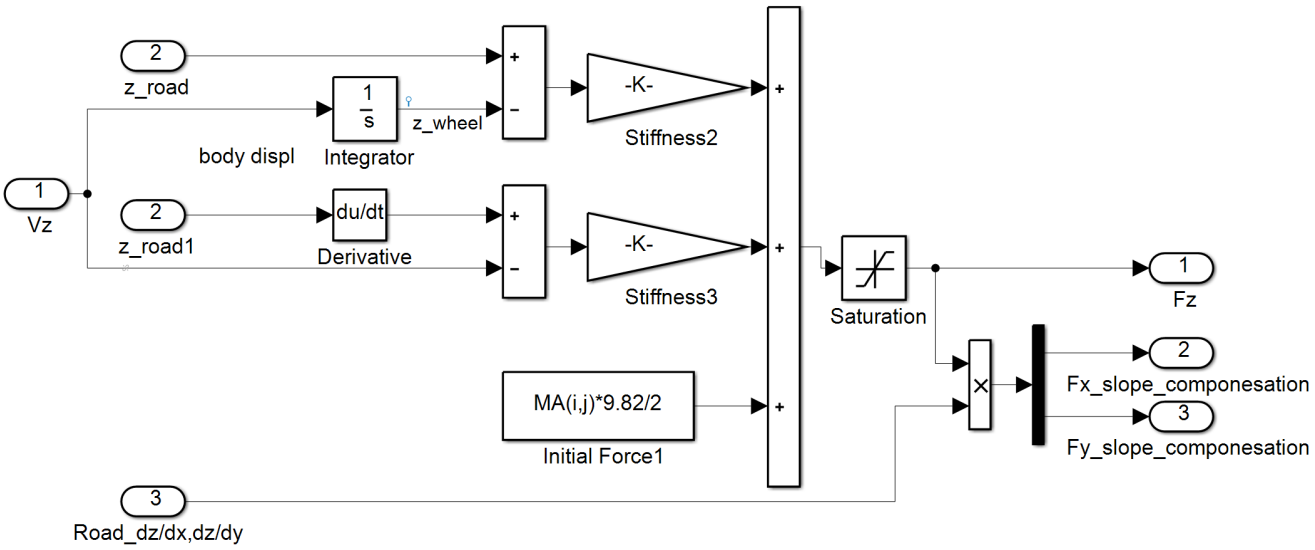

Figure 5.21: *Normal load F_z generation in the VTM, i.e. block "Fz_calculation" in figures D.4, and 5.5.*

where c_z express vertical stiffness of the tyre, and c_{dz} represents damping properties of a tyre in the vertical direction. Vertical distance of the wheel hub z_{wij} is obtained from the multibody vehicle model. It denotes the vertical distance between the wheel hub and the global coordinate system. Vertical distance of the road z_{rij} is obtained from the pre-processed road profile. It denotes vertical distance between the the road coordinate and the global coordinate system. Slope resistance R_{sl} representation is rather of approximate character, because small angle approximation

$$\alpha_{sl} \approx \tan \alpha_{sl} \tag{5.53}$$

is utilized for taking into account gravity resultant on the inclined road. Road slopes dz_r/dx_r and dz_r/dy_r are used directly in the compensation of the longitudinal force F_{xFzij}, and lateral force F_{yFzij}

$$F_{xFzij} = F_{zij} \frac{dz_{rij}}{dx_{rij}}, \; and \tag{5.54}$$

$$F_{yFzij} = F_{zij} \frac{dz_{rij}}{dy_{rij}}. \tag{5.55}$$

Implementation in the VTM is visualized in the Figure 5.21. Compensations are applied to the forces generated by the tyre model, see Figure D.4, which are updated with the number of tyres on the side of the axle n_{as}

$$F_{xcompij} = F_{xij} n_{asj} + F_{xFzij}, \; and \tag{5.56}$$

$$F_{ycompij} = F_{yij} n_{asj} + F_{yFzij}. \tag{5.57}$$

This approach does not result in the expected slips of the wheels directly, because compensation for the road inclination bypasses the tyre model. Slips of the wheel in longitudinal κ and lateral direction α are compensated by the driver model in form of the torque demand M_y and steering angle δ.

Global Simulation Platform (GSP)

This environment is focused on power-train system and its components, which are further used for evaluation of the vehicle performance in available drive cycles. However, chassis is very simple and neglects suspension dynamics in vertical and lateral direction. Tyre-road contact is not modeled at all. Hence, the tyre representation is very simple. All vehicle controllers and actuators are represented with high fidelity. Platform is based on the MATLAB/Simulink environment where vehicle definition can be easily changed and scaled.

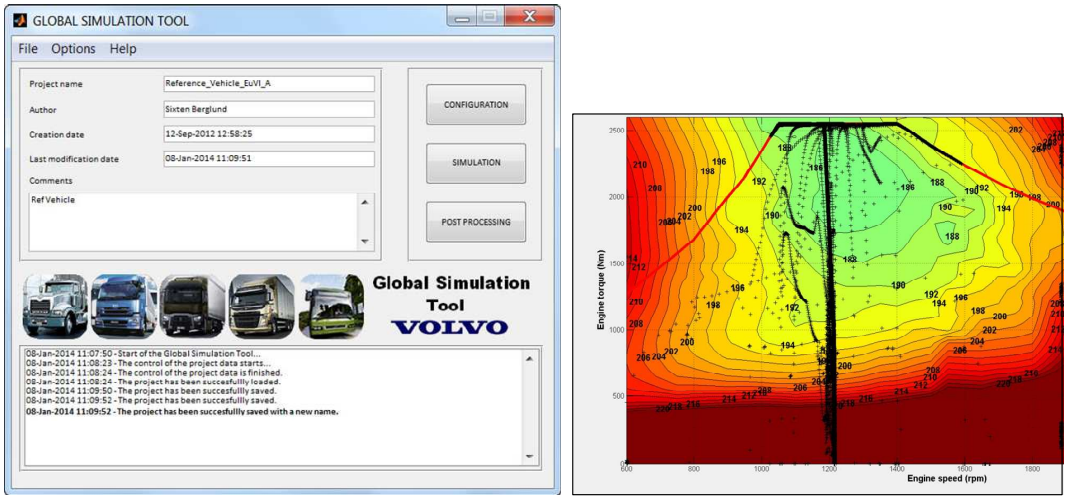

Figure 5.22: *GST interface*

GSP is also common repository of vehicle and machine simulation models. Unified model structure helps to reuse model components and data. It is focused on evaluation of fuel consumption and performance of vehicle plants.

Global Simulation Tool (GST)

GST is the graphical interface of GSP and provides a user friendly environment which can be easily maintained, see Figure 5.22. This environment actually contains compiled GSP models, which does not require user to make any direct changes in Simulink software. Hence, it does not demand any special training and it can be used outside of product development area within Volvo Group.

GSP&VTM combination

A combination of VTM and GSP platform was made within MSc. thesis [19]. This combination diminishes weaknesses of both models by joining high-fidelity chassis and power-train models of the vehicle. However, complexity, computational inefficiency and time to setup desired combination are serious disadvantages of this model.

Complete Vehicle Models (CVM)

Complete Vehicle Models is based on NASTRAN programing language. It concerns elastic behavior of the vehicle components. Vehicle structure is defined with discrete elements and evaluated with FEM solvers. However, such level of complexity is payed by high computational expensiveness of the model. Work with such program requires special training. CVM mainly evaluates

- static analysis,
- handling,
- comfort,
- vibration environment,
- durability, and
- engine induced vibrations.

5.5 Model B

Newly developed model B, visualized in Figure 5.23, aims to provide evaluation of the operating cycle with the selected vehicle and tyres combination. Vehicle template was taken from the VTM library. Top level of the Simulink layout is visualized in Figure 5.23. VTM truck template was transformed in order to be consistent with the representation of the model A. Environment description also accords to the Model A, and it consists from the velocity and vertical profiles of the track. Model B contains empirical MF tyre model, described in Section 5.4, and newly developed linear tyre model, described in Section 5.1. Both models includes the surrogate model for evaluation of the rolling resistance coefficient, described in Section 5.1. Power-train and driver model development are described in Section 5.3. Model B is executed from the from the MATLAB script, which calls all necessary components of the model, see E.

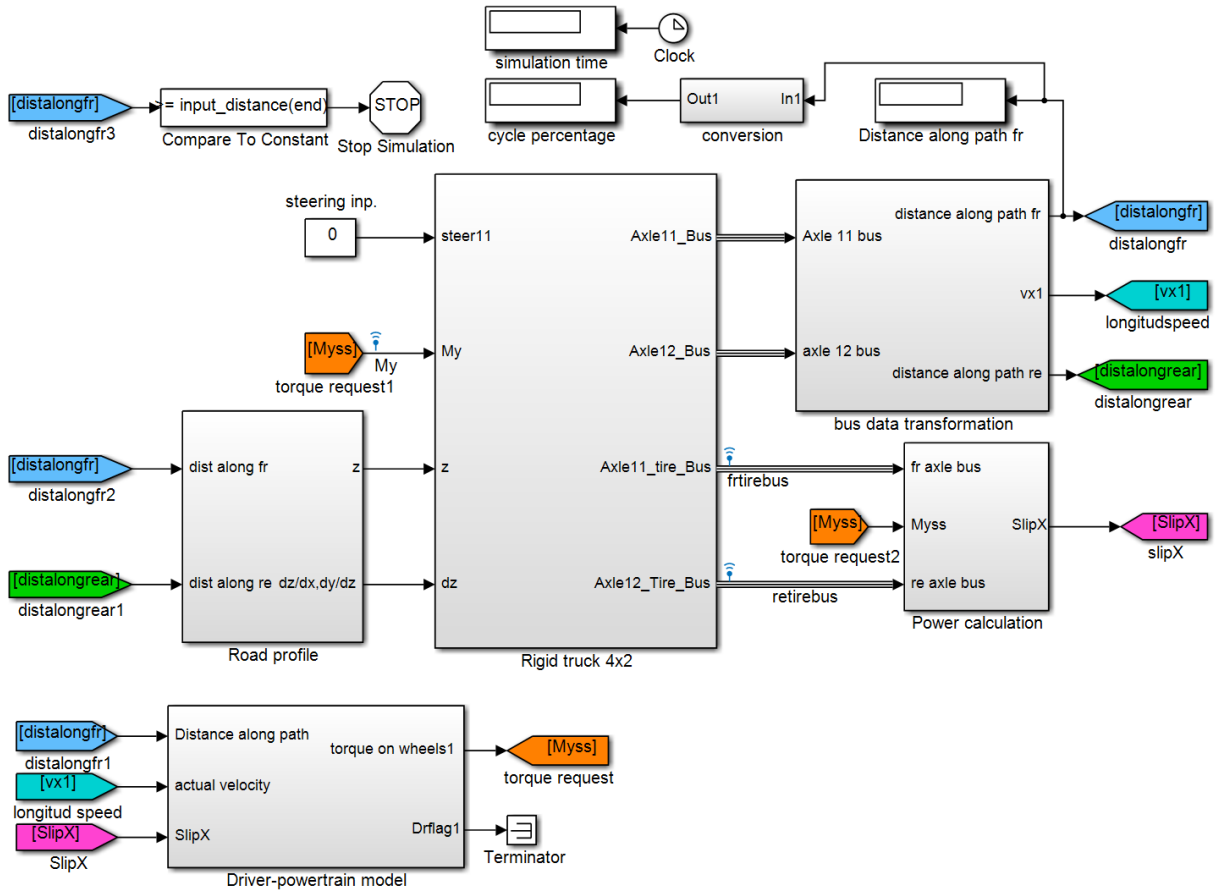

Figure 5.23: *Structure of high-fidelity Model B*

5.6 Constraining events

Tyre selection optimization routine requires models of objective functions and constraints, described in Section 2.2. Current set of constraints are ride comfort, handling and start-ability, see [34]. Set of constraints ensures that the vehicle can be used in the selected operating environment. Newly developed high-fidelity joint model B enables to implement former constraining events. Constraining events contained in the model A can not cope with different vehicle combinations. This would be the main benefit of constraining events using the model B, which can evaluate various vehicle combinations, without need to change the constraining event definition.

Current set of constraints

Implementation of the current set of constraints to the model B is discussed in this section. Feasibility of constraining events implementation to the model B is outlined. Limitations in model B are discussed.

Ride comfort

Ride comfort can not be evaluated in the model B directly, because tyre-road contact is represented with single contact point in both tyre models (MF and linear tyre). Enhancement of the tyre model for advanced tyre-road contact and flexible belt model are required in order to consider short wavelength road irregularities. However, this solution would require even more tyre parameters than in current definitions of tyre models. This can be simplified by logging of the displacement of the tread from simulation environments with more advanced tyre models (CVM) and using them in model B. Sensor in the vehicle cab can be used in order to evaluate vertical component of the acceleration in the cab, which can be used as a the vehicle response to the given road profiles.

Handling

Steady-state cornering can be evaluated with MF tyre or linear tyre of model B for combination of constant velocity $v_x = const.$ and steering angle ν, which does not result in large slip angles. Overhead script would run the vehicle simulation for short period of time with fixed steering angle $\nu = const.$, and constant velocity $v_x = const.$ on the leveled road ($z_{tr} = 0$, $dz/dx = 0$, $dy/dx = 0$). Steady state response to the fixed steering angle ν of the vehicle can be compared with lateral acceleration a_y of the vehicle combination, measured in specified position on the vehicle.

This can be implemented, by connecting constant steering angle request to the vehicle template (currently $\nu = 0$). Easiest change of environment definition is by defining of the new operating cycle with the few sample points of constant velocity $v_x = const.$ and zero sample points for vertical profile $z_{tr} = 0$. Corresponding $dz/dx = 0$ is calculated from the vertical profile automatically. Road camber $dy/dx = 0$ is default setting in the model B. Lateral acceleration can be measured in one of the vehicle sensors, e.g. cab. Various values of lateral accelerations can serve as a performance measure or for comparison with the acceleration threshold (constraint).

Start-ability

Definition of the former start-ability constraining event in model A is described in Section 5.4. Brief idea about implementation of the start-ability model to the model B is described bellow.

Threshold of α_{slmax} for given vehicle combination can be defined. Overhead script executes joint model, which evaluates whether the vehicle can drive off at slope α_{slmax}. Environment definition can be easily implemented by adding a linearly increasing signal to the vertical profile z_{tr}, which reflects increasing road angle. Road angles are derived from the vertical profile automatically. Start-ability constraint is fulfilled if $v_x \ngeq 0$ at simulation time, e.g. $t = 0.1s$.

Following method can be also used as a performance measure for comparison of the different tyres. The road slope $\alpha_{sl.}$ in the model B increases, until $v_x > 0$. Slope $\alpha_{sl.}[k]$, when vehicle velocity tends to $v_x \leqq 0$ is the break, when vehicle can not drive off anymore. Slope $\alpha_{sl.}[k-1]$ is the maximum slope which satisfies start-ability constraint.

For purpose of start-ability constraining event, MF tyre is a more suitable tyre model, reflecting non-linear behavior of the tyre in the region of high slips κ. However, MF tyre model requires empirical data for each tyre, which is limiting for the tyre selection purposes. Simple linear tyre model, which has been developed for the purpose of verification of the objective function is not very suitable, because it can not reflect the real tyre behavior in the region of high slips κ, which can occur during the drive off on an inclined road. Detailed model of the power-train is required in order to model start-ability well-enough. This would imply adding complexity to the model B.

New constraints proposal

As the VTM is designed for the evaluation of the vehicle dynamic behavior, it allows to introduce new tyre related constraints taking into account important vehicle performance and safety measures, which can help to improve tyre selection process.

Braking

Braking performance of the vehicle is one of the most critical vehicle safety measure. It is highly dependent on the tyre characteristics, especially longitudinal slip stiffness $c_{F\kappa}$, which is influenced by the tread depth *dep*. Braking performance is influenced by the available road-friction μ and power capacity of the vehicle braking system, resistances of the vehicle and load transfer, caused by the deceleration of the vehicle. One of the possible braking performance measures can be the braking distance, where the vehicle brakes from the selected velocity v_x to standstill, and resulting stopping distance x_{stop} serves as a measure, see [37], [14]. Braking performance constrain can be defined as

$$x_{stop} \leq x_{stopmax}, \tag{5.58}$$

where $x_{stopmax}$ is the maximal stopping distance.

Stopping distance of the vehicle combination can be evaluated by a short simulation of model B on the custom operating cycle. Operating cycle is defined with a set of sample points defining a leveled road and step change of the set velocity v_{set}, e.g. step $20\,to\,0\,m/s$. Simulation is stopped with use of the "Stop simulation" block when the velocity of the front axle fulfills the condition $v_{x1} \leq 0$. Resulting stopping distance is the last value in the distance along path array x, i.e. logged signal `Distance_along_path(end)`.

Model B uses traction control, described in 5.3, which aims to reduce requested braking/driving torque to selected value of longitudinal slip threshold κ_{max}, discussed in Section 5.1. However, this simplification does not follow the real braking strategy of the truck. Current model of brakes in the model B, described in 5.8, is rather simple and does not capture complex behavior of the vehicle electronic brake system (EBS), which regulates braking request on different wheels in order to deliver best braking performance wrt. actual vehicle and environment conditions. The MF tyre version of model B approximates tyre performance during braking more accurately than the linear tyre model.

Vehicle stability

Lateral stability of the vehicle combination is strongly influenced by the selection of the proper set of tyres and its distribution among vehicle axles. A set of tyres and their cornering characteristics, especially cornering stiffness $c_{F\alpha}$, influence lateral vehicle stability during cornering events. Steady-state cornering was proposed in the handling constraint. Following constraint candidates aims on vehicle oscillatory stability due to dynamic maneuvers. MF tyre model of the model B seems to be more suitable for such dynamic maneuvers, because high values slip angles α can be attained.

High speed off-tracking

Vehicle off-tracking is the lateral deviation of the first vehicle unit front axle, and the axle with highest off-tracking during dynamic maneuver. This measure gives an idea about space required by the vehicle combination during specified maneuver ([4]).

Implementation of the vehicle combination off-tracking constraining event to the model B is possible. Operating cycle with sample points expressing leveled road and constant velocity needs to be created or replaced with constant input Simulink block. Single sine wave steering input is connected to the vehicle template by Simulink block "Sine Wave" for one period. Then the steering input of the vehicle switches to zero for few seconds. Position of each axle from axle buses needs to be logged, and their trajectories can be compared with the front axle trajectory in post-processing MATLAB script. Difference between highest deviating axle from the deviation of front axle is subject to the constraint.

Rearward amplification

Rearward amplification is the relationship between the relative movements of the first and the last vehicle units during dynamic maneuver. This constraint expresses tendency of the vehicle combination to swing-out and rollover ([4]).

Implementation of the vehicle combination rearward amplification constraining event to the model B is possible. Operating cycle and lane change steering input are same as described in high speed off-tracking constraining event. Lateral acceleration profiles of a first and last unit are logged. Post-processing MATLAB script finds the peak amplitudes of the acceleration profiles of first and last unit. Ratio between last and first peak amplitudes is subject to the rearward amplification constraint.

Constraining events summary

Selection of relevant constraints needs to be implemented to the model B, and constraint thresholds should be specified by a literature research. Source of such limiting values of constraints can be obtained from norms for selected vehicle combinations, legislation or internal manufacturer standards. It is impossible to list all possible constraints for any tyre selection problem. Constraints do not have to stay only within the simulation model boundaries, therefore new constraints such tyre packaging can become a part of the optimization routine as well.

6 Verification of the model A

This chapter aims to provide insight into the verification of the computationally efficient model A by the high-fidelity model B. Verification methodology is introduced in Section 6.1. Description and results of the model A objective function verification are summarized in Section 6.2. Section is divided to qualitative verification and sensitivity analysis. Qualitative verification aims to find the difference between different modeling principles of the model A and the model B. Sensitivity analysis aims to investigate influence of the changing tyre design variables on the energy consumption of the model A and the model B.

6.1 Verification strategy

Comparison of the fuel consumption seems to be easiest way how to compare both models. However, this could not be done, because VTM environment lacks a representation of the power-train. Additional implementation of the detailed power-train would make whole model very complex, therefore the implementation of the different vehicle combinations would be more difficult. Nevertheless, we can compare the behavior of the fuel consumption $f_c(x)$ $[g/s]$ in case of model A with tractive power

$$P_{tr}(t) = M_y(t)\Omega_y(t) \tag{6.1}$$

of model B, where M_y represents input drive torque transferred from power-train to the wheel and Ω_y wheel rotational speed. Only $M_y > 0$ is considered, because it represents tractive energy, not braking. These quantities are comparable, because fuel consumption can be translated to the power with use of the calorific value of the fuel HU $[J/g]$. We can also compare total amount of energy during a drive cycle

$$E_{tr} = \int_0^{t_{sim}} M_y(t)\Omega_y(t)dt \tag{6.2}$$

or its trend when changing boundary conditions with total amount of fuel

$$F_c = \int_0^{t_{sim}} f_c(t)dt \tag{6.3}$$

or its energy equivalent.

It is important to be aware of the fact that model A is actually not using a power-train model for the vehicle control strategy. Therefore, even a very precise model B including detailed power-train model would not show the same results, due to lack of interaction of the power-train with dynamics of the vehicle in model A. This allows us to compare tractive power in both models.

Different definition or lack of driving resistances, described in Section 5.2, cause deviations. Therefore, it seems wise to go directly to the area of focus, which is rolling resistance. Alternatively we can compare resistive powers due to rolling resistance. Rolling resistance moment could be derived by the Euler equation of motion of the wheel

$$M_{yRR} = -\dot{\Omega}_y I_{yy} + M_y - F_x R_l, \tag{6.4}$$

where the product of angular acceleration $\dot{\Omega}_y$ and polar moment of inertia I_{yy} represents moment of inertia due to the acceleration of wheel mass around wheel rotational axis. In addition the product of tractive force F_x and loaded tyre radius R_l stands for available tractive moment, and M_y is driving moment which is supplied to wheel from drive-train. Since we have both rolling resistance moment M_{yRR} and rotational velocity Ω_y of each wheel represented in both models, we can define resistive power due to rolling resistance as

$$P_{RR}(t) = M_{yRR}(t)\Omega_y(t). \tag{6.5}$$

Such a verification is more convenient than tractive power, because these rolling resistance powers can be compared directly. Difference make the style of drive cycle following in case of model A. Due to inverse dynamic technique of model A, where power-train serves only as ex-post calculator of the fuel consumption, power-train model does not have any impact on control strategy or influence the drive cycle in any manner. Therefore, model B is even more accurate from the point of view of actual driving, because it reflects the dynamic vehicle properties. However,

tractive power and energy consumption balance	$P_{tr}(t)$ *vs.* $f_c(t)$
energy balance	E_{tr} *vs.* F_c
tractive power balance	$P_{trA}(t)$ *vs.* $P_{trB}(t)$
resistive power by rolling resistance balance	$P_{RR_A}(t)$ *vs.* $P_{RR_B}(t)$

Table 6.1: Possible verification measures

this difference between the models, due to the different control strategy (different use of traction power, braking) is not that significant when considering rolling resistance power compared to when we take into account whole power-train as previously proposed and try to find similar trends of both models during the drive cycle. Summary of proposed verification methods could be found in Table 6.1.

6.2 Verification of the model A operating costs

Verification of model A is provided by model B, which is based on VTM, described in Section 5.4. This tool can not be used without modifications, because it is not primarily used for simulation of drive cycles. Derived model B is summarized in the Section 5.5.

Simulation of both models is described in C.1. Operating cycle provided in model A was used, see [10]. These simple operating cycles consists of vertical and set velocity profiles, in form of sampled points with respect to the cycle distance. For processing of these road cycle data, a script in model A was used as a base. Model A preprocesses road data using linear interpolation. This solution is computationally efficient, but the slope is changing considerably due to the coarse sampling frequency of original data. Such road profile is not very close to reality and brings additional perturbations to the high fidelity model B. The road profile was interpolated using a spline and re-sampled with higher sampling frequency in order to provide same input to both of the models. Therefore model B suspension is not excited with additional perturbations and interpretation of the verification results will be easier.

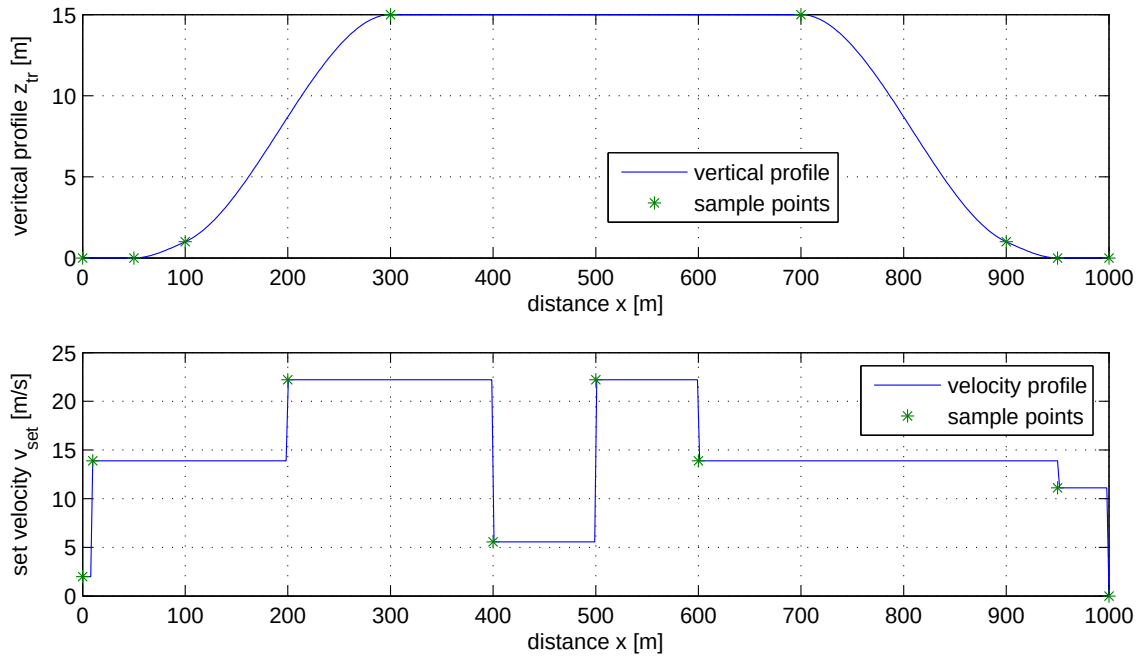

Figure 6.1: *Testing operating cycle 1505 (1km), contains set velocity and vertical profiles*

VOLVO FH500 Rigid truck 4x2, fully loaded		
curb weight	[kg]	7066
laden weigh	[kg]	17918
wheel base	[m]	6
curb front axle	[kg]	5231
laden front axle	[kg]	6870
curb rear axle	[kg]	1835
laden rear axle	[kg]	11048
front tyres		2
rear tyres		4
engine		12.8l, 6 cylinder
maximum power		368kW@1400-1900 rpm
maximum torque		2500Nm@1050-1400 rpm
number of gears		12

Table 6.2: Selected truck basic parameters

In the first loop of the verification process, qualitative comparison of model A actual fuel consumption f_c $[g/s]$ is compared with tractive power on the drive shafts P_{tract} $[W]$ for model B, described in Section 6.1. Both simulations are provided with the same model of the truck, which is rigid 4x2 truck, described in Table 6.2. Simple longitudinal driving cycle defined with vertical road profile and speed profile is used, see Figure 6.1. Both models use same tyre with parameters described in Table 6.3. Model B has implemented surrogate model, described in Section 2.2, 5.1 and in [34]. It supplies model with detailed representation of the rolling resistance, based on actual driving conditions and tyre design variables. Total amount of fuel consumed per driving cycle F_c $[l]$ of model A is compared with total amount of tractive energy E_{tr} $[kJ]$.

Tyre 315/80 R22.5 (pac2002_315_80R22_5.tir)		
parameters	**units**	**values**
tyre inflation pressure p	[Pa]	$8e05$
unloaded section width w_t	[m]	0.315
tread depth dep	[m]	0.011965
unloaded tyre diameter d	[mm]	1.096
vertical stiffness k_z	[N/m]	$1e06$
vertical damping c_z	[N/m.s]	$1e03$
valid longitudinal slip range	[-]	$\langle -1.5; 1.5 \rangle$
USE MODE	[-]	14

Table 6.3: Characteristic tyre parameters

Qualitative verification of model A (first loop)

In order to get a first idea about how both models differ from each other a simple qualitative analysis was made. The driving cycle, described in Figure 6.1, was chosen in order to find out, how both models work and highlight differences. Even though the control strategy of models differ significantly, rough correlation is expected.

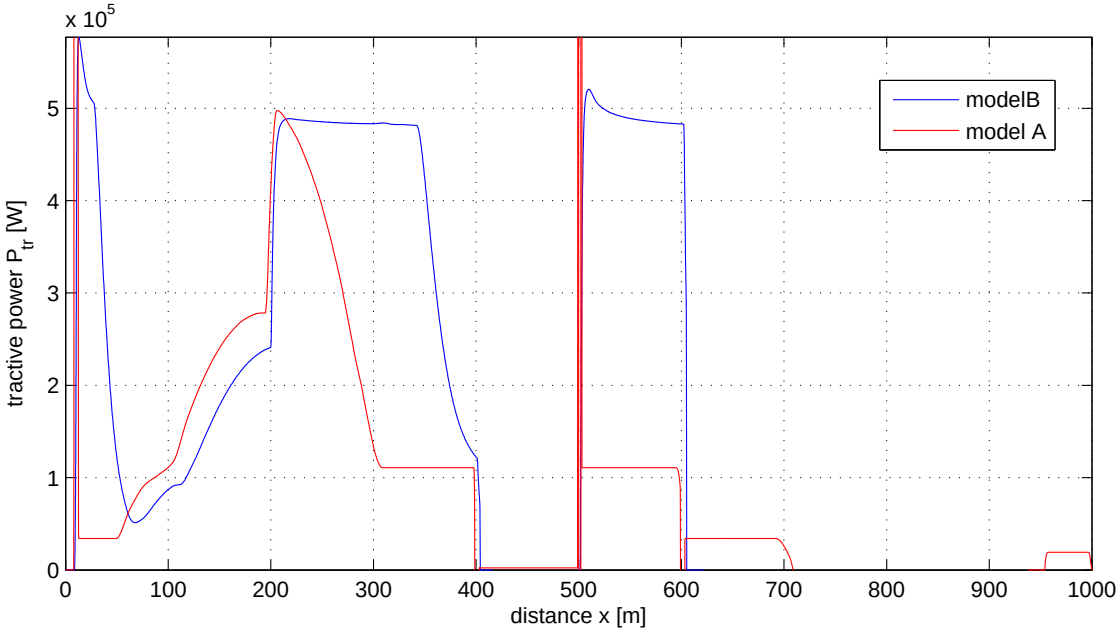

Figure 6.2: *Tractive power P_{tr} comparison*

In the Figure 6.2, can be seen a comparison of both, model A and B in terms of tractive power P_{tract}, defined in Eq. (6.1). Up to the distance of sudden step change in set speed v_{set}, we can see that both models follow the same trend of mean value of P_{tract}. However, model B reacts with significantly smaller amplitude, but it introduces phase shift. The phase shift is probably caused by the energy of the vehicle stored in the inertia of the vehicle of model B and driver logic, including lags between modes representing neuro-muscular lags of the driver, described in Section 5.3. Model A completely lacks such behavior. It is not covered at all, because tractive power P_{tract} is a function of set speed v_{set} and sum of resistances $\sum F_{resi}$. When the set velocity v_{set} step occurs, model A follows velocity profile with actual velocity v_x, which means that acceleration of the wheel vehicle is absolutely unrealistic and depends on the step size of the acceleration vector. Such behavior is not very realistic, because a real truck is limited by the maximum power of the engine and many other drive-train constraints. Model B copes with sudden step in set speed v_{set} by driving torque demand, according to the request from used driver model. Sudden drops of the tractive power are caused by the traction control, which prevents model B from saturating wheels during high drive torque requests.

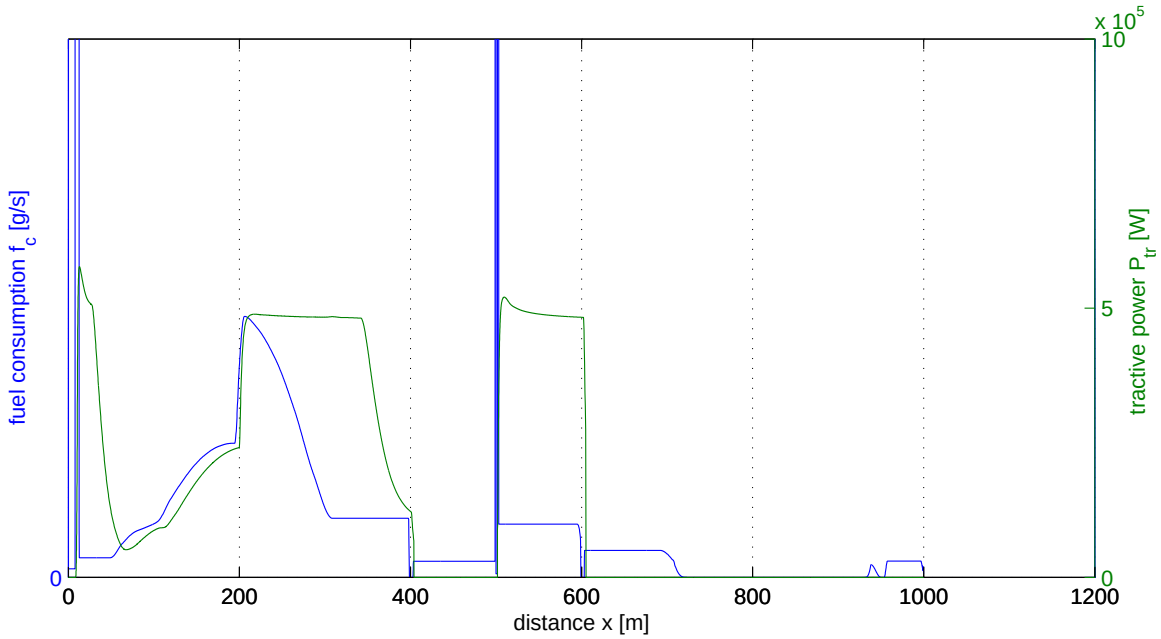

Figure 6.3: *Fuel consumption f_c vs. tractive power P_{tr}*

Figure 6.3 compares a trend of fuel consumption f_c of model A with tractive power P_{tract} of model B. This comparison adds complexity to the model A, because model of the power-train calculates fuel consumption f_c inversely, more discussed in Section 5.3. Therefore we have more realistic trend of control strategy of the vehicle. However, the power-train in this model is not in the feedback loop, hence it does not influence the dynamics of the vehicle. Resulting sudden accelerations of the model A cause unrealistic values of fuel consumption at given time step, because of the extensive extrapolation of the engine speed in the engine map of fuel consumption. Even though this value holds only during one time step, its amplitude is so high that it influence overall consumption of the vehicle considerably.

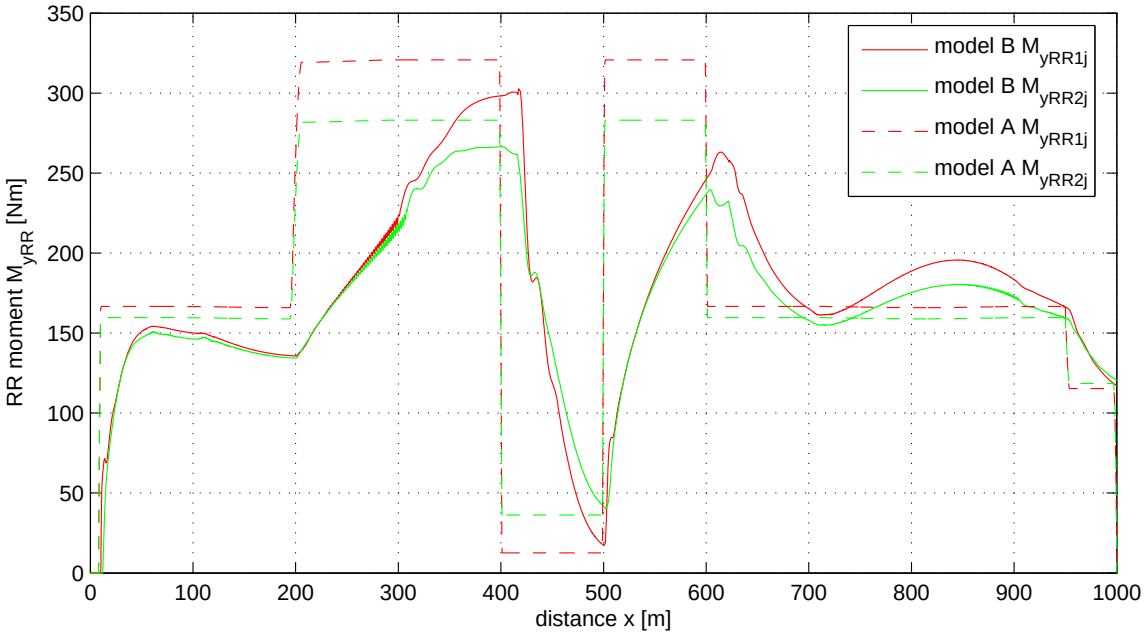

Figure 6.4: *Rolling resistance moments M_{yRR} comparison, values for wheels on ($1j$ = front axle, $2j$ = rear axle)*

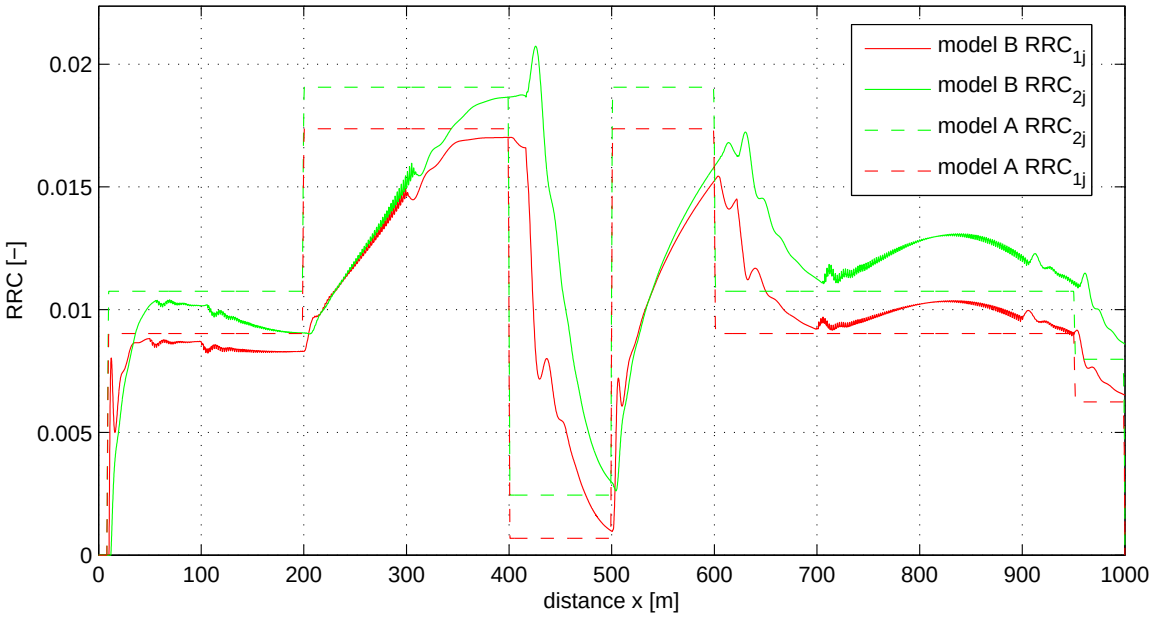

Figure 6.5: *Rolling resistance coefficient f comparison, values for wheels on (1j = front axle, 2j = rear axle)*

Figure 6.4 shows a comparison of rolling resistance moments M_{yRR} of both models with respect to the distance along the path x. Both models are using the surrogate model for rolling resistance developed within the TyreOpt research project, described in [34]. It is dependent on the velocity v_x, displayed on the Figure 6.6, tyre design variables $\mathbf{x}$ (p, w_t, dep, d_0), vertical load F_{zij} on each of the wheel, see Figure 6.7, and produces rolling resistance coefficient, see Figure 6.5.

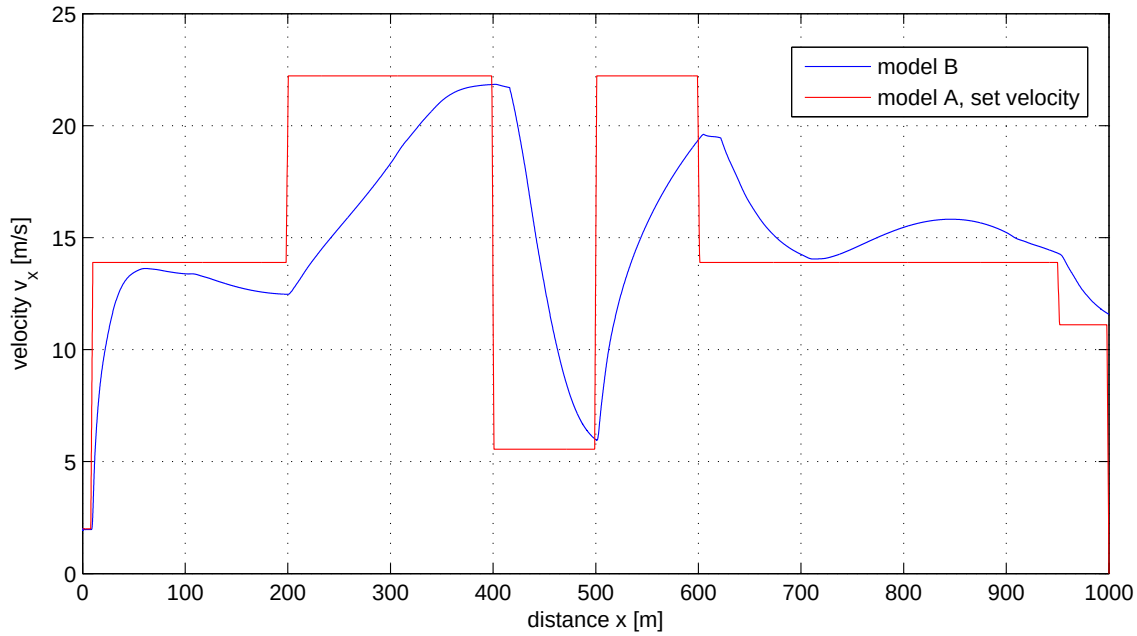

Figure 6.6: *Velocity profile v_x, (velocity profile of model A = v_{set})*

Axle loads of both models were set to the exact same values for a loaded vehicle at standstill, described in Table 6.2. Therefore both models represents the same vehicle, tyre and environment. As can be seen from the Figure 6.7, normal reaction on the wheels F_{zij} in model B varies during the drive cycle, because a more realistic representation of vehicle chassis and tyre. On the other hand, constant value of wheel normal reaction ($F_{zij} = const.$) of model

A, does not consider load shift or any other chassis phenomena. Model A velocity v_x is following velocity profile

$$v_x = v_{set}, \tag{6.6}$$

which does not represent realistic behavior of the truck, because acceleration depends only on step size. As discussed in Section 5.3, kinematic models, as model A, cannot provide realistic representation of transients, because of lacking feedback between vehicle dynamics and power train, driver model. Such behavior in transients also proves lack of any tyre model which would reflect slip deformation of tyre, because such tyre can transmit any requested torque M_y. Tyre model, described in 5.4, is in fact only kinematic ration between linear velocity and rotation of the drive shaft and arm of traction force.

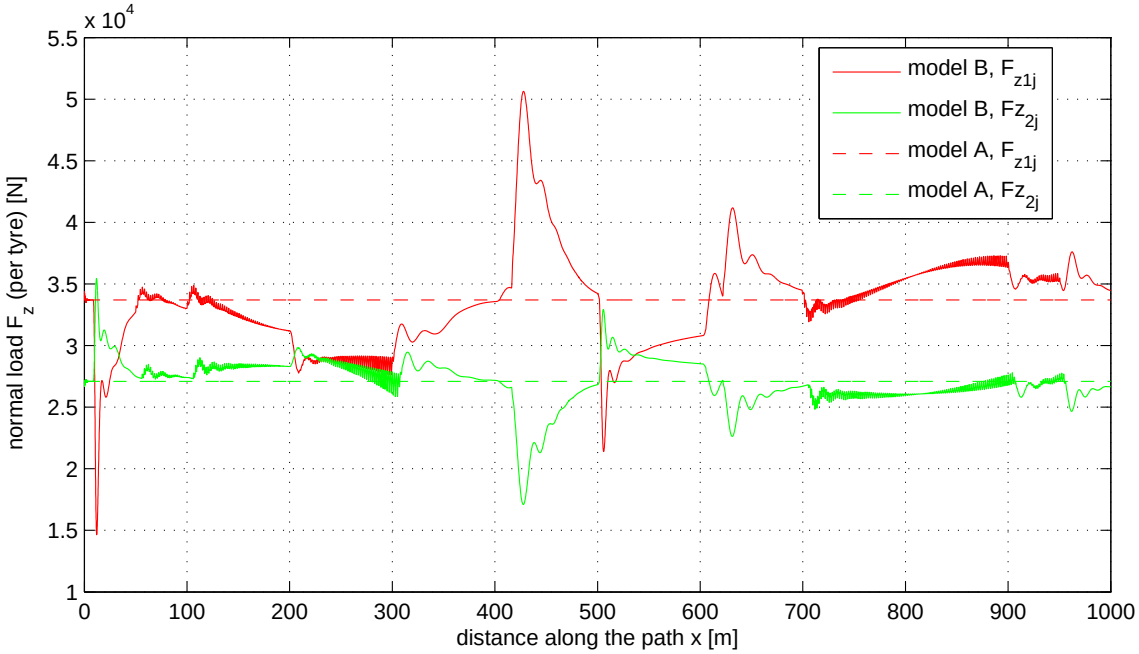

Figure 6.7: *Normal reactions under wheels F_z comparison, values for wheels on ($1j$ = front axle, $2j$ = rear axle)*

Conclusions of qualitative verification

First loop of verification proved differences caused by different modeling approaches to both models. Model A provides a good balance between computational power and fuel consumption at level road profiles and smooth velocity changes. With increasing profile complexity, model A deviates even more from real vehicle behavior. Model A requires further changes in order to provide more physical results. Limitation of the maximum requested power would help to prevent large deviations of fuel consumptions in transient. Resulting fuel consumption would be closer to reality.

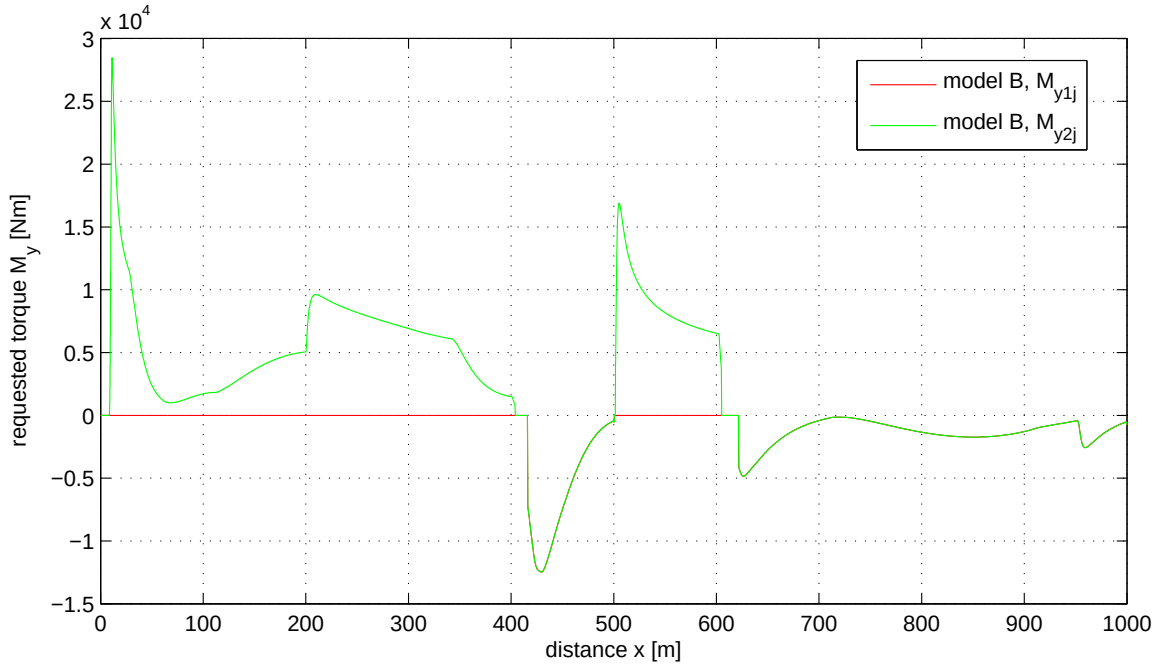

Figure 6.8: *Model B - requested torque M_y, values for wheels on ($1j$ = front axle, $2j$ = rear axle)*

From the results of the torque on drive shafts M_y, see Figure 6.8, could be seen large oscillations from the beginning of the cycle, until 200m. This is caused by too high torque request by the driver model. Traction control is preventing saturation of the wheels by switching to sailing mode, see Section 5.3. Such behavior does not follow real vehicle-driver behavior and induces perturbations to the vehicle suspension, visible on Figure 6.7. Hence driver model and control strategy of the model B requires further improvement.

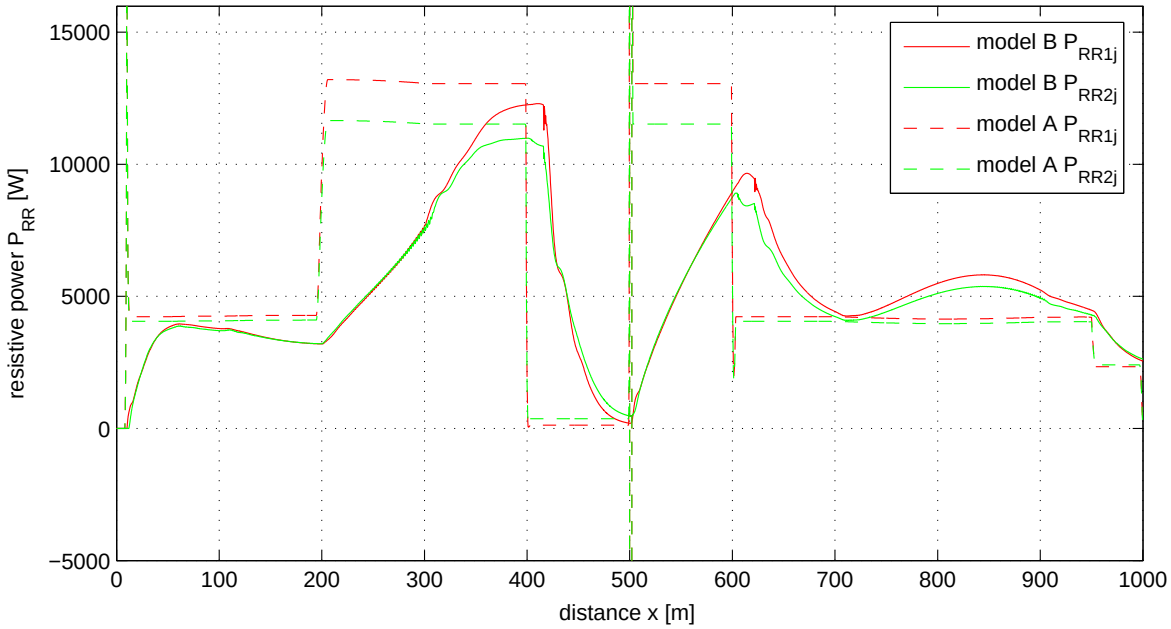

Figure 6.9: *Rolling resistance powers P_{RR} comparison (scaled), values for wheels on ($1j$ = front axle, $2j$ = rear axle)*

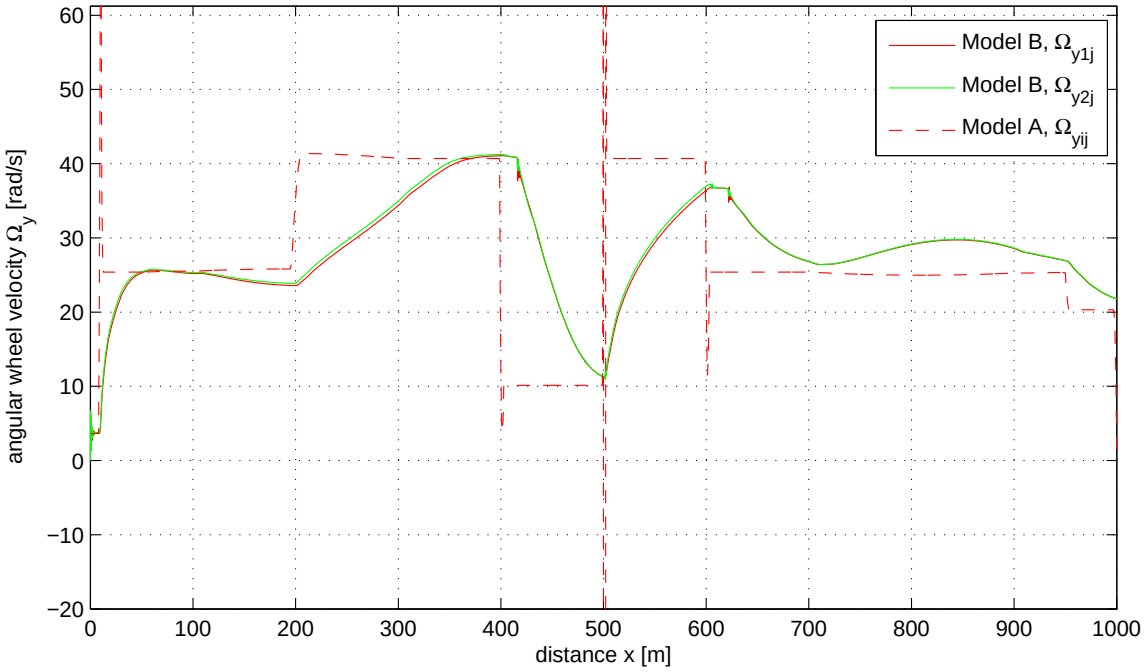

Figure 6.10: *Wheel angular velocities Ω_y comparison (scaled), values for wheels on ($1j$ = front axle, $2j$ = rear axle, ij = front&rear axle)*

Sensitivity analysis (second loop)

This section aims to evaluate behavior of the Model A with respect to the tyre design parameters. This requires multiple simulations for each design variable. By comparison of the tractive powers P_{tr} on the drive shafts as a function of the tyre design parameters of both models on selected road cycle can be evaluated suitability of the model A for evaluation of the operating cycles. When one design variable changes within interval specified in Table C.5, other variables are set to reference values.

First, quantitative comparison with empirical tyre model represented in VTM, summarized in Table C.2, was done on 4 tyres, described in D.1. Total tractive energy on drive shafts E_{tr}, defined in Section 6.1, is used in order to compare both models. Relevant tyre parameters and drive cycle representation were exported to model A. Drive cycle, visualized in the Figure 6.1, was utilized. For the detailed description of the verification with empirical tyre data, see Table C.2.

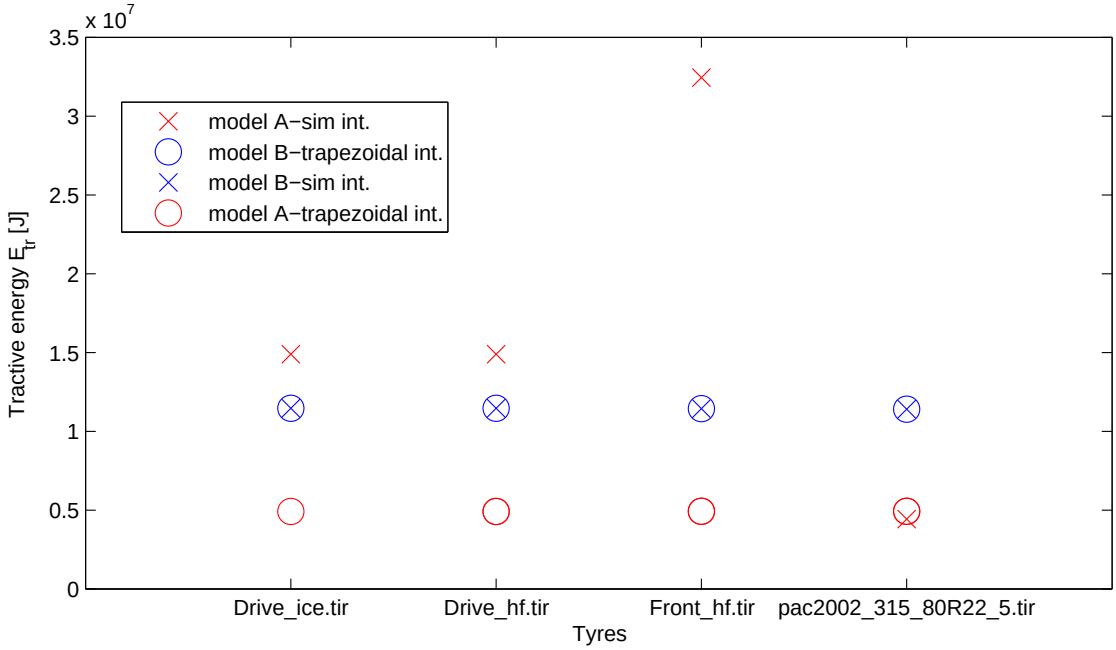

Figure 6.11: *Comparison of tractive energy E_{tr} (traction only) on the road 1505 (10km), described in C.1.*

Tractive energy on the drive shafts E_{tr} were calculated in 2 different ways. First was numerical integration in Simulink, described in [25]. As a comparison method was used trapezoid quadrature, described in [26], which is in fact integration of the linearly interpolated sample points of the tractive power on the drive shafts P_{tr}, see Figure 6.2. In Figure 6.11, can be seen that these 2 methods of evaluation of the tractive energy varies significantly in case of the model A. Trapezoid is approximation method which does not capture transient behavior of the model A, discussed in the first loop of verification. Simulations described in the Table C.2, proves that sudden increase of the set velocity v_{set}, visualized in the Figure 6.1, is the cause of the sudden tractive energy E_{tr} rise, see Figure 6.12. Transients of the model A can strongly influence results of the total energy consumption, hence the fuel consumption f_c as well.

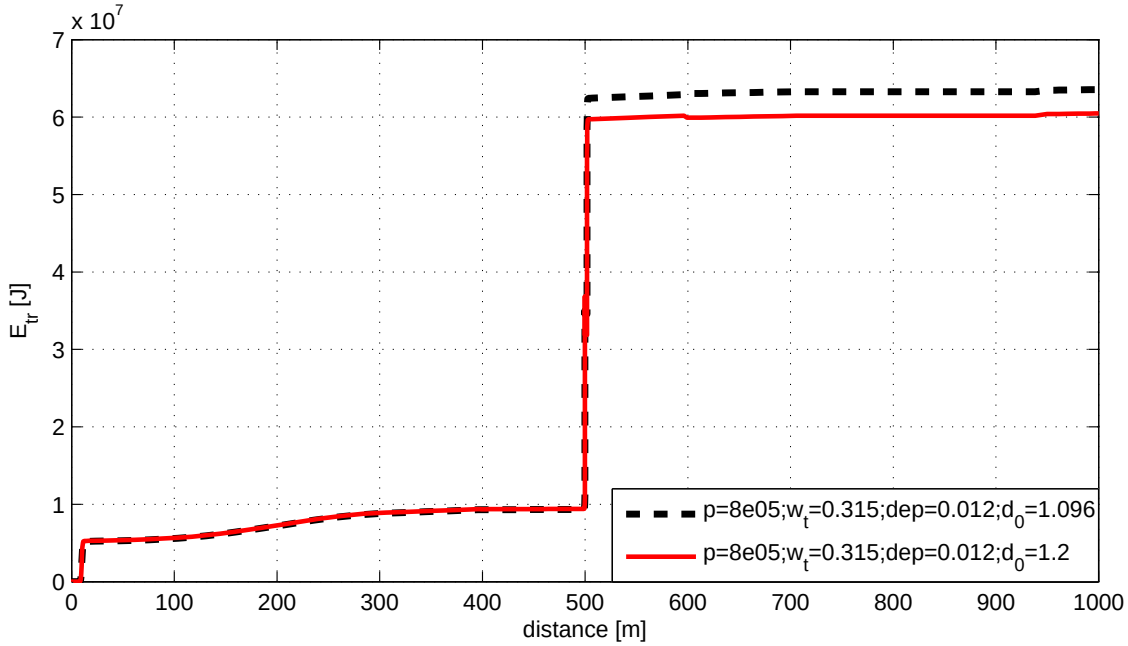

Figure 6.12: *Tractive energy $E_{tr} = f(x)$ trend of the model A, by Simulink integration of $P_{tr}(s)$ on the road 1505 (10km), described in C.1.*

Influence of the changing tyre design variables on a tractive energy E_{tr} will be compared between model A and B. This comparison aims to find out how sensitive are both models on the change tyre design variables. High fidelity model B captures dynamic behavior of the chassis and control strategy of the model B is based on the forward approach with simple driver model. Therefore profiles of normal load $F_z(x)$ and velocity $v_x(x)$, discussed in Section 6.2, are the major differences between compared joint models. Both normal load F_z and velocity v_x are inputs of the surrogate model for evaluation of the rolling resistance f. Therefore consumption of the tractive energy E_{tr} varies for both joint models.

Both joint models are showing relatively good correlations of tractive energy E_{tr} orders. However, by normalizing of E_{tr} of each model by

$$e_{tr} = \frac{E_{tr}}{maximum\,(E_{tr})}, \tag{6.7}$$

could be better seen the sensitivity to changing tyre design variables. Details of simulations are described in Table C.3. Change of the normalized tractive energy e_{tr} with regard to varying inflation pressure p, on the shortened road 365, can be seen on the Figure 6.13. Both of the models are following decreasing tendency of the rolling resistance f, discussed in Section 4.3, which is visualized on the same figure with fixed values of velocity v_x, and normal load F_z.

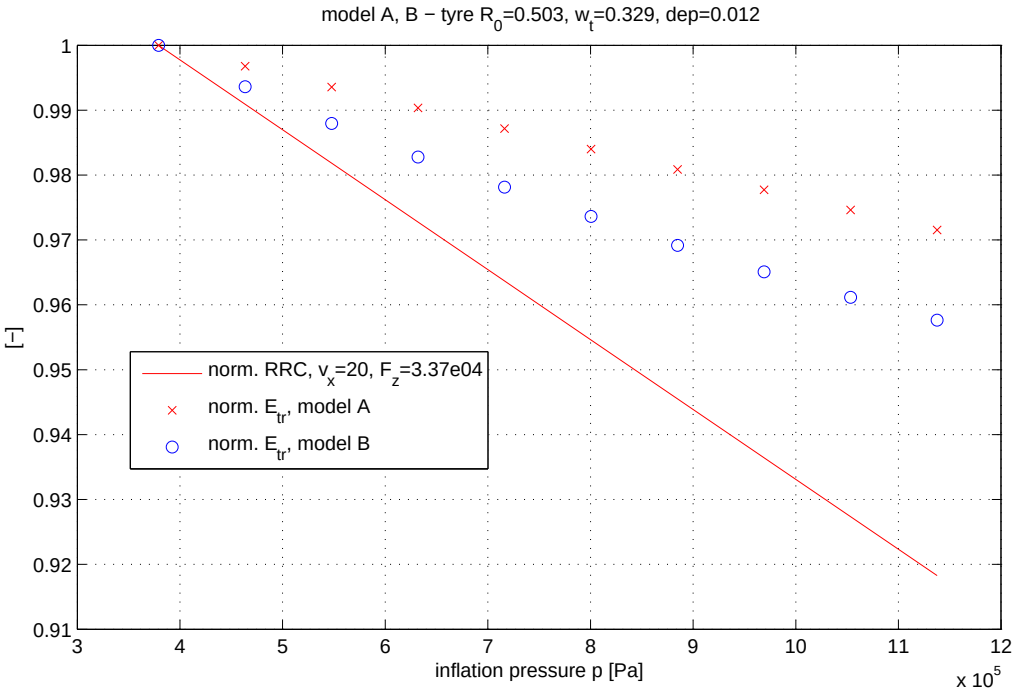

Figure 6.13: *Normalized tractive energy $e_{tr} = f(p)$ of model A, B on road 365 (10km), described in C.2.*

Change of the normalized tractive energy e_{tr} with regard to varying unloaded radius R_0, on the shortened road 365, can be seen on the Figure 6.14. Both of the models are following decreasing tendency of the rolling resistance f, discussed in Section 4.3, which is visualized on the same figure with fixed values of velocity v_x, and normal load F_z.

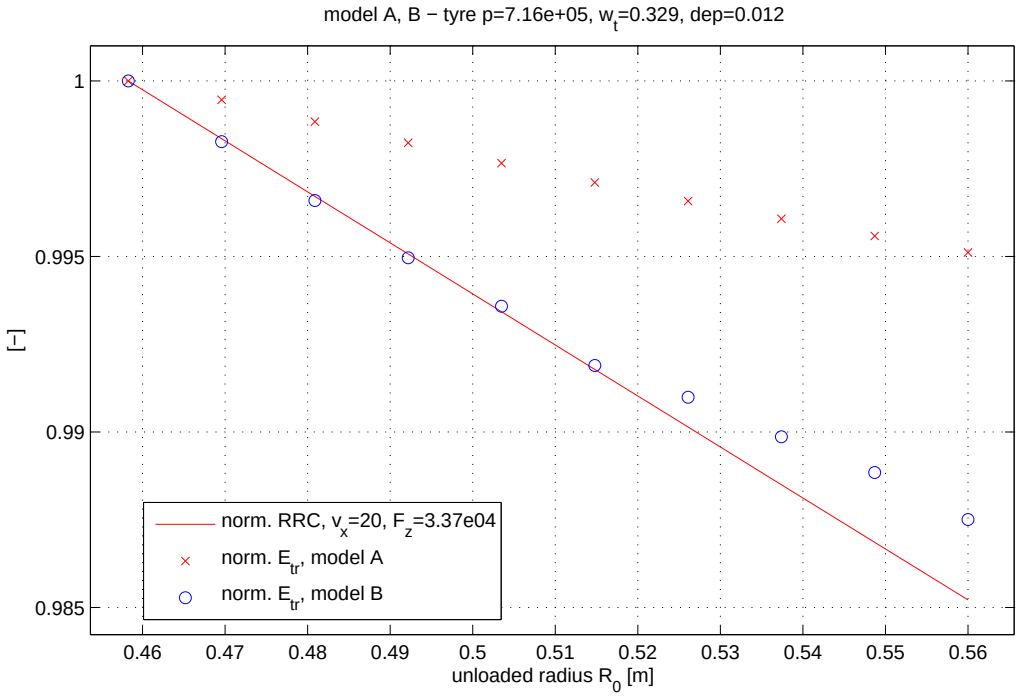

Figure 6.14: *Normalized tractive energy $e_{tr} = f(R_0)$ of model A, B on road 365 (10km), described in C.2.*

Change of the normalized tractive energy e_{tr} with regard to varying width of the tyre w_t, on the shortened road 365, can be seen on the Figure 6.15. Both of the models are following increasing tendency of the rolling resistance f, discussed in Section 4.3, which is visualized on the same figure with fixed values of velocity v_x, and normal load F_z.

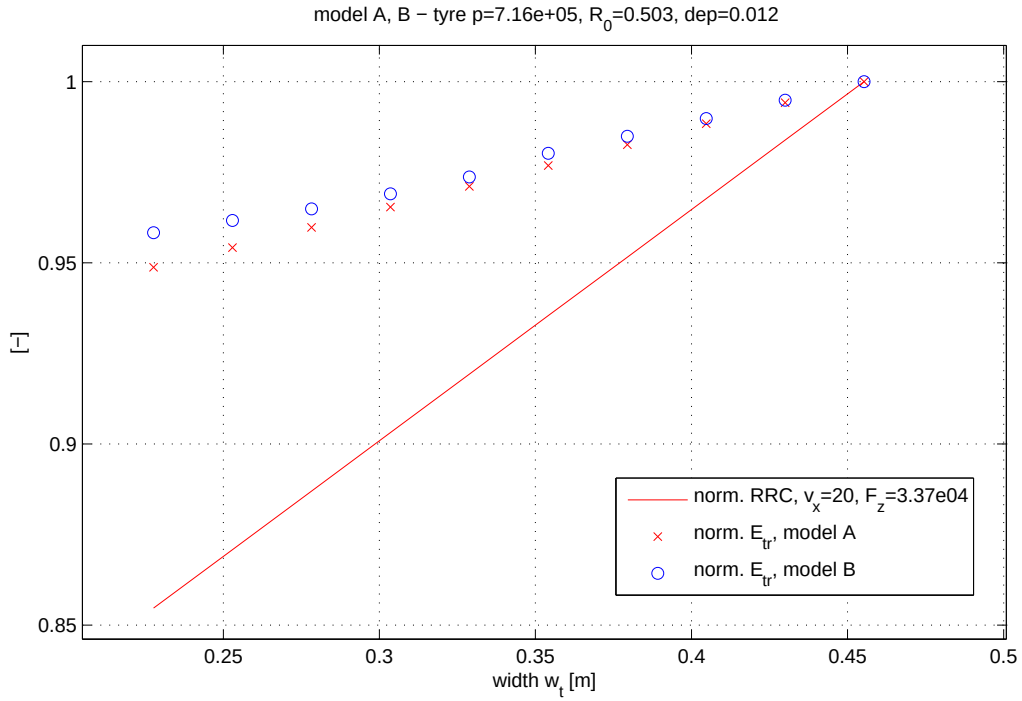

Figure 6.15: *Normalized tractive energy $e_{tr} = f(w_t)$ of model A, B on road 365 (10km), described in C.2.*

Quantitative results of the tractive energy E_{tr} with regard to the changing tyre design variables, on the shortened road 365, can be found in the Figures C.4, C.5, and C.6.

From the tendencies of tractive energy E_{tr} with changing tyre design variables is also notable that both considered models have different sensitivity to tyre design variables within one model. This is notable when the difference between worst and best result of tractive energy E_{tr} for each tyre design variable is considered wrt. to other tyre design variables within the same model. This is a serious issue for the tyre selection problem, because energy performance of two different tyres can theoretically result with different rank in both considered models.

From presented trends of the $e_{tr} = f(p)$, $e_{tr} = f(R_0)$, and $e_{tr} = f(w_t)$ can not be distinguished what is the contribution of the different velocity $v_x(x)$, and normal load $F_z(x)$ profiles to the difference in the tractive energy E_{tr} between joint models. Contribution of the normal load F_z to the tractive energy E_{tr} can be found out by the comparison of the E_{trA} with logged velocity profile $v_x(x)$ from the model B and tractive energy of model B E_{trB}. Velocity profile $v_x(x)$ was logged from the model B for each tyre design variable combination and implemented to the model A. Simulation of vehicle with various tyre design variables, on the shortened road 365, is summarized in Table C.4. Difference in tractive energies E_{tr} of model B, model A, and model A with logged velocity profile $v_x(x)$ for varying tyre design variables is visualized in figures 6.16, 6.17, 6.18. Trend of tractive energy E_{tr} of modified model A with logged velocity profile $v_x(x)$ from model B shows better correlation with trend of tractive energies of model B than original model A for all values of tyre design variables. Remaining difference of modified model A and model B is influenced by constant normal load F_z of model A, different simulation methods, and changing tyre characteristics. However, it can be concluded that the influence of control strategy to the energy consumption is more significant than the response from the vehicle chassis for vehicle with the same tyres on both axles. Importance of the vehicle chassis fidelity is expected to rise with the vehicle complexity, such as longer vehicle combinations and various tyres along vehicle combination axles.

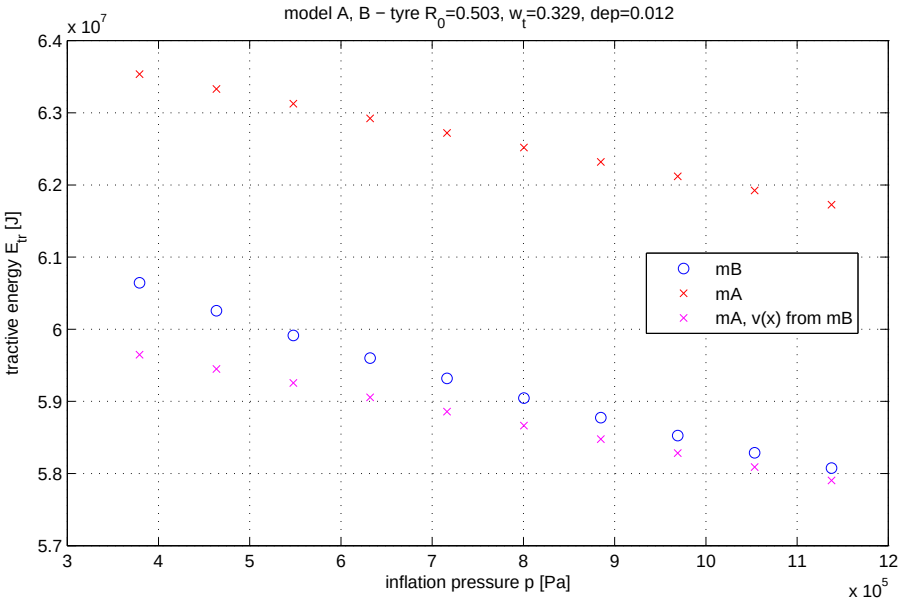

Figure 6.16: *Tractive energy $E_{tr} = f(p)$ of model A, modified model A, and model B on road 365 (10km), described in C.2.*

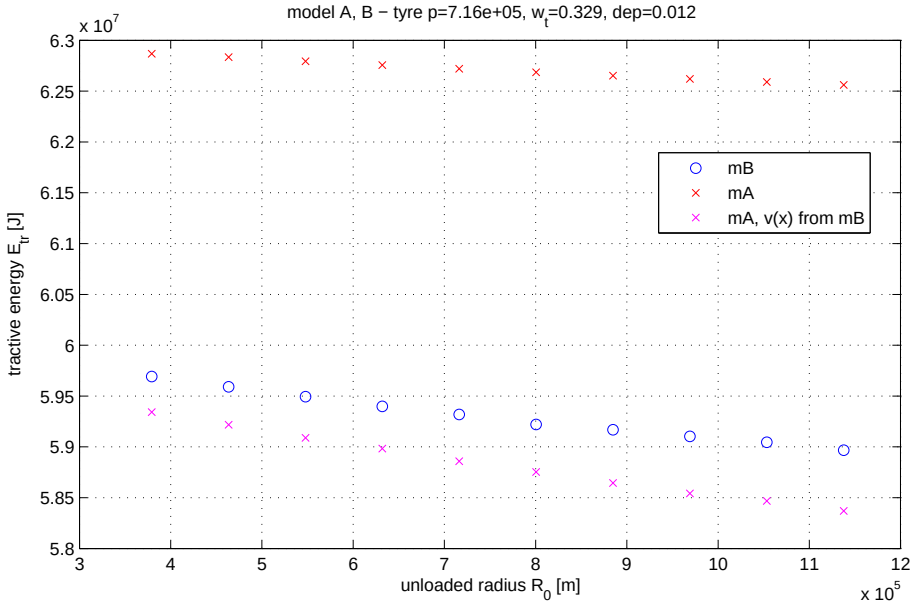

Figure 6.17: *Tractive energy $E_{tr} = f(R_0)$ of model A, modified model A, and model B on road 365 (10km), described in C.2.*

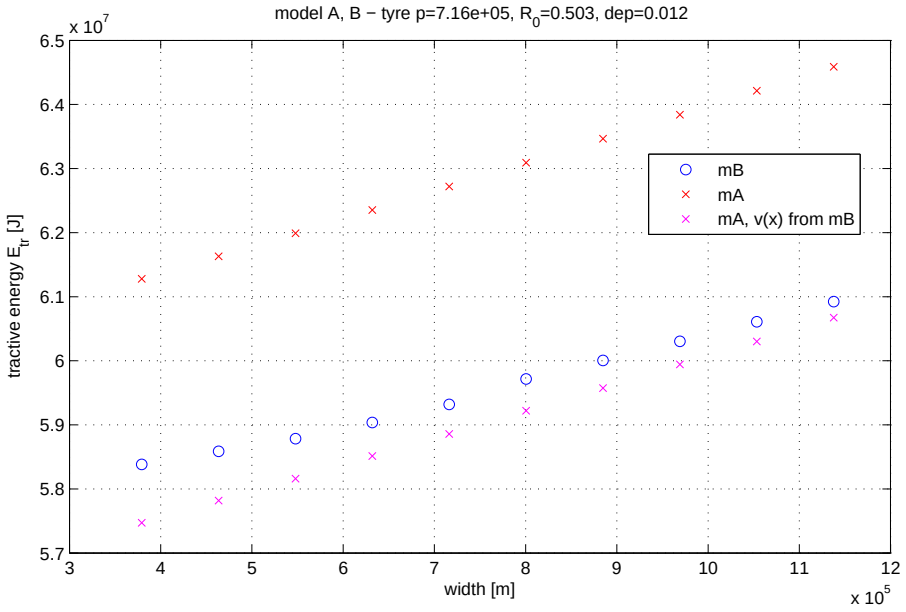

Figure 6.18: *Tractive energy $E_{tr} = f(w_t)$ of model A, modified model A, and model B on road 365 (10km), described in C.2.*

7 Conclusions and Future work

7.1 Project conclusions

Tyre-Opt project results and proper literature were reviewed, see Chapter 2 and 4, in order to provide sufficient information base for all thesis activities. Requirements and criteria for the model B were proposed in the Chapter 3. Criteria were evaluated by the project stakeholders in order to match the criteria with proper weights. Specialists at Volvo GTT vehicle analysis tools provided evaluation of each tool. After processing and discussion of the results, VTM was chosen as a base for the newly developed model B.

High fidelity model B provides relatively detailed model of the vehicle chassis, due to the multibody vehicle representation of the vehicle, provided in VTM. Developed environment enable to assess different vehicle combinations, because modularity of model B and various vehicle templates in VTM library. Newly developed linear tyre model and regression model of the loaded radius, described in Section 5.1, enable model to provide sensitivity analysis of changing tyre design variables on total tractive energy. Implemented surrogate model provides detailed representation of the rolling resistance coefficient, described in Section 5.1. Power-train and driver model development and implementation are described in Section 5.3. Model B includes all necessary environment and tyre data pre-processing in order to be able to evaluate behavior of the same vehicle, tyres and environment as provided in model A. Feasibility of constraining events implementation to the high-fidelity model were discussed and candidates for new constraints are proposed in Section 5.6.

Comparison quantities for the verification of the model A operating cycle were chosen, see Section 6.1. Limitations of the inverse dynamic approach for evaluation of the fuel consumption were discussed in Chapter 6. Such technique is suitable for smooth road profiles and velocity profile without any step change. Suggestions for improvement of the model A were proposed, summarized in Section 7.2. Model A will provide satisfactory representation of the vehicle performance with suggested modifications and limitation for the smooth drive cycles without transients.

The main cause of different energy consumption between model A and model B was found in varying velocity profiles of both models, caused by different modelling principles, i.e. driver models. However, difference caused by the distinct velocity profiles seems relatively constant within the models. Therefore the tyre selection process should not be affected by this phenomena, unless results of both models are compared.

Sensitivity analysis proved that different fidelity of models can influence tyre selection process, even though the difference in energy consumption of both models are not significant. Both models proved different sensitivity of tractive energy on various tyre design variables. This can lead to slightly different result of tyre selection process, because some of the tyre design variable has larger weight that the others in both models.

7.2 Future work

Optimization framework of the TyreOpt research project requires joint model for evaluation of the objective function and constraints. Main aim of this thesis project is the modelling and verification of the fuel consumption. Advanced tyre-wear model should be developed in order to verify its former representation in model A. Model B can serve as a base for development of the constraining event models, discussed in Section 5.6,which should verify model A constraints. Implementation of the former set of constraining events to the model B will ensure evaluation of various vehicle combinations.

Representation of the power-train and driver model in model B was designed for various vehicle combinations, but it is rather simple and it could be improved in order to bring more realistic results. Connection of the model B with GSP platform, described in 5.4, would ensure very detailed fuel consumption results. Detailed road definition, including lateral description of the road and micro profile, could be added in order to capture influence on the rolling resistance. Handicap of simple power-train model can be solved by cooperation with research projects aimed on power-train development, which seems to be mutually beneficial for both involved parties, as both groups aim to improve vehicle performance.

For better quality of the model A drive cycle's evaluation is desirable to introduce restriction of the maximum engine power. Such constraint will provide more accurate results of the energy consumption at more dynamic drive cycles. Dynamic drive cycles could be handled by pre-processing of the velocity profile by models, which are using forward approach and driver model. Similar approach can be used for the normal load, when higher-fidelity models serves as a pre-processing of the drive cycle data. This solution should bring better representation of the model A dynamic chassis behavior than the introduction of the simple load transfer model. Importance of higher fidelity

representation of the vehicle chassis is expected to be proven on more complex vehicle combinations and especially when various tyres are assumed over the vehicle axles.

Model B is prepared for the future improvements of the surrogate model for rolling resistance coefficient, such drive and brake torque, road friction and slip angle influence on rolling resistance. Relevant inputs are available, therefore relatively fast implementation is expected. Extension of the surrogate model for the force generation characteristics would make the vehicle model more consistent, as the FEM truck tyre from UOIT would be the only source of the tyre characteristics. This may also facilitate future validation of the tyre selection process.

References

[1] *Using the PAC2002 Tire Model*. ADAMS/Tyre 2005 r2 Help.

[2] R. Ali, R. Dhillon, M. El-Gindy, F. Öijer, I. Johanson, and M. Trivedi, *Prediction of rolling resistance and steering characteristics using finite element analysis truck tyre model*, International Journal of Vehicle Systems Modelling and Testing, 8 (2013), pp. 179–201.

[3] J. Allen, *Rigid ring quarter-vehicle model for durability and ride comfort predictions*. The Pennsylvania State University The Graduate School, Department or Mechanical Engineering, 2007.

[4] J. Aurell and C. Winkler, *Standard test procedures for the lateral stability of heavy vehicle combinations*, ROAD TRANSPORT TECHNOLOGY, (1998).

[5] M. S. Bazaraa, H. D. Sherali, and C. M. Shetty, *Nonlinear programming Theory and Algorithms*, John Wiley & Sons, Hoboken, NJ, USA, third ed., 2006.

[6] I. Besselink, *Shimmy of Aircraft Landing Gears*, PhD thesis, Delft University, September 2000.

[7] A. Booker, J. Dennis, J.E., P. Frank, D. Serafini, V. Torczon, and M. Trosset, *A rigorous framework for optimization of expensive functions by surrogates*, Structural optimization, 17 (1999), pp. 1–13.

[8] P. C. Cacciabue, *Modelling driver behaviour in automotive environments: critical issues in driver interactions with intelligent transport systems*, Springer, London, 1. aufl.; illustratition ed., 2007; 2010.

[9] S. Chae, *Nonlinear Finite Element Modeling and Analysis of a Truck Tire*, PhD thesis, The Pennsylvania State University, 2006.

[10] Z. Chen and S. Prathaban, *Modeling of tyre parameters influence on transport productivity for heavy trucks*. Diploma work- Department of Applied Mechanics, Chalmers University of Technology, Göteborg, Sweden, no: 2013:67, 2013.

[11] L. Eriksson, *Simulation of a vehicle in longitudinal motion with clutch engagement and release*, IFAC Workshop: Advances in Automotive Control, Karlsruhe, Germany, 2001.

[12] L. R. Federico Millo and M. Andreata, *Numerical Simulation for Vehicle Powertrain Development, Numerical Analysis - Theory and Application*, InTech, 2011.

[13] G. Genta, *Motor Vehicle Dynamics: Modeling and Simulation*, American Society of Mechanical Engineers, 1997.

[14] G. Genta and L. Morello, *The Automotive Chassis*, Springer Science+Business Media B.V., 2009.

[15] A. Gosavi and S. (e-book collection), *Simulation-based optimization: parametric optimization techniques and reinforcement learning*, vol. 55.; 55, Springer, Boston, 2014.

[16] K. Grosch and A. Schallamach, *Tyre wear at controlled slip*, Wear, 4 (1961), pp. 356 – 371.

[17] L. Guzzella and A. Amstutz, *The QSS toolbox manual*, ETH, June 2005.

[18] E. M. T. Hendrix and B. G. Toth, *Introduction to Nonlinear and Global Optimization*, Springer-Verlag, New York, NY, USA, 2010.

[19] S. Janardhanan, *Function development and verification environment for active safety functions of heavy commercial vehicles*, 2013.

[20] P. Lindroth, *Product Configuration with respect to Multiple Criteria — a Mathematical Programming Approach*, Licentiate thesis, Department of Mathematical Sciences, Chalmers University of Technology and Department of Mathematical Sciences, University of Gothenburg, Göteborg, Sweden, 2008.

[21] P. Lindroth, M. Patriksson, Z. Šabartová, and A.-B. Strömberg, *Optimizing truck tyres- how to improve the realism of simulation-based optimization through physical constraints*, Orbit medlemsblad for Dansk Selskab for Operationsanalyse og Svenska OperationsAnalysFöreningen, 23 (2014).

[22] G. Lino and Antonio, *Vehicle Propulsion Systems, Introduction to Modeling and Optimization*, Springer-Verlag Berlin Heidelberg, 3rd ed., 2013.

[23] MathWorks, Inc., *MATLAB Data Analysis*, 3 Apple Hill Drive Natick, MA 01760-2098, March 2015.

[24] ——, *MATLAB Mathematics*, 3 Apple Hill Drive Natick, MA 01760-2098, March 2015.

[25] ——, *Simulink User's Guide*, 3 Apple Hill Drive Natick, MA 01760-2098, March 2015.

[26] C. Moler, *Numerical Computing with MATLAB*, Society for Industrial and Applied Mathematics, 2004, ch. 6, pp. 165–184.

[27] H. Naunheimer, B. Bertsche, J. Ryborz, and W. Novak, *Automotive transmissions*, Springer Berlin Heidelberg, 2011.

[28] N. S. Nise, *Control Systems Engineering, International Student Version, 6th Edition*, Wiley, 6th edition international student version ed., April 2011.

[29] H. B. Pacejka and I. J. M. Besselink, *Tire and vehicle dynamics*, Butterworth-Heinemann, 3rd ed. ed., 2012.

[30] J. P. Pauwelussen, *Essentials of Vehicle Dynamics*, Butterworth-Heinemann, 2015.

[31] T. A. Runkler, *Data analytics: models and algorithms for intelligent data analysis*, Springer Vieweg, Wiesbaden; New York, 2012.

[32] H. Stenvall, *Driving resistance analysis of long haulage trucks at volvo*, 2010. 101.

[33] Volvo GTT, *PERF Users Manual*.

[34] Z. Šabartová, *Mathematical modelling for optimization of truck tyres selection*, licentiate's thesis, Chalmers University of Technology and University of Gothenburg, 2015.

[35] Z. Šabartová, P. Lindroth, A.-B. Strömberg, and M. Patriksson, *Integration of expert knowledge into radial basis surrogates for global optimization.* preprint.

[36] Z. Šabartová, P. Lindroth, A.-B. Strömberg, and M. Patriksson, *An optimization model for truck tyres selection*, in Proceedings of the 4th International Conference on Engineering Optimization 2014. Aurelio Araujo (ed.), Lisbon, Portugal, September 2014, pp. 561–566.

[37] J. Y. Wong, *Theory of ground vehicles*, Wiley, 4. ed., 2008.

A Requirement analysis

A.1 Collected data

evaluation list of criteria weights w_i														
stakeholder k_i/criteria c_i	**1**	**2**	**3**	**4**	**5**	**6**	**7**	**8**	**9**	**10**	**11**	**12**	**13**	**14**
1	5	4	3	2	2	2	2	2	2	2	2	5	4	5
2	5	4	3	3	2	5	2	3	4	4	3	4	3	5
3	5	4	3	3	3	5	3	2	4	4	3	4	3	4
4	5	4	2	5	3	5	5	1	1	1	5	1	5	5
5	4	4	3	1	3	5	3	-	-	-	1	4	2	4
resulting w_i	4.8	4	2.8	2.8	2.6	4.4	3	2	2.75	2.75	2.8	3.6	3.4	4.6

Table A.1: Evaluation list of criteria weights w_i

evaluation of tools e_{ij}																	
	i	**1**	**2**	**3**	**4**	**5**	**6**	**7**	**8**	**9**	**10**	**11**	**12**	**13**	**14**	**avg.**	**weigh. avg.**
exp. 1	**VTM**	5	3	2	2	4	3	5	4	5	4	1	2	4	4	3.50	**11.73**
	GSP	-	-	4	-	-	-	-	-	-	-	-	-	-	-	4	**11.20**
exp. 2	**PERF**	5	3	4	1	1	3	-	5	1	3	3	4	5	5	3.31	**11.51**
exp. 3	**VTM**	4	-	3	3	4	4	4	3	-	4	-	3	3	4	3.55	**12.04**
	PERF	2	-	3	1	3	2	1	3	-	3	-	4	4	4	2.73	**9.19**
	GSP	3	-	4	1	4	2	1	3	-	3	-	3	3	4	2.82	**9.48**
	GSP&VTM	4	-	4	3	4	4	4	3	-	4	-	2	3	4	3.55	**11.96**
	CVM	3	-	2	5	3	4	4	3	-	3	-	1	3	4	3.18	**10.71**
exp. 4	**VTM**	4	3	2	4	2	3	5	4	3	4	2	2	4	4	3.29	**10.96**
	GST	3	2	4	2	4	2	1	5	1	2	1	4	5	1	2.64	**8.46**
	GSP	3	2	4	2	4	2	1	5	3	3	1	3	4	4	2.93	**9.54**
	GSP&VTM	4	3	4	4	4	3	5	3	3	4	2	1	3	2	3.21	**10.43**
exp. 5	**CVM**	-	-	-	-	-	4	4	-	-	-	-	-	-	-	4.00	**14.80**
	GST	3	2	5	3	4	2	2	5	3	4	4	-	4	5	3.54	**11.31**
	GSP	3	2	5	3	4	2	2	5	3	4	4	-	4	5	3.54	**11.31**

Table A.2: Expert's evaluation of Volvo GTT analysis tools e_{ij}

A.2 Results

Criteria weights		
Rank	**Criteria**	**Weight w_i**
1	simple vehicle longitudinal drive cycle simulation	4,8
2	edit-ability	4,6
3	definition of the tyre model	4,4
4	definition of the resistances	4
5	learning time	3,6
6	approximate time to set the simulation	3,4
7	vehicle stability (handling) related simulations	3
8	detailed definition of an environment	2,8
9	vehicle comfort related simulations	2,8
10	power-train definition	2,8
11	possibility to provide continuous change of the tyre design parameters	2,75
12	possibility to define variety of truck types and combinations	2,75
13	vehicle start-ability related simulations	2,6
14	computational efficiency	2

Table A.3: Resulting criteria weights

Results		
Rank	**Platform**	**s_j**
1	CVM	12,77
2	VTM	11,57
3	GSP&VTM	11,20
4	PERF	10,35
5	GSP	10,38
6	GST	9,89

Table A.4: Results of the model B platform decision process

B Model B

B.1 Linear tyre - longitudinal version

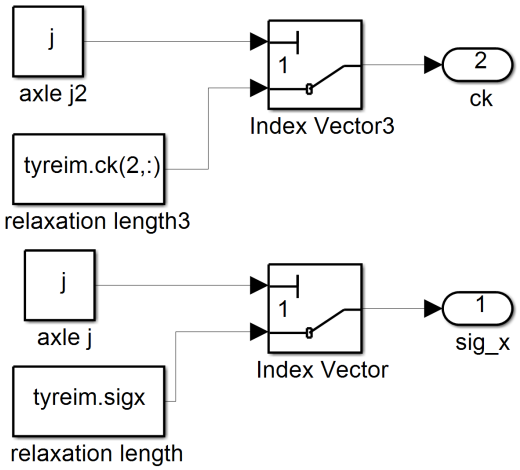

Figure B.1: *Linear tyre characteristics, i.e. block "linear tyre characteristics" in Figure 5.5.*

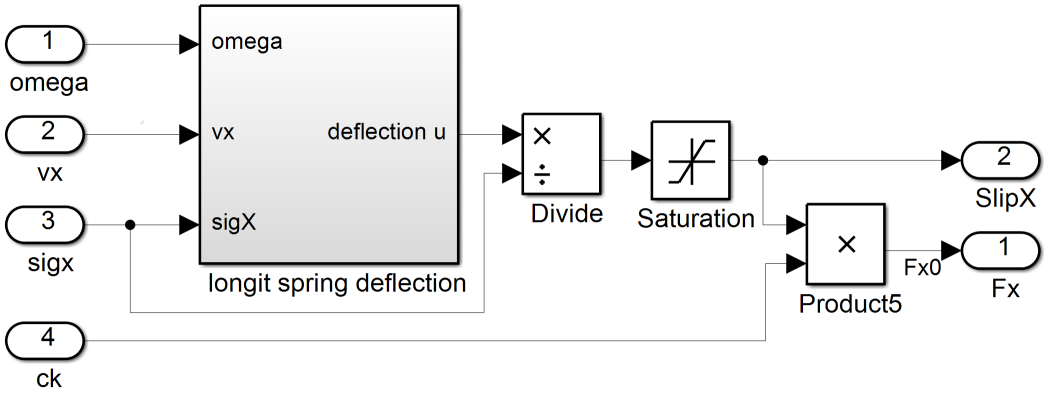

Figure B.2: *Transient linear tyre model, i.e. block "Transient linear tyre" in Figure 5.5.*

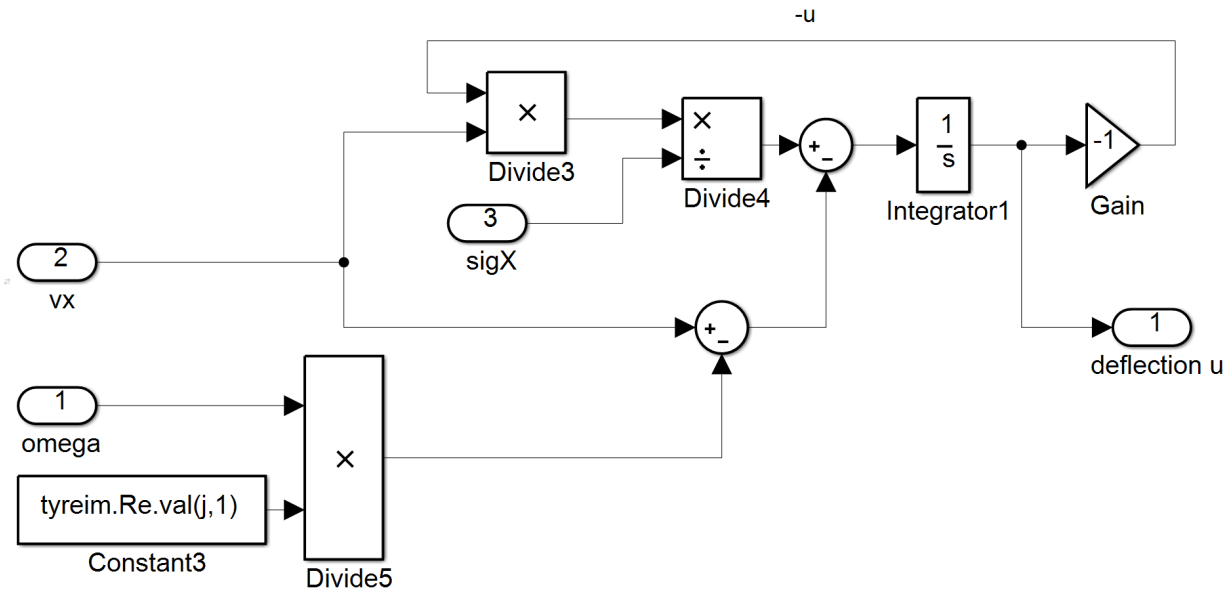

Figure B.3: *Longitudinal spring deflection, i.e. block "longit spring deflection" in Figure B.2.*

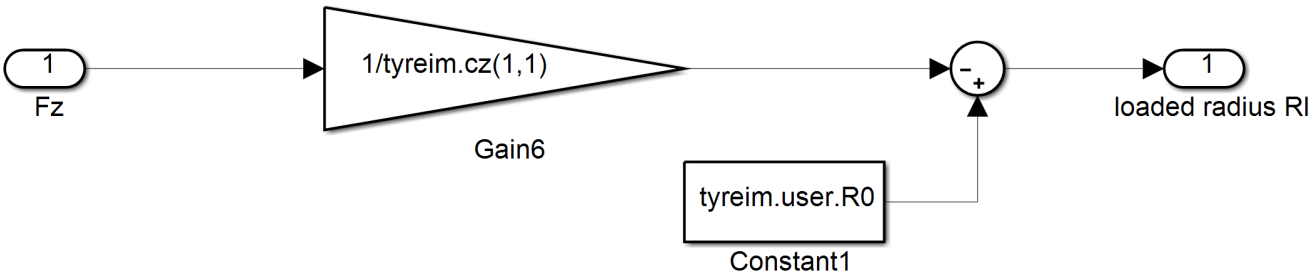

Figure B.4: *Vertical dynamics of the tyre, i.e. block "Subsystem" in Figure 5.5.*

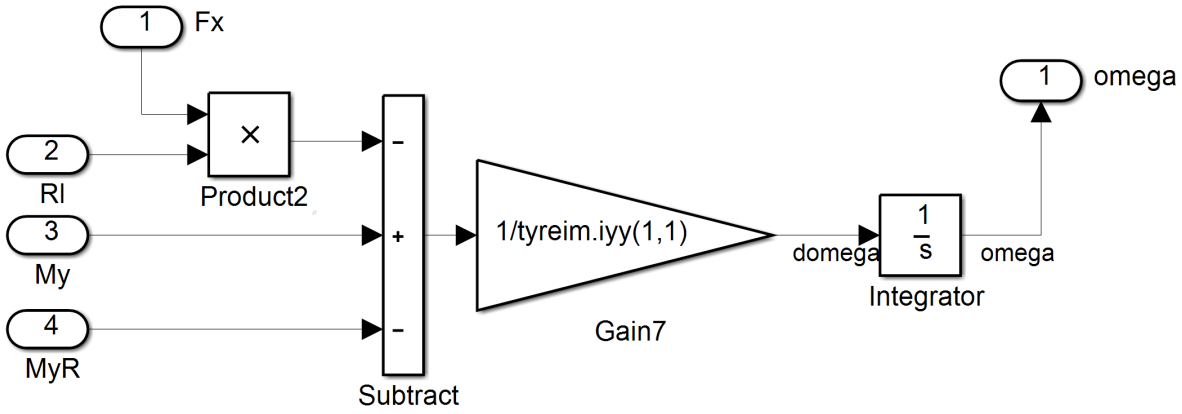

Figure B.5: *Equation of motion of the wheel, i.e. block "Euler equation of motion" in Figure 5.5.*

C Verification data

test no.	**L1.1**
description	qualitative verification of model A
tyres	model B - MF, surrogate - pac2002_315_80R22_5.tir, cf. D
	model A - surrogate, pararmeters derived from the pac2002_315_80R22_5.tir, cf. D
track	road 1505 (1km), cf. C.1
model	A, B
pre-processing/mod.	model A - tractive energy Simulink block, finer pre-processing of an environment
outputs	$P_{tr_{A,B}}(x)$,$P_{RR_{A,B}}(x)$,$f_{c_A}(x)$,$M_{y_{A,B}}(x)$, $f_{R_{A,B}}(x)$, $M_{yRR_{A,B}}(x)$, $\Omega_{y_{A,B}}(x)$, $F_{z_{A,B}}(x)$
goal	comparison of qualitative behaviour of both models, find the differences

Table C.1: Verification details of L1.1

test no.	**L2.1**
description	qualitative verification of model A - transients
tyres	model B - MF (4), surrogate - pac2002_315_80R22_5.tir, Drive_ice.tir, Front_hf.tir, Drive_hf.tir, cf. D
	model A - surrogate, paramateters derived from the MF (4) tyres, cf. D
track	road 1505 (1km), cf. C.1
model	A, B
pre-processing/mod.	tractive energy E_{tr} from simulink integration of $P_{tr} \geq 0$ for A, B
post-processing 2	tractive energy E_{tr} from trapezoid int. of $P_{tr} \geq 0$ of A, B
outputs	$E_{tr} = f(tyres)$ (trapz, sim) and $E_{tr} = f(tyres, x)$ (sim)
goal 1	show ΔE_{tr} between trapz. simulink on road 1505 (infl. by transients)
goal 2	proof transient problem of model A - higlight the numerical issue in model A

Table C.2: Verification details of L2.1

test no.	**L2.2**
description	sensitivity analysis
tyres	linear tyre, various p, w_t, d, cf. Table C.5
track	reduced road 365 (10km), cf. Figure C.2, reduced road 521 (10km), cf. Figure C.3
model	A, B
pre-processing/mod.	simulink integration of $P_{tr} \geq 0$ for A, B (E_{tr})
post-processing 1	normalization of the tractive energy E_{tr}, presentation of the figures
outputs	$E_{trA} = f(p)$, $E_{trB} = f(p)$, $E_{trA} = f(w_t)$, $E_{trB} = f(w_t)$, $E_{trA} = f(d)$, $E_{trB} = f(d)$ (both mod. A, B simulink int.)
goal 1	influence of the tyre design variables p, d, w_t on total energy consumption E_{tr}

Table C.3: Verification details of L2.2

test no.	L2.3
description	sensitivity analysis with modified model A
tyres	linear tyre, various p, w_t, d, cf. Table C.5
track	reduced road 365 (10km), cf. Figure C.2, reduced road 521 (10km), cf. Figure C.3
model	A, B
pre-processing/mod.	simulink integration of $P_{tr} \geq 0$ for A, B (E_{tr})
pre-processing	logg of the normal load profile $F_z(x)$, and velocity profile $v_x(x)$ of the model B
pre-processing	import of the logged profiles $F_z(x)$, and $v_x(x)$ from the model B to the model A
outputs	$E_{trA,Amod} = f(p)$, $E_{trB} = f(p)$, $E_{trA,Amod} = f(w_t)$, $E_{trB} = f(w_t)$, $E_{trA,Amod} = f(d)$, $E_{trB} = f(d)$ (both mod. A, B simulink int.)
goal 1	influence of the normal load $F_z(x)$ and control strategy $v_x(x)$ on the energy consumption E_{tr}

Table C.4: Verification details of L2.3

C.1 Environment data

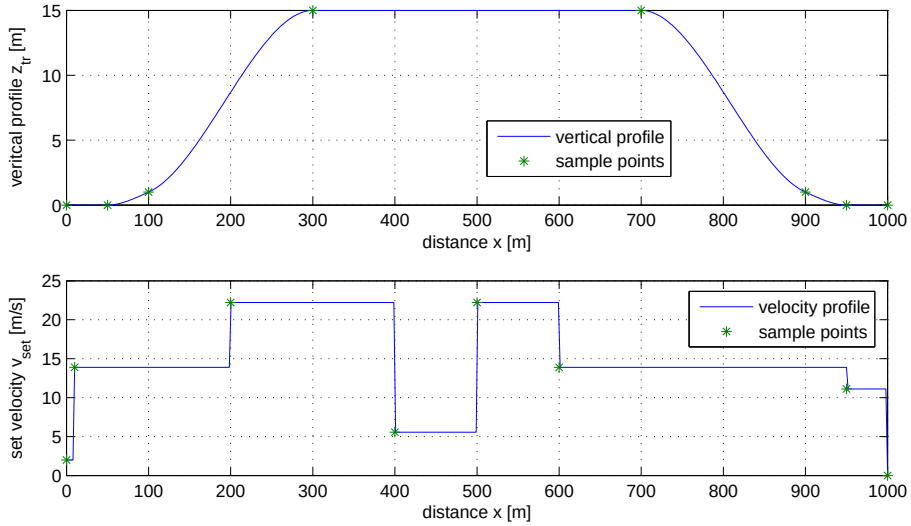

Figure C.1: *Testing road cycle 1505 (1km)*

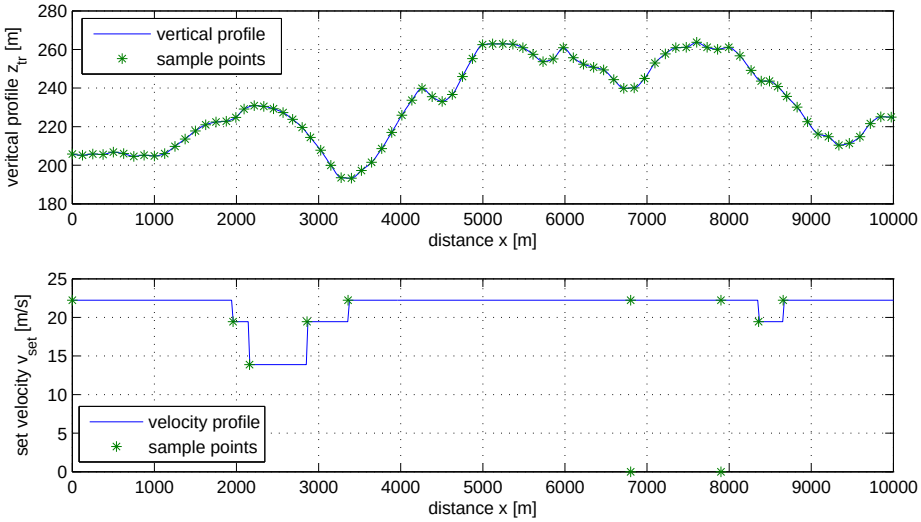

Figure C.2: *Reduced road 365 (10km)*

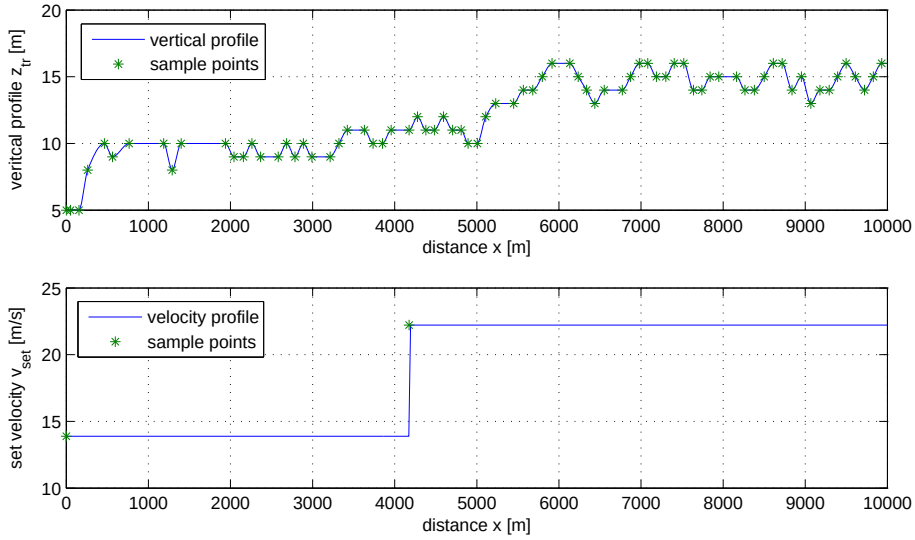

Figure C.3: *Reduced road 521 (10km)*

C.2 Sensitivity analysis

Verification matrix			
changing variable	**operation range**	**reference value**	**evaluated variable values**
tyre pressure p [psi]	$\langle 55 - 165 \rangle$	110	$[55; 66; 77; 88; 99; 110]$ $[121; 132; 143; 154; 165]$
tyre diameter d [mm]	$\langle 916.57 - 1120 \rangle$	1018	$[1018.29; 1038.63; 1058.97; 1079.31; 1099.66; 1120]$ $[916.57; 936.91; 957.26; 977.60; 997.94]$
tyre width w [mm]	$\langle 227.66 - 455.31 \rangle$	341	$[227.66; 250.43; 273.19; 295.96; 318.72; 341.49]$ $[364.25; 387.02; 409.78; 432.55; 455.31]$
tyre depth dep [mm]	$\langle 0 - 23.93 \rangle$	12	$[11.97]$

Table C.5: Variable values in sensitivity analysis

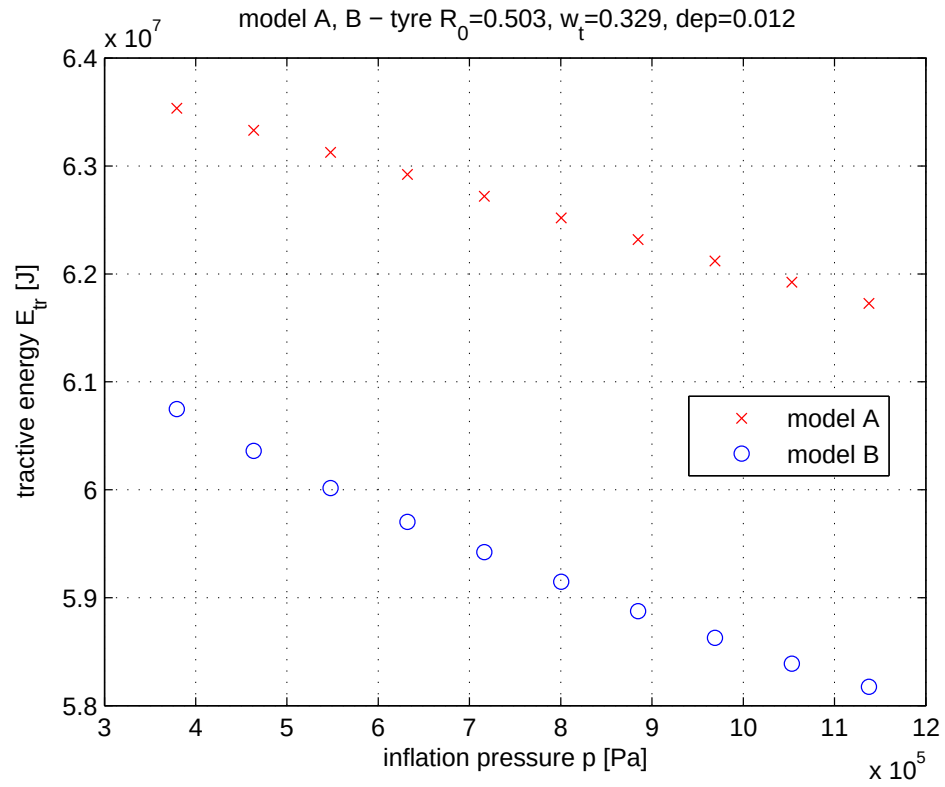

Figure C.4: *Tractive energy $E_{tr} = f(p)$ of the model A, B on the road 365 (10km)*

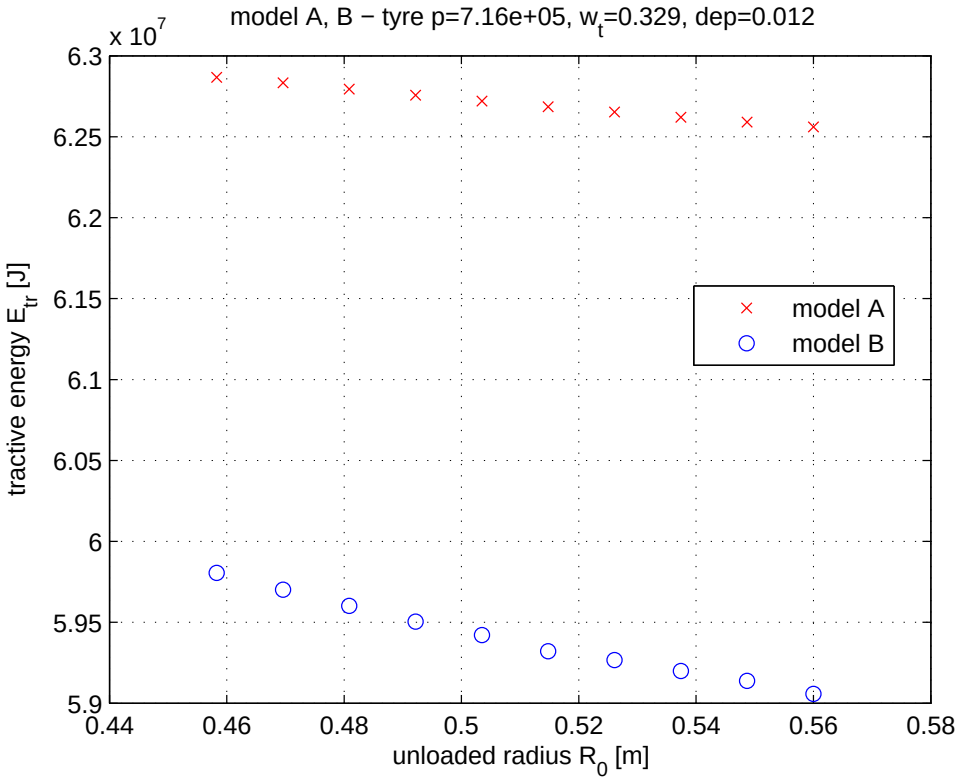

Figure C.5: *Tractive energy $E_{tr} = f(R_0)$ of the model A, B on the road 365 (10km)*

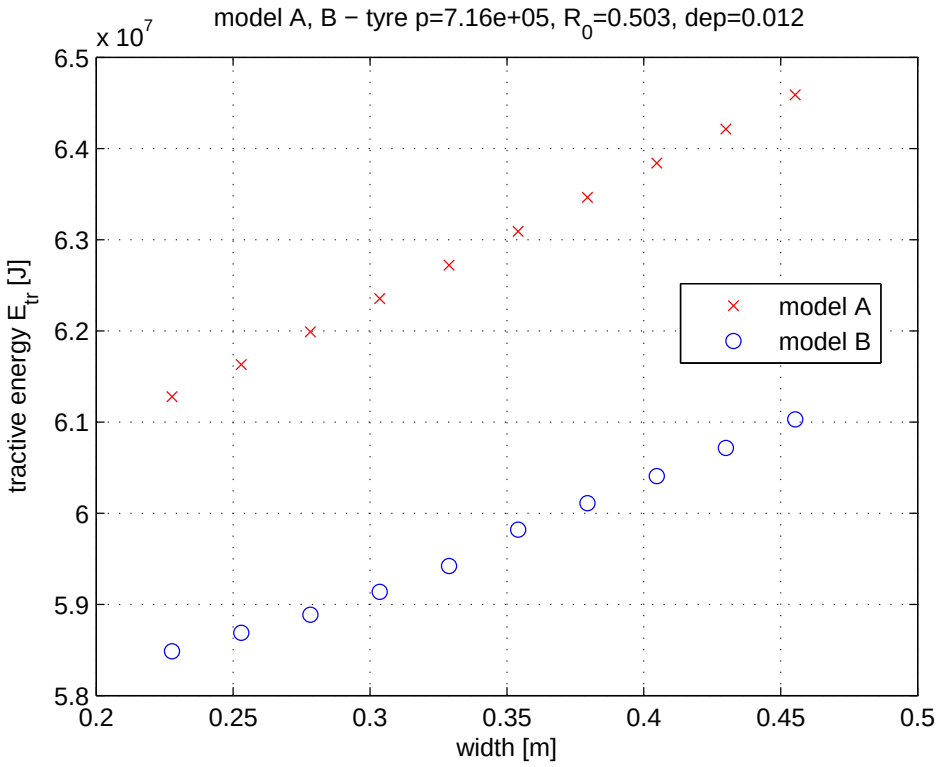

Figure C.6: *Tractive energy $E_{tr} = f(w_t)$ of the model A, B on the road 365 (10km)*

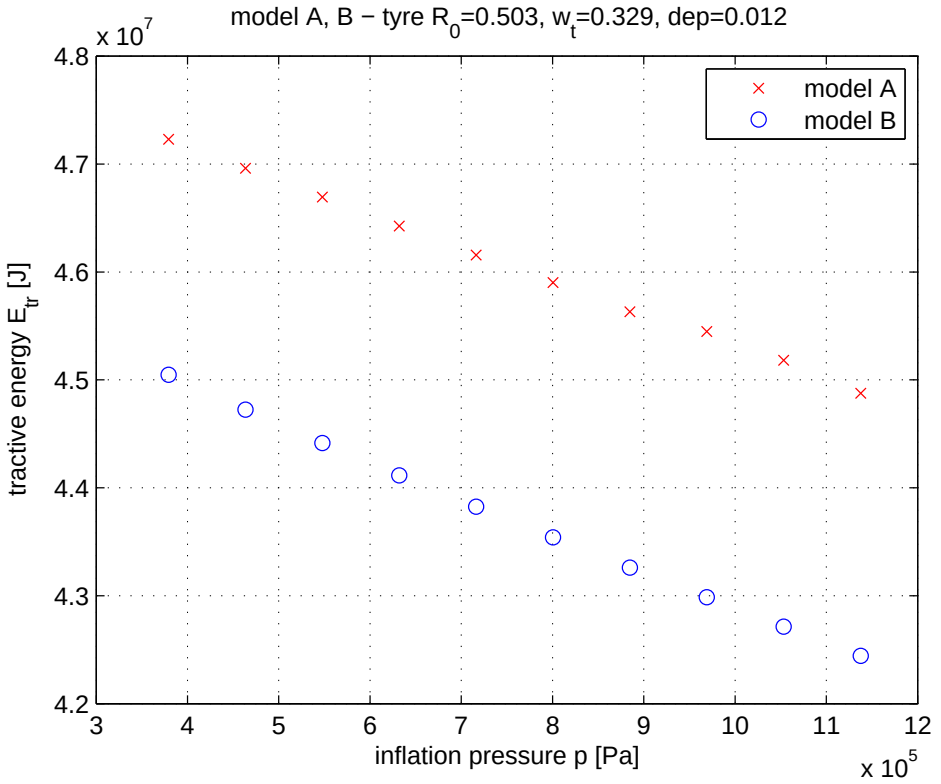

Figure C.7: *Tractive energy $E_{tr} = f(p)$ of the model A, B on the road 521 (10km)*

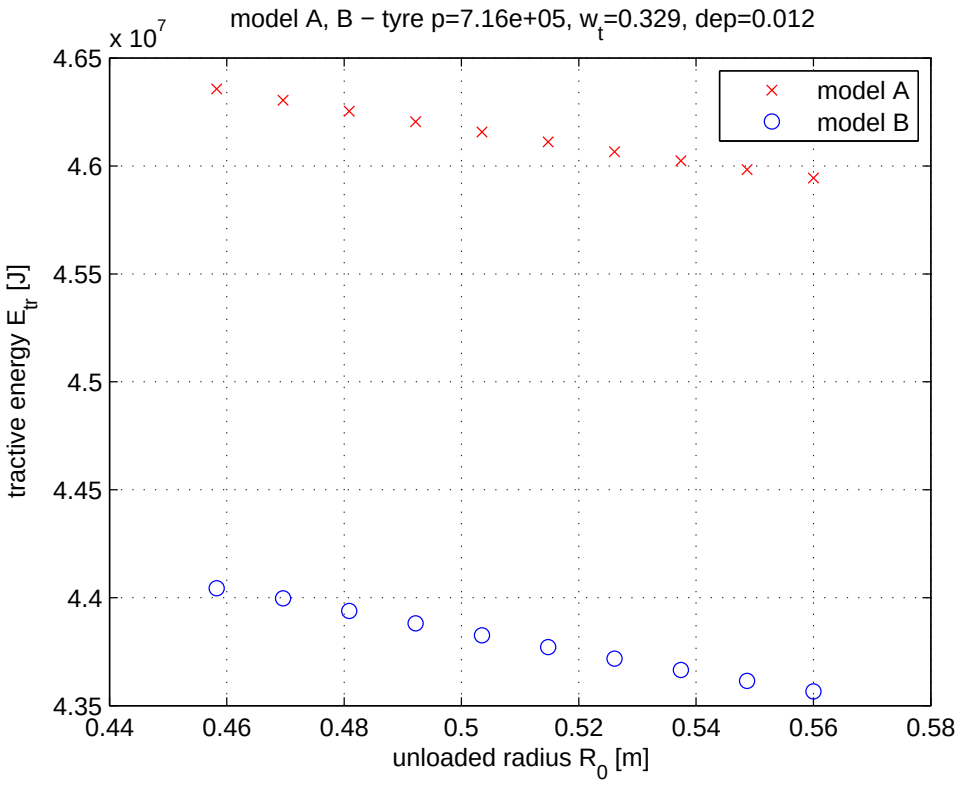

Figure C.8: *Tractive energy $E_{tr} = f(R_0)$ of the model A, B on the road 521 (10km)*

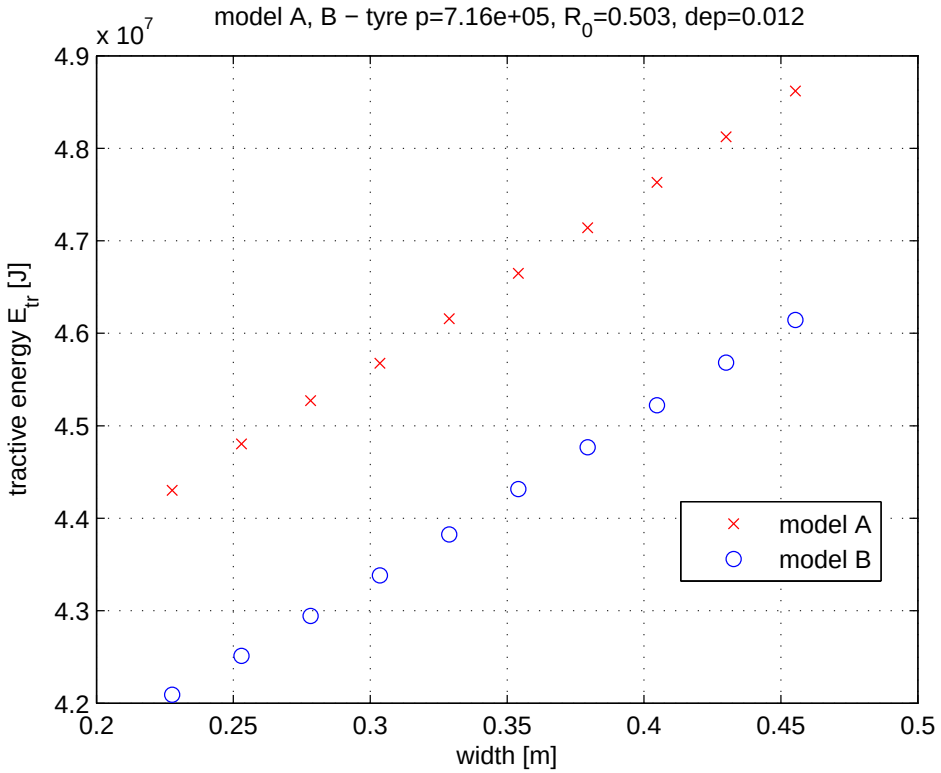

Figure C.9: *Tractive energy $E_{tr} = f(w_t)$ of the model A, B on the road 521 (10km)*